THE PROCEEDINGS OF THE PHYSICAL SOCIETY

Section A

VOL. 63, PART 11 1 November 1950 No. 371 A

The Hard Components of Scattered Gamma-Rays

BY P. B. MOON

Physics Department, University of Birmingham

MS. received 13*th March* 1950, *and in final form* 5*th May* 1950

ABSTRACT. A summary is given of theoretical information on the three processes by which gamma-rays can be elastically scattered by atoms, viz. Rayleigh scattering by bound electrons, Thomson scattering by the nuclear charge and (exceptionally) nuclear resonant scattering.

Interference between the three scattered waves is considered and shown to be of practical importance as between Rayleigh and Thomson scattering of hard gamma-rays at large angles.

The calculated intensities of Rayleigh, Thomson and Compton scattering are plotted against angle of scattering for gamma-ray energies of 2·8 and 0·41 MEV., and for scatterers of Al, Cu and Pb. The graphs illustrate the dominance of Rayleigh scattering at very small angles for all energies, and the comparable intensities of Rayleigh and Thomson scattering at high energies and large angles.

The unidentified hard component found by Pollard and Alburger in the large-angle scattering of 2·8-MEV. gamma-rays by various elements is interpreted as a mixture of Rayleigh and Thomson scattering; theoretical and experimental intensities show reasonable agreement for both light (Al) and heavy (Pb) scatterers.

Experiments on the scattering of 0·41-MEV. gamma-rays at about 115° are reported. In agreement with theory, about 2% of the radiation scattered from lead is found to retain the full energy; for copper and aluminium, the proportion of elastically scattered photons is much smaller.

§ 1. INTRODUCTION

THE scattering of gamma-rays in matter is mainly due to the Compton effect, which involves the ejection of an electron from the scattering atom and a substantial loss of energy by the gamma-ray. Three types of scattering are, however, known to be possible in which the only loss of energy is the small amount taken up by the recoil of the scattering atom. The processes in question are:

(i) scattering by bound electrons, without the removal of any electron from its bound state;

(ii) scattering by the nuclear charge as a whole;

(iii) scattering due to nuclear resonances.

These processes will be considered in turn, the possibility of interference between them examined, and some experiments with 0·41-MEV. gamma-rays reported.

§ 2. SCATTERING BY BOUND ELECTRONS (RAYLEIGH SCATTERING)

Rayleigh scattering is well known in the X-ray region, since it is the coherent scattering responsible for X-ray interference phenomena. In the γ-ray region, its existence is shown by the success of crystal spectroscopy, which has recently been extended to energies above 1 MeV. (Lind, Brown and DuMond 1949) but there seems to have been no deliberate experimental study of the scattering process. Franz (1935) has extended into the γ-ray region the calculations of Debye (1930) on the coherent scattering of X-rays, the Thomas–Fermi approximation to the electron distribution being assumed. * The following discussion will be based upon Franz's non-relativistic calculations which, as he shows, should give the total Rayleigh scattering cross section to within about 20% even for the heaviest elements and for the energetic Th C″ γ-ray. Throughout the gamma-ray region, this cross section is a small fraction of that for Compton scattering, the ratio of the two being about $2{\cdot}1 \times 10^{-5} Z^{5/3} E_0/E$, where Z is the atomic number of the scattering atom, E the energy of the γ-ray and E_0 the self-energy of the electron (0·511 MeV.).

The Rayleigh scattering is mainly at small angles; Franz's results† show that more than three-quarters is scattered by less than the angle $2 \sin^{-1} [2{\cdot}6 \times 10^{-2} Z^{1/3} E_0/E]$.

This characteristic angle θ_0 is about 16° for 0·41-MeV. radiation scattered by lead, and about $1\frac{1}{2}$° for 2·8-MeV. radiation scattered by aluminium. For angles much less than θ_0 Debye's treatment is valid and shows that as the angle of scattering θ approaches zero, the intensity of Rayleigh scattering is proportional to Z^2 and independent of E—results familiar in the X-ray field but having special importance for γ-ray crystal spectroscopy, where the background from inelastic scattering is so much more serious.

When $\theta > \theta_0$, Franz's equations lead to the expression

$$S_{\mathrm{R}} = \frac{\mathbf{e}^4 Z^2}{E_0{}^2} \frac{\pi}{2u^3} \frac{1+\cos^2\theta}{2} \,\mathrm{cm}^2 \qquad \ldots\ldots(1)$$

for the cross section *per unit solid angle*, where $u = 2{\cdot}43 \times 10^{-2} Z^{1/3} (E/E_0) \sin \frac{1}{2}\theta$.

Inserting numerical values, one finds

$$S_{\mathrm{R}} = \frac{8{\cdot}67 \times 10^{-33}}{\sin^3 \frac{1}{2}\theta} \left(\frac{ZE_0}{E}\right)^3 \frac{1+\cos^2\theta}{2} \,\mathrm{cm}^2. \qquad \ldots\ldots(2)$$

§ 3. SCATTERING BY THE NUCLEAR CHARGE (NUCLEAR THOMSON SCATTERING)

The cross section for scattering by the nuclear charge may be obtained from Thomson's classical equation for the scattering of X-rays by free electrons, by inserting the nuclear mass M and charge $Z\mathbf{e}$ in place of the electronic mass $\mathbf{m}$ and charge $\mathbf{e}$.

The total cross section is $\frac{8\pi}{3} \frac{Z^4 \mathbf{e}^4}{M^2 \mathbf{c}^4}$ and the cross section per unit solid angle at angle θ is

$$S_{\mathrm{T}} = \frac{Z^4 \mathbf{e}^4}{2M^2 \mathbf{c}^4} (1+\cos^2\theta) = 2{\cdot}39 \times 10^{-32} \frac{Z^4}{A^2} \frac{1+\cos^2\theta}{2} \,\mathrm{cm}^2, \qquad \ldots\ldots(3)$$

where A is the nuclear mass (^{16}O = 16).

---

* My thanks are due to Dr. Franz and to Professor R. E. Peierls for valuable discussions of this paper, and to Mr. J. Woodward for the last factor of equation (1), omitted by Franz because he was concerned with small angles of scattering.

† Last pair of equations (un-numbered) on his page 316; θ_0 is the angle for which $u = 2\pi$.

§ 4. RESONANT NUCLEAR SCATTERING

Resonant nuclear scattering is the nuclear analogue of the well-known resonance fluorescence of atoms and may be described as virtual absorption and re-emission, by a nucleus, of a gamma-ray that has the right energy to raise the nucleus from its ground state to an excited level. The angular distribution will depend upon the type of transition concerned—electric dipoles, for example, will scatter unpolarized radiation with an intensity varying as $(1+\cos^2\theta)$. At exact resonance, the cross section would be of the order of the square of the γ-ray wavelength (say, 10^{-20} to 10^{-22} cm^2), and much larger than even the Compton cross section. Yet the process has so far not been observed, because of the impossibility of securing exact resonance for all pairs of emitting and scattering nuclei, even when they are of identical type. The widths of gamma-ray lines, and of the corresponding nuclear resonances, are usually much less than the Doppler shifts due to the recoil velocities and to the velocities of thermal agitation of the emitting and scattering nuclei. Taking as an example the γ-ray with which this paper is mainly concerned—the 0·41-MEV. transition in ^{198}Hg following the β-decay of ^{198}Au—one may suppose the scatterer to be mercury, which contains about 10% of ^{198}Hg, or a compound of mercury. The recoil of the emitting nucleus takes about 0·425 electron volt, and an equal amount of kinetic energy goes to the scattering nucleus when it absorbs the photon, which is therefore too low in energy by about 0·85 ev. for exact resonance. (See Kuhn (1929) and Pollard and Alburger (1948) for discussions of the corresponding question for ^{208}Pb and ^{24}Mg respectively.) The thermal shift (in either direction according to whether the two nuclei are approaching or receding from one another) is somewhat smaller but still a considerable fraction of an electron volt. The width of the nuclear resonance is not known, but unless the transition were of electric dipole type (which is unlikely because the gamma-ray suffers appreciable internal conversion) it is probably 10^{-4} ev. or less. Thus an individual photon has a strong chance of resonant scattering only by those few nuclei (about 1 in 10^8 if the width of the resonance is 10^{-4} ev.) whose thermal velocities with respect to that of the emitting atom compensate closely enough for the recoil shift. Even if recoil were totally prevented by the binding of the nuclei in a crystal lattice, resonant scattering would still be effective only for the few pairs of nuclei whose thermal velocity components along the line joining them are almost exactly equal. Nuclear resonant scattering will therefore usually have an effective cross section very much *less* than that for Compton scattering, and only in exceptional cases can it be expected to be comparable even with Rayleigh or Thomson scattering. It would, of course, be a most remarkable coincidence if resonance were to occur with gamma-radiation emitted and scattered by nuclei not of identical type.

§ 5. INTENSITIES AND ANGULAR DISTRIBUTIONS OF COMPTON, RAYLEIGH AND THOMSON SCATTERING

Figures 1 (*a*) and 1 (*b*) show the Compton, Rayleigh and Thomson cross sections per unit solid angle for scattering of 2·8-MEV. and 0·41-MEV. gamma-rays by aluminium, copper and lead; symbols denoting the three elements appear on the lines and indicate points calculated from the Klein–Nishina formula* for Compton scattering, from equation (2) for Rayleigh scattering and from equation (3) for Thomson scattering. Detailed and accurate calculations would entail more labour, and would occupy much more space in presentation, than the present discussion warrants.

---

* I am indebted to Mr. A. Storruste for help with the Klein–Nishina calculations.

It will be noted that at very small angles the Rayleigh scattering is predominant, Compton scattering coming next and Thomson scattering being negligible in comparison with either. For the higher energy and at larger angles, the Thomson component may equal or surpass the Rayleigh, though both are then small compared with the Compton component.

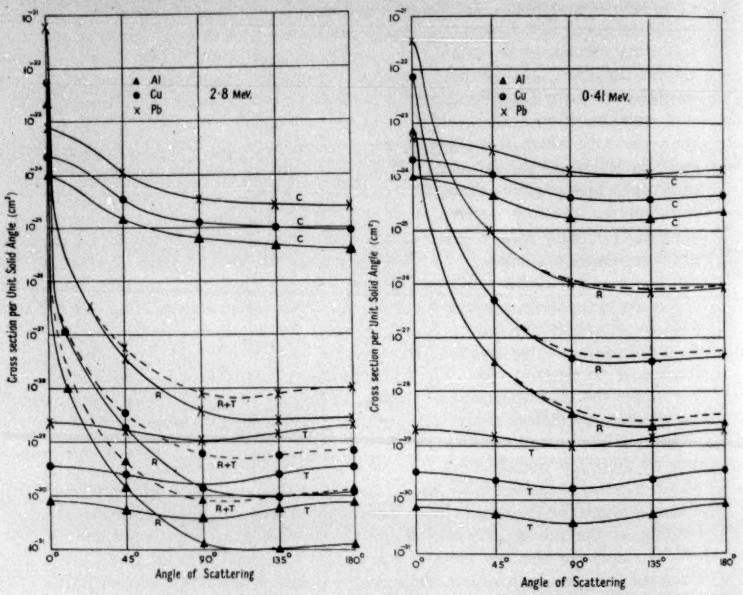

(*a*) (*b*)

Figure 1. Calculated cross sections in cm² per unit solid angle for scattering of gamma-rays by Al (▲), Cu (●) and Pb (×). C=Compton scattering, R=Rayleigh scattering, T=Thomson scattering. (*a*) 2·8 Mev., (*b*) 0·41 Mev.

§6. INTERFERENCE BETWEEN RAYLEIGH, THOMSON AND RESONANT SCATTERING

The scattering by Rayleigh, Thomson and resonance processes from an individual atom will not be coherent with the incident wave, because of the displacements of frequency caused by recoil and thermal motions, but they will presumably be coherent with one another. This is certain as between Rayleigh and Thomson scattering, because the waves result respectively from the motion of the negative and positive charges of a single system—the nucleus and its electrons—acted upon by the same electromagnetic field. If, as is assumed in Debye's and Franz's calculations, the electrons may be treated as a charge-distribution symmetrical about the nucleus, the phase of the resultant wave scattered by them will be the same as that of the wave scattered by the nuclear charge. The interference will therefore be constructive, with an intensity $A_R^2+2A_RA_T+A_T^2$, where A_R and A_T are the amplitudes of the Rayleigh and Thomson waves in the direction and at the distance of the point of observation. The resultant intensity is indicated by the broken lines, marked R+T in Figure 1 (*a*).

As was seen in § 4, resonant nuclear scattering will seldom be comparable in intensity with Rayleigh scattering. Though their *amplitudes* will of course be less unequal, there are two reasons for believing that interference between them will not give a ' cross term ' comparable with the Rayleigh intensity. The first is that, at exact resonance, the resonantly scattered wave will be in quadrature with the waves scattered (non-resonantly) by the electrons and by the nuclear charge. It is true that on one side of the resonance the two waves will come into phase, but on the other their phases will become opposite. Since the effective width of the gamma-ray line vastly exceeds the intrinsic width of the nuclear resonance, those photons that are strongly scattered will be uniformly distributed in frequency over the width of the resonance, and the constructive and destructive interference on the two sides of the peak will balance out. The other argument depends on the fact that the resonant scattering is *strong* scattering by a very *small fraction* of the nuclei; for an individual nucleus and an individual photon that are in resonance, the resonant scattering is much greater than the Rayleigh scattering, while well outside the resonance the reverse is true. Thus, quite apart from the phases, the amplitudes of the two waves will almost always be so unequal that the resultant intensity will be closely equal to that of the larger component.

Similar arguments hold good for interference between resonant and Thomson scattering.

§ 7. EXPERIMENTS OF POLLARD AND ALBURGER

During a search for resonant nuclear scattering, Pollard and Alburger (1948) investigated, by absorption in lead, the energy-distribution of ' ^{24}Na ' gamma-rays (2·8 and 1·4 Mev.) scattered at about 135° from Mg, Al, Pb and Hg. They found in each case a scattered component having an absorption coefficient characteristic of the 2·8-Mev. component of the original radiation. Since the ' ^{24}Na ' gamma-rays are in fact emitted from the product nucleus ^{24}Mg, any resonant scattering should have been found with Mg but not with the other scatterers. Though the ' hard component ' from Mg seemed somewhat more intense than that from the neighbouring elements Al, the difference was not significantly more than the experimental error. The intensity of this unidentified hard component compared with that of Compton scattering appears from their absorption curves to be about 0·02 for Pb and about 0·004 for Al. However, the efficiency of their counter for the hard component was probably five or ten times greater than for the Compton component, which at 135° would have an energy of about 0·32 Mev.; moreover, the hard component would escape more readily from the thick (' up to 1 inch ') scatterers that were used. Thus the true relative intensities are probably of the order of 10^{-3} for Pb and 2×10^{-4} for Al. Figure 1 (*a*) shows that the calculated ratio S_{R+T}/S_C for Pb at 135° is $10^{-28}/3\times10^{-25}$ or about 3×10^{-4}; the corresponding ratio for Al is $10^{-30}/5\times10^{-26}$ or about

2×10^{-6}. Theory and experiment thus agree within a factor of ten, and little more could be expected in view of the use of non-relativistic theory and the Thomas–Fermi electron distribution, the sensitivity of the ratio to the exact angle of scattering, and the uncertainty of the corrections made above for counter efficiency and for absorption in the scatterers. It will be noted that for lead the Rayleigh scattering should be the principal contributor, while for aluminium the Thomson scattering is the larger. Any other source of hard γ-radiation, such as bremsstrahlung, would help to explain the discrepancy between theory and experiment.

§ 8. EXPERIMENTS WITH 0·411 Mev. GAMMA-RAYS

The large-angle scattering of gamma rays of much lower energy (0·41 Mev.) by aluminium, copper and lead has been studied using a method similar to that of Pollard and Alburger. The apparatus is shown in section to scale in Figure 2.

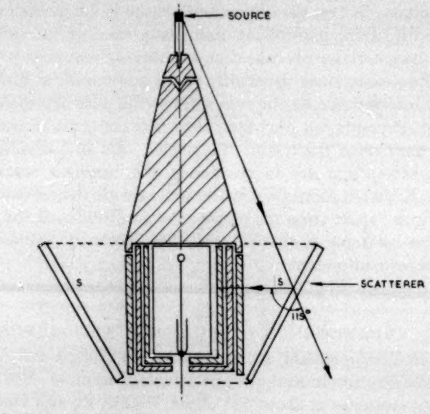

Figure 2. Experimental arrangement for scattering of 0·41-Mev. gamma-rays.

The source (a gold foil irradiated in the Harwell pile) was enclosed in a glass tube, just thick enough to prevent the ^{198}Au β-rays from reaching the scatterer, which was a hollow truncated cone of lead, copper or aluminium; the copper-walled Geiger–Müller counter was shielded from direct radiation by a solid lead cone. The whole apparatus was suspended by wires in the middle of a large room.

The source-holder was firmly and symmetrically mounted on an inverted cone of lead which fitted snugly into a conical hole in the top of the shielding cone; the source could thus be drawn up by a thread into a lead block above the apparatus, and accurately replaced. Various absorbers of lead could be placed round the counter; the outermost of these was made shorter than the others and fitted against an annular projection on the shielding cone. This ‘ staggering ’ of joints in absorbers is important when, as in the present work, it is desired to continue an absorption curve to less than a thousandth of the initial intensity.

The difference between the rates of counting with the source in place (R_1) and with the source removed (R_1') is a measure of the scattered intensity plus any radiation penetrating through the shield. The corresponding difference ($R_2 - R_2'$) when the scatterer is absent represents penetration through the shield, and thus $(R_1 - R_1') - (R_2 - R_2')$ represents the scattered intensity. Scattering from the air or other nearby objects was estimated to be at most a few per cent of that from the conical scatterer. The lead and copper scatterers each had a superficial mass of about 3·5 gm/cm^2, and the aluminium one about 2·5 gm/cm^2, so that a substantial fraction of the radiation incident upon them was scattered.

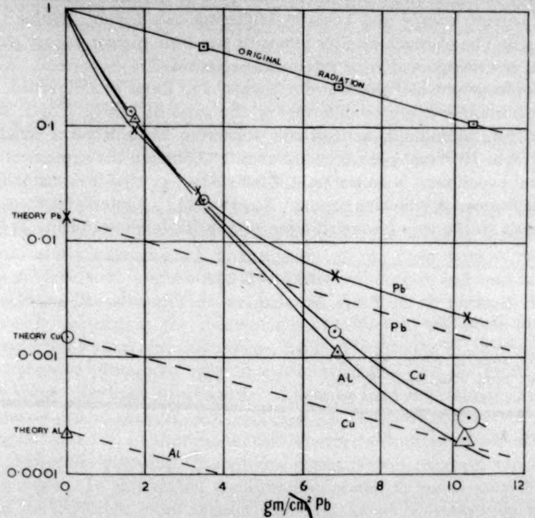

Figure 3. Absorption of gamma-rays scattered at 115° by Al (△), Cu (○) and Pb (×). Original energy 0·41 Mev.

Figure 3 shows semi-logarithmic absorption curves for the scattered radiation; the vertical heights of the symbols indicate the statistical probable error of the experimental points. The line marked ‘ original radiation ’ was obtained by replacing the scatterer by a very thin cone carrying small fragments of the source on the circle passing through the points S of Figure 1; this was judged to be the ‘ average ’ position of the scattering material, and corresponded to a mean angle of about 115°.

The points marked ‘ theory ’ represent in each case the ratio of Rayleigh to Compton scattering intensity at 115°, as obtained from Figure 1.(*b*), multiplied by the estimated ratio of their respective chances of emergence from the thick scatterers—a factor of about two. No correction was made for counter sensitivity, since according to Bradt *et al.* (1946) the copper-walled counter should be almost equally sensitive to the Rayleigh and Compton components of 0·41 and 0·22 Mev. respectively. The broken lines are drawn through these points parallel to the experimental absorption curve for the original radiation; as the Compton radiation is filtered out, the experimental curves should become asymptotic to these lines.

For lead, experiment and theory agree quite as well as could be expected; for copper, they are at least not inconsistent; for aluminium, the experimental absorption curve could not be carried far enough to permit even a tentative conclusion.

Mr. A. Storruste, who has been working in this laboratory on problems of bremsstrahlung, informs the author that hard bremsstrahlung due to β-rays from the source or to Compton electrons produced in the scatterer will not reach the counter in intensities comparable with that of the hard radiation observed. For the primary energy and angle of scattering in question, double Compton scattering will be of much smaller intensity and little greater energy than single Compton scattering, and may safely be neglected.

The experiments of Pollard and Alburger, and those here reported, together involve gamma-ray energies differing in the ratio of nearly 7 to 1, scattering elements from aluminium to lead and scattering cross sections ranging from about 10^{-26} to $10^{-30}\,\mathrm{cm}^2$ per unit solid angle. Although the agreement between theory and experiment is only rough, it is satisfactory that it is maintained over such wide ranges. A following paper by Storruste (1950) shows that the agreement also extends to the angular distribution of the Rayleigh scattering at 0·41 MeV.

REFERENCES

Bradt, H., Gugelot, P. C., Huber, O., Medicus, H., Preiswerk, P., and Scherrer, P., 1946, *Helv. Phys. Acta*, **19**, 77.

Debye, P., 1930, *Phys. Z.*, **31**, 419.

Franz, W., 1935, *Z. Phys.*, **98**, 314.

Kuhn, W., 1929, *Phil. Mag.*, **8**, 625.

Lind, D. A., Brown, T. R., and DuMond, J. W. M., 1949, *Phys. Rev.*, **76**, 1838.

Pollard, E. C., and Alburger, D. E., 1948, *Phys. Rev.*, **74**, 926.

Storruste, A., 1950, *Proc. Phys. Soc.* A, **63**, 1197.

The Rayleigh Scattering of 0·41 Mev. Gamma-Rays at Various Angles

By A. STORRUSTE
Physics Department, The University of Birmingham

Communicated by P. B. Moon; MS. received 5th May 1950

ABSTRACT. A report is given on some measurements of the Rayleigh cross section for scattering of 0·41 Mev. gamma-rays by lead, copper and aluminium. At smal langles the Rayleigh cross section in lead is found to decrease rapidly with increasing angle of scattering from approximately 12 times the Compton cross section at 3° to a value equal to the Compton cross section at 12°. In copper the Rayleigh cross section is found to equal the Compton cross section at 4·5°. In aluminium no substantial excess scattering above the Compton cross section is found, the smallest angle at which measurements were taken being 3°. At 60°, 90°, 120° and 150° the hard component of the scattered radiation from lead is found to be respectively 1·77, 1·14, 0·88 and 0·66% of the Compton component as calculated by the Klein–Nishina formula.

---

§1. INTRODUCTION

In a preceding paper (Moon 1950) is given a summary of theoretical predictions regarding the elastic scattering of gamma-rays, in addition to reports on an experimental investigation of the cross section for elastic scattering of 0·41 Mev. gamma-rays by aluminium, copper and lead at a mean angle of 115°. The aim of the present work has been to check the angular distribution by extending the measurements to various angles of scattering. Moon's paper shows that, for this energy, Rayleigh scattering by bound electrons is much the most prominent type of elastic scattering and the terms 'elastic scattering' and 'Rayleigh scattering' will here be used interchangeably.

The theory predicts that at small angles of scattering, up to about 12° in lead, 4·5° in copper and 2·5° in aluminium, the Rayleigh scattering should exceed the inelastic Compton scattering, though its intensity will decrease rapidly with increasing angle. In this region the Compton scattering varies very little with angle and the Rayleigh cross section has been found by measuring the total cross section and subtracting the Compton cross section calculated from the Klein–Nishina formula.

At larger angles of scattering the hard component of the scattered radiation from lead has been measured directly by filtering out the soft Compton component by absorption in conjunction with variation of the bias-setting of the scintillation counter used.

§2. MEASUREMENTS AT SMALL ANGLES OF SCATTERING

For good resolving power a detector for gamma-rays of small size and high efficiency is important. This was achieved by using a light guide in connection with a scintillation counter. A section of the apparatus is shown in Figure 1 (*a*). A natural scheelite crystal of volume about 0·8 cm^3 was put at the end of a Perspex rod 50 cm. in length guiding the light from the phosphor to an eleven-stage E.M.I. photo-multiplier. To improve the efficiency, immersion oil was used between the phosphor and the Perspex rod and between the Perspex rod and the glass, and the phosphor was covered with aluminium foil. The apparatus was suspended by fish line in the middle of a large room. The source was placed in a thin-walled glass tube which could be drawn up to the ceiling by a thread or lowered to fit accurately into an outer glass tube fastened to the suspension system, the joint between the two tubes being a ground cone. A double lead cone 10 cm. in length, with a maximum diameter of 1·8 cm., was accurately fixed to the lines half way between the source and the phosphor.

The scatterers used were rings of aluminium, copper and lead having cross sections of 22 mm. × 5 mm., 6·5 mm. × 5 mm. and 2 mm. × 5 mm. respectively. About eight rings of each element were used, the smallest having an inner radius of 10 mm. with the radius increasing by 5 mm. for each successive ring. The rings were suspended by threads from the ceiling. Each was accurately centred by a thin disc of paper fixed to the ring and having a centre hole just large enough to pass over the double lead cone.

The source used was a 50 mg. gold wire irradiated in the Harwell pile and had a strength of about 100 mc. The scattering from the walls of the room, mainly

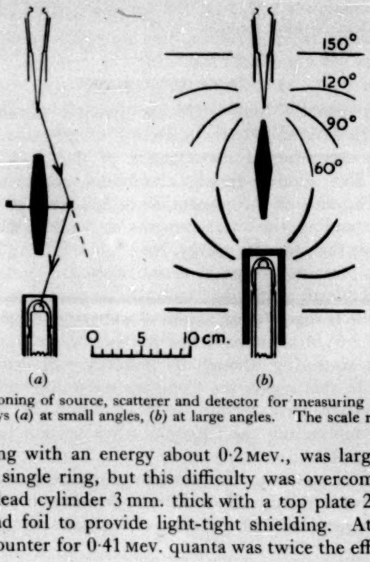

(*a*) (*b*)

Figure 1. The positioning of source, scatterer and detector for measuring the elastic scattering of gamma-rays (*a*) at small angles, (*b*) at large angles. The scale refers to (*b*).

Compton scattering with an energy about 0·2 MeV., was large compared to the scattering from a single ring, but this difficulty was overcome by shielding the phosphor with a lead cylinder 3 mm. thick with a top plate 2 mm. thick, as well as using some lead foil to provide light-tight shielding. At the bias used the efficiency of the counter for 0·41 MeV. quanta was twice the efficiency for 0·2 MeV. quanta.

The first measurements were taken with the source and the phosphor 40 cm. apart, the angle of scattering ranging from 7·5° to 35°. In this arrangement the rate of counting R_1 with a scatterer in place was for all scatterers a few times the rate of counting R_2 with the scatterer absent. R_2 was about 600 counts per minute and was mainly due to scattering from the walls of the room. The next series was performed with a distance of 60 cm. between source and phosphor, the scattering angle ranging from 5° to 20° and the spread in angle of scattering in one ring being about 3°. For measurements at smaller angles, the distance from source to phosphor was increased to 100 cm. The rate of counting R_1–R_2 due to scattering in the ring decreases, however, with the fourth power of the distance, and since the distance to the walls and the floor of the room was only about 200 cm. the background rate of counting was relatively large. Even the rather hard scattered radiation from the volume of air between source and phosphor was appreciable. For these reasons, it was not possible to make reliable measurements at angles of scattering less than about 3°. On the other hand, elastic scattering at angles greater than about 25° for lead and 10° for copper could not be studied by this method because the cross section became small compared with that for Compton scattering.

The results are plotted in Figure 2. The absolute value of the observed cross section was found by measuring the strength of the source directly with the same counter and weighing and measuring the scatterers. At larger angles where the Rayleigh scattering should be a very small fraction of the Compton scattering, the observed values were equal to the calculated Compton cross section to within the expected accuracy of about 10%. The curve of the observed total cross section was, therefore, fitted to the calculated Compton cross section at the largest angles; the difference between this curve and the Compton curve at smaller angles gives the Rayleigh scattering cross section, indicated by R in Figure 2. The energy of the Compton and Rayleigh components being nearly equal, the correction for the variation of the counter efficiency with energy was never more than 10%. The results indicate clearly the rise in cross section at small angles in the case of lead and copper. In the case of aluminium where no Rayleigh scattering was detected, the statistical probable error, indicated by the sizes of the symbols in the figure, was rather large and the too small value observed at 3° was partly due to the absorption by the ring of the gamma-rays scattered in the air. The results are in close agreement with theory and show the difference between scattering by a light and a heavy element.

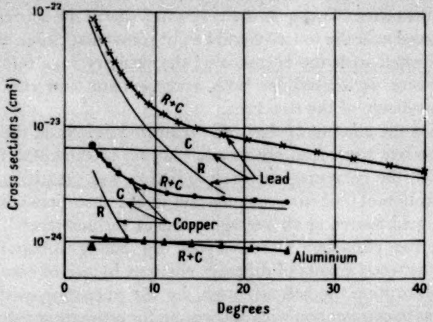

Figure 2. The total cross sections per unit solid angle for the scattering at small angles of 0.41 MeV. gamma-rays by lead, copper and aluminium, the decomposition into Compton and Rayleigh scattering being indicated. For aluminium, no Rayleigh component is detectable.

§ 3. MEASUREMENTS AT LARGE ANGLES OF SCATTERING

Measurements of elastic scattering become easier again at angles greater than about 60°, because the Compton scattering, though relatively much more intense, is then of appreciably lower energy and can be effectively removed by absorbers and by using a suitable bias in the recording system to discriminate against the weaker scintillations.

For measuring the elastic scattering at large angles the source and phosphor were placed 16 cm. apart. The scatterers used were sheets of lead formed into appropriate figures of revolution about the line joining the source and the phosphor, giving mean scattering angles of 60°, 90°, 120° and 150°. The scatterer at 90° was of course part of a sphere, and the scatterer at 150° was for convenience made plane as shown in Figure 1(*b*). The arrangement was similar to that described by Gentner (1936). Two sets of scatterers were made, the ones placed near the source having a thickness of 1 mm., and the scatterers placed near the phosphor having a thickness of 2 mm. When placing a scatterer near the phosphor, owing to the comparatively large size of the phosphor, there is some spread in scattering angle and some uncertainty in estimating the absorption of the Rayleigh scattered gamma-rays in the scatterer itself. The latter, however, does not vary much from one scatterer to the other. Owing to the very small size of the source (27 mg. gold) the scatterers placed near the source could be put somewhat closer, the uncertainty then being connected with the entrance of the primary rays into the scatterer. Measurements were performed for both arrangements and the results shown beneath are the average of the two runs.

For measuring the amount of elastically scattered radiation, the scattered rays had first to penetrate some lead absorbers, varying in thickness from 5 mm. to 10 mm., by which the percentage of hard radiation was greatly increased. The amount of absorption of 0·41 Mev. gamma-rays in the absorbers was measured by placing a small gold source at an average point of the scatterer. The radiation which reached the phosphor was analysed by taking integral bias curves. Discrimination between quanta of different energies by use of bias curves is very similar to the absorption method although, for the phosphor used, less efficient. Using bias curves in conjunction with absorption for estimating a small percentage of hard gamma-radiation is, however, believed to be superior to the absorption method alone, and has been used here to avoid shifting of absorbers. The decomposition of the bias curves into Compton and Rayleigh scattered radiation was made by the aid of experimental bias curves for the original radiation and the Compton scattered radiation alone. The former of these was obtained by using a small fragment of the source, the latter by removing the absorbers from around the phosphor and using very thin scatterers. As a result the counting rate due to the primary radiation decreased by a factor of 35 from the lowest to the highest bias setting used; the corresponding factors for the Compton scattered radiation at 60°, 90°, 120° and 150° were 320, 720, 1,450 and 2,300 respectively.

For calculating the absolute cross section for the elastic scattering of the 0·41 Mev. gamma-rays, each scatterer was divided into six sections and the contribution from each one added to give the observed rate of counting. The result, together with the observed cross section for Rayleigh scattering by lead at small angles, is shown in Figure 3. The total probable error is not simple to estimate. The observed rate of counting due to the Rayleigh scattered gamma-rays was high enough to give a reasonable statistical probable error, being about 5% at 60°, 90°, 120° and 8% at 150° for a counting time of 10 minutes at the highest bias settings used. As much longer counting times were used, the probable statistical errors are less than the above values. The errors made in analysing the curves and the uncertainties in connection with the calculations mentioned above may be higher and cannot be estimated accurately. In addition the correction made for the Compton scattering of the hard gamma-rays from the source was rather large at 60° as will be seen from the discussion below. The probable errors indicated by the heights of the symbols in the figure show how the accuracy of the result is believed to vary with angle of scattering. For comparison the theoretical cross section for elastic scattering is drawn as a curve. At small angles the values are obtained from Debye (1930), at larger angles the curve is taken from Moon (1950).

The energy distribution of the primary gamma-radiation from the source was checked by replacing the double lead cone in Figure 1 with lead absorbers up to 5 cm. in thickness and using 1 cm. of lead shielding around the phosphor. The result was in agreement with previous data for ^{198}Au *. At 60° the two hard gamma-rays will give rise to Compton scattered quanta of energies about 0·52 MeV. and 0·40 MeV. As the intensity of the 0·52 MeV. gamma-rays was calculated to be almost of the same order of magnitude as the Rayleigh scattered 0·41 MeV. radiation, it was assumed best to use only about 8 mm. of lead absorbers. Then the combination of the 0·40 MeV. and the 0·52 MeV. gamma-rays, striking the phosphor with intensities in the ratio 2·4 : 1, was assumed to give approximately the same slope of the bias curve as the 0·41 MeV. quanta for the bias settings used and in all amounted to 44% of the total hard radiation found by analysing the bias curve. At the larger angles of scattering all Compton scattered gamma-rays were softer than the Rayleigh scattered 0·41 MeV. radiation and hence gave less trouble.

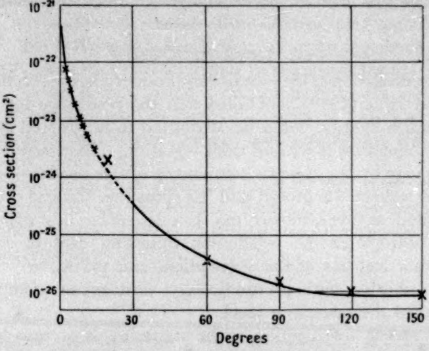

Figure 3. The measured cross section per unit solid angle for the elastic scattering of 0.41 MeV. gamma-rays by lead at various angles of scattering with the predictions from theory drawn as a curve.

ACKNOWLEDGMENT

The writer is indebted to Professor P. B. Moon for providing him with excellent facilities in the laboratory and for helpful guidance throughout the work.

REFERENCES

Debye, P., 1930, *Phys. Z.*, **31,** 419.
Gentner, W., 1936, *Z. Phys.*, **100,** 445.
Moon, P. B., 1950, *Proc. Phys. Soc.* A, **63,** 1189.

---

* Dr. P. E. Cavanagh and others at Harwell have informed Professor P. B. Moon of the existence of a 0·67 MeV. gamma-ray of intensity 1·5% and a 1·08 MeV. gamma-ray of intensity 0·4% following the beta-decay of ^{198}Au.

γ-Radiation from the Resonant Capture of Protons by ^{7}Li Nuclei

By S. DEVONS* and G. R. LINDSEY†

* Imperial College of Science, London
† Cavendish Laboratory, Cambridge

MS. received 1st *June* 1950

ABSTRACT. Further measurements have been made of the angular distribution of the γ-radiation in the reaction ^{7}Li(p, γ)^{8}Be. The results indicate approximate isotropy, at resonance, for both spectral components (17·6 and 14·8 Mev.) of the radiations. The difficulties in reconciling the properties of the γ-radiation with results of recent experiments on the scattering of protons by lithium are discussed.

§ 1. INTRODUCTION

In a recent investigation of the γ-radiation produced in the reaction ^{7}Li(p, γ)^{8}Be, Devons and Hine (1949) concluded that the resonance for this process, at 440 kev. proton energy, could be attributed to an excited state of ^{8}Be with total angular momentum $J = 1$ and odd($-$)parity. This state of ^{8}Be should be produced primarily by the S-wave component of the incident proton beam and from the triplet state of the proton and ^{7}Li spins (i.e. ^{7}Li and proton spins anti-parallel), provided, as was assumed, the ^{7}Li nucleus has odd parity. In this way the observed isotropy of the γ-radiation following capture could be readily explained. Other features of the γ-radiation, and particularly the variation of its angular distribution with proton energy, also appear compatible with this characterization of the resonance level.

However, a recent investigation of the scattering of protons by ^{7}Li nuclei, in the same range of proton energies, gave results which apparently require for their interpretation the assignment of different symmetry properties to the levels of ^{8}Be.‡

The main difficulty in assigning properties to the resonance level of ^{8}Be which are compatible with both γ-radiation and scattering measurements lies in the inadequacy of the proton S-wave component to account for the resonance in the elastic scattering cross section, whereas the approximate isotropy of the γ-radiation is strongly indicative of a proton S-wave. Cohen (1949) finds that the magnitude of the scattering cross section can be correctly accounted for if it is assumed that the resonance level of ^{8}Be is a $J = 1, +$ state, produced by the proton p-wave. To fit the experimental results he also chooses a particular value for the relative contributions of the triplet (proton and ^{7}Li spins anti-parallel) and quintuplet (spins parallel) 'spin' states in the formation of the ^{8}Be state. If this interpretation of the scattering data is made, there is sufficient information to enable the angular distribution of the γ-radiation at resonance to be predicted. This γ-radiation consists of two components (Walker and McDaniel 1948), one of 17·6 Mev. and the other approximately 14·8 Mev., corresponding to transitions to the two lowest states of ^{8}Be. If both these states are assumed to have the symmetry $J=0, +$, then the predicted angular distribution for both components is $1+0{\cdot}703\cos^2\theta$, in obvious conflict with experiment. In order to avoid this conflict, Christy (1949) has suggested that the lower of these two states of ^{8}Be has the symmetry $J=2, +$ and the other $J=0, +$, and that the angular distribution of the two components separately is *not* isotropic, though the mixture is fortuitously so. On the basis of this interpretation, the spectral composition of the radiation should vary substantially with the angle (relative to the direction of the incident protons) at which the radiation is observed.

---

‡ Only brief reports of the measurements (Fowler, Lauritsen and Rubin 1949) and their interpretation (Cohen 1949, Christy 1949), have been published. In addition we wish to acknowledge several private communications from Professor Christy in which he gave us more details of the experiments and their interpretation.

We shall return to a more detailed discussion of this interpretation after presenting experimental evidence that the spectral composition does not change greatly, if at all, with angle.

§ 2. EXPERIMENTAL

The γ-radiation produced by bombardment of thin evaporated targets of metallic lithium was studied by means of an electron pair spectrometer similar to that described by Walker and McDaniel. The arrangement used is represented in Figure 1. Relevant characteristics of the apparatus are :

Spectrometer. Magnet gap 5·0 cm.; maximum magnetic yield 8,000 gauss; average spacing of counter pair 20·4 cm.; two pairs of counters, 2, 3 and A, B, each 1 cm. diameter and 6 cm. long; lead converter foil 320 mg/cm^2; coincidence resolving time 1·5 μsec.

Target. Lithium metal evaporated on copper 0·7 mm. thick; target thickness 10 to 25 kev. stopping-power for 450 kev. protons; proton current 15–30 μa.; energy homogeneity approx. 10 kev. The distance between the target and the centre of the converter foil was 8 cm.

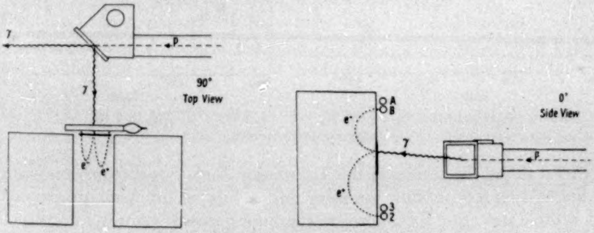

Figure 1. Experimental arrangement.

The spectrum of the γ-radiation was studied at two angles, 0° and 90° with respect to the direction of the proton beam (Figure 1). Coincidences were recorded between all four counter pairs A3, A2, B3, B2 and corrected firstly for random coincidences and secondly for the effects of pairs originating elsewhere than in the lead converter. The coincidence rates were normalized to the same total γ-radiation flux by monitoring the γ-radiation with a large lead-shielded counter kept in a fixed position. The energy of the proton beam used in all the observations was adjusted (within one or two kev.) to give a maximum intensity, i.e. the radiation observed was due almost completely to the 440 kev. resonance in the capture process.

Figure 2 shows the corrected results. The resolution from the pair B3 was too poor to provide useful information. Results from the two pairs B2, A3 are combined since they correspond to identical geometrical conditions. In each case the results obtained at 0° and 90° are shown superposed.

In order to estimate how small a change in spectral composition could be detected, an attempt was made to calculate the theoretical resolution curves of the spectrometer. The main factors governing the resolution are the ratio of the counter widths to the distances between them and the thickness of the lead converter. The calculation took account of the three-dimensional geometry of the target converter, baffles and counters and of the angular distribution of electrons and positrons produced by the γ-radiation.

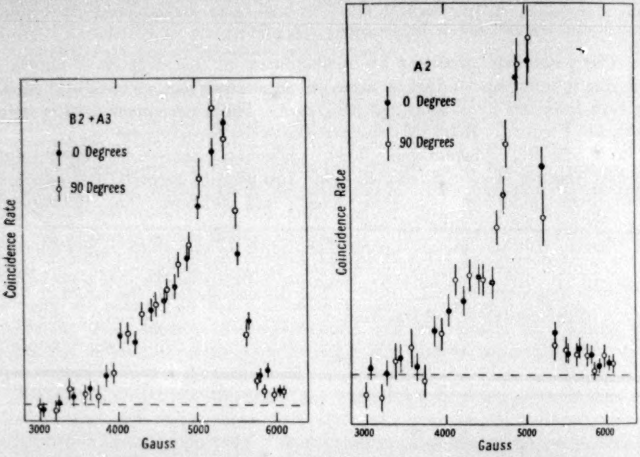

Figure 2 (*a*).

Figure 2 (*b*).

Experimental spectra.

Figure 3 shows the results of this calculation for a γ-spectrum consisting of a sharp line at 17·6 MeV. of unit intensity and a line of intensity proportional to K and width 2 MeV., and for a converter stopping power (Δ MeV.) corresponding to the thickness used in the experiments. The calculated curves indicate a better resolution than was actually obtained. This may be due to such factors as the neglect of scattering of electrons produced in the converter by the walls and baffles, and scattering in the converter itself.

The results are, however, sufficient to show that the intensity of the 14·8 MeV. component is approximately 0·5 of that of the 17·6 MeV. component, in agreement with previous results, and that the ratio of the two components does not change greatly with angle, probably by less than 20%.

§ 3. THEORETICAL

It can be seen at once that the above results are consistent with the interpretation of the resonance given by Devons and Hine. The assignment of the resonance to the proton S-wave results in isotropy of the γ-radiation irrespective of any further particularization of the symmetry properties of the resonance or lower states of ^{8}Be. The fact that the γ-radiation widths for the two components are of comparable magnitude suggests that the two transitions are of the same multipolarity, but this would be the case if either or both the lower states of ^{8}Be were $J=2, +$ or $J=0, +$, with the assignment $J=1, -$ for the resonance level.

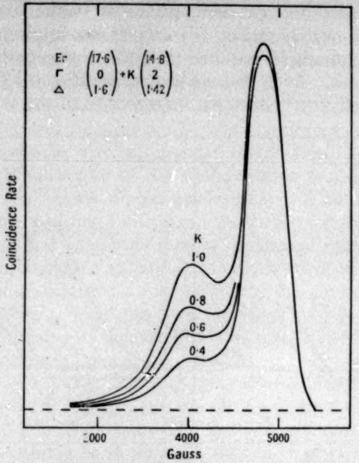

Figure 3. Calculated spectrum for pair A2.

The choice between $J=0$ and $J=2$ for the lower states must then depend on evidence other than the properties of the radiation at resonance (cf. Devons and Hine 1949, p. 79).

The evidence from the study of the proton elastic scattering indicates that the resonance is produced by the p-wave component. The ^{8}Be resonance level might then be a $J=0$, 1, 2, or 3, + state. $J=0$, 2, + are ruled out by the absence of α-particle competition, and $J=3$ is very unlikely in view of the large radiation width. Column 1 of the Table shows the angular distribution of both 17·6 and 14·8 Mev. components if it is assumed that both low states are $J=0, +$ (transition: magnetic dipole). It is possible to obtain isotropy for both components with

Angular Distribution of Radiation from a State $J=1, +$

R	Formation of ^{8}Be resonance level	$(J=1,+)\rightarrow(J=0,+)$	$(J=1,+)\rightarrow(J=2,+)$		
		(1) M.D. only	(2) E.Q. only	(3) M.D. only	(4) Mixed E.Q.+M.D.
∞	Triplet state only	+1·00	+0·430	+0·077	−0·275
0	Quintuplet state only	−0·143	−0·073	−0·017	−0·144
4	4×triplet+1×quintuplet	+0·703	+0·316	+0·058	−0·220

The angular distribution is in all cases of the form $1+\alpha\cos^2\theta$. The figures indicate the magnitude of α. M.D.=magnetic dipole; E.Q.=electric quadrupole.

this assignment $J=1, +$ to the resonance level and $J=0, +$ to both lower states, but this would require a relative contribution R from triplet and quintuplet 'spin states' in the formation of ^{8}Be of $\frac{1}{5}$ as opposed to 4 required to interpret the scattering data (Cohen 1949).

Columns 2, 3 show the calculated radiation distributions for the transition $J=1, + \rightarrow J=2, +$ taken as either pure magnetic dipole or pure electric quadrupole, with three different assumptions as to the formation of the ^{8}Be resonance state: (i) entirely triplet, (ii) entirely quintuplet and (iii) the ratio, $R=4$, of triplet and quintuplet required to explain the scattering data in terms of the p-wave component. As in the case of the transition $J=1, + \rightarrow J=0, +$, in this case also the radiation is isotropic, irrespective of the relative strengths of magnetic dipole and electric quadrupole, if we take $R=\frac{1}{5}$. (This value of R in fact corresponds to formation of the $J=1$ state of ^{8}Be with equal probability in its three sub-states $J_z=0, \pm 1$, and therefore gives isotropic radiation for any symmetry properties of the lower states of ^{8}Be.)

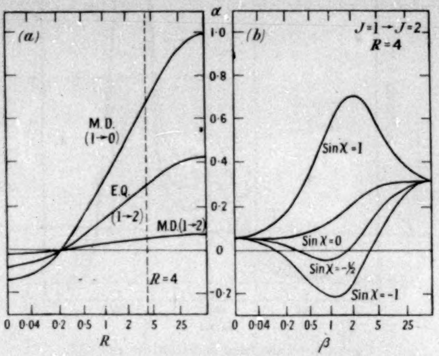

Figure 4. Theoretical angular distributions.

The general expressions for the angular distribution of the γ-radiation assuming p-wave resonance forming $J=1,+$ state are:

(*a*) for transition to $J=0, +$ states (magnetic dipole)

$$I(\theta) \propto 1+\cos^2\theta\,(5R-1)/(5R+7);$$

(*b*) for transitions to $J=2, +$ states (mixed electric quadrupole, magnetic dipole),

$$I(\theta) \propto 1+\cos^2\theta\,(5R-1)\,\frac{(4+45\beta\sin\chi+9\beta^2)}{(260R+268)+12\beta\sin\chi(1-5R)+3\beta^2(35R+41)}.$$

R (real, positive) represents relative contributions of triplet and quintuplet spin states, β (real, positive) the ratio of quadrupole to dipole amplitudes, and χ (real) the phase difference of the multipoles.

It may also be pointed out that the assumption $J=0, +$ or $J=2, +$ for the lower levels is compatible with the approximate equality of the radiation widths of the two γ-components since transitions to both of these lower levels may have similar multipolarities.

The variation of the predicted angular distributions with R is shown in Figure 4 (*a*).

If, however, we retain the value of $R=4$ indicated by the scattering experiment, we can only get isotropic radiation for both γ-components by assuming that *both* lower states of ^{8}Be are of the type 2, +, that both transitions are mixed dipole and quadrupole, and adjusting the relative amplitudes and phases of the components to give the desired isotropy. This is illustrated in Figure 4 (*b*), where the angular distribution is shown for the whole range of relative amplitudes and phase differences. It is possible in this way to obtain an interpretation of the resonance which is consistent with both the scattering data and the properties of the radiation at resonance. However, this is a rather artificial interpretation depending on the fortuitous values of four quantities (two amplitude ratios and two phase differences), and, in addition, leads to the rather implausible result that both lower states of ^{8}Be have $J=2$, even parity.*

An alternative interpretation, proposed by Christy, is that one of the lower states of ^{8}Be has $J=0$ and the other $J=2$. The transition to the $J=0$ state would then be magnetic dipole with an angular distribution $1+0{\cdot}7\cos^2\theta$, and the observed isotropy at resonance of the total radiation is achieved by taking the other transition to be mixed dipole–quadrupole with an angular distribution $1-\alpha\cos^2\theta$. Column 4 of the Table shows the largest values that α can take for any phase-difference and amplitude ratio of dipole and quadrupole. It is clear that isotropy of the combined radiation can only result if the weaker (14·8 Mev.) component has the distribution $1+0{\cdot}7\cos^2\theta$, i.e. the ground state of ^{8}Be must be identified with $J=2, +$ and the 3 Mev. state with $J=0, +$. If the ratio of 17·7 to 14·8 Mev. components measured at 0° is taken to be 2 : 1, then to get the observed overall isotropy a value of $\alpha=-0{\cdot}17$ is required, which is just within the permitted range (Figure 4 (*b*)). But with these assumptions the ratio of intensities of the 17·6 and 14·8 Mev. components should range with angle from 2 : 1 at 0° to 4·1 : 1 at 90°. The measurements described above almost certainly rule out a variation of this magnitude.

If, then, the value of R used to interpret the scattering data is adopted, one may conclude that assignment of the resonance to the p-wave component can only be made consistent with the properties of the γ-radiation at resonance if one also assumes both lower states of ^{8}Be to have $J=2$. If this value of R is not adopted, an interpretation consistent with a p-wave resonance can be obtained with any assignment of the values $J=0$, 2 to the lower levels. Finally, it should be remembered that in all the calculations the very plausible assumption has been made that the ^{7}Li nucleus has odd parity, and it seems unlikely that the converse assumption would substantially simplify the interpretation.

ACKNOWLEDGMENT

One of us (G. R. L.) is indebted to the Royal Commissioners for the Exhibition of 1851 for the award of an overseas scholarship. The experimental work was done in the Cavendish Laboratory.

REFERENCES

Christy, R. F., 1949, *Phys. Rev.*, **75**, 1464.
Cohen, E. R., 1949, *Phys. Rev.*, **75**, 1463.
Devons, S., and Hine, M. G. N., 1949, *Proc. Roy. Soc.* A, **199**, 56, 73.
Fowler, W. A., Lauritsen, C. C., and Rubin, S., 1949, *Phys. Rev.*, **75**, 1463.
Walker, R. L., and McDaniel, B. D., 1948, *Phys. Rev.*, **74**, 315.

---

* This interpretation may also conflict with the properties of the γ-radiation away from resonance. Detailed calculations have not been made to check this point.

The Density Distribution inside Nuclei and Nuclear Shell Structure

By W. J. SWIATECKI
Department of Mathematical Physics, University of Birmingham

Communicated by R. E. Peierls; MS. received 5th *April* 1950

ABSTRACT. A method of evaluating the density distribution of particles inside a heavy nucleus is described. The results are used to show that the electrostatic repulsion between protons is too weak to produce a nucleus sufficiently hollow to explain the observed ' closed shells ' at $N, Z = 50, 82$.

§ 1. INTRODUCTION

Due to the electrostatic repulsion between protons, the density near the centre of a nucleus is decreased. The question of the magnitude of this effect has lately become important in connection with the interpretation of closed shells in nuclei. It is known that one can go some way towards a theoretical explanation of the observed shells by assuming a ' wine-bottle potential ' instead of a conventional ' square well '* (Feenberg and Hammack 1949). The most obvious interpretation of such a potential is in terms of a decreased central density caused by the repulsion between protons. A method of calculating the proton and neutron densities will be developed and the results applied to test the above hypothesis.†

In the following calculations the nucleus is pictured as a drop of nuclear matter whose properties are described by an energy density $\epsilon(n_n, n_p)$, a function of the neutron and proton densities. Recognition of the quantum mechanical nature of nuclear matter is contained in the derivation of the form of $\epsilon(n_n, n_p)$. Apart from that, the derivation of the densities follows classical lines.

In §§ 2 and 3 the function $\epsilon(n_n, n_p)$ will be found from the empirical properties of nuclear matter as revealed by the binding energy formula and supplemented by calculations based on simplified models of the nucleus.

In § 4 $\epsilon(n_n, n_p)$ will be used to determine the densities $n_n(r)$ and $n_p(r)$ as functions of the distance from the centre, by minimizing the total energy with respect to the densities.

In the remaining sections the associated potential wells will be derived and the results applied to test the hypothesis of the wine-bottle potentials as used to explain the positions of closed shells in nuclei.

§ 2. NUCLEAR ENERGY DENSITY FUNCTION

The total energy density can be written as

$$\epsilon(n_n, n_p) = \epsilon_v(n_n, n_p) + \tfrac{1}{2} e v n_p, \qquad \ldots\ldots(1)$$

where ϵ_v = energy density due to specifically nuclear forces, v = electrostatic potential, en_p = charge density associated with the protons. Let us define a standard nucleus by $N=Z=A/2$ with electrostatic forces assumed absent. Let the densities be then $n_\mathrm{n}=n_\mathrm{p}=n_0$ and $\epsilon_v(n_0, n_0)=\epsilon_0$. For moderate density deviations we may approximate to ϵ_v by a quadratic,

---

* An alternative explanation has been proposed by Maria Goeppert-Mayer, *Phys. Rev.*, 1949, **75**, 1969, in terms of spin–orbit coupling. This model will not be discussed in the present paper.

† Calculations of neutron and proton densities exist (Feenberg 1941). The method which will be derived here is much simpler and gives the dependence on the parameters entering it in an explicit manner.

$$\epsilon_v(n_\mathrm{n}, n_\mathrm{p})=\epsilon_0+P\phi+\tfrac{1}{2}Q\phi^2+\tfrac{1}{2}S\psi^2, \qquad \ldots\ldots(2)$$

where $\phi=\frac{1}{2}(n_\mathrm{n}+n_\mathrm{p})-n_0=n-n_0$, $\psi=\frac{1}{2}(n_\mathrm{n}-n_\mathrm{p})$, and ϵ_0, P, Q, S are constants. P, S and ϵ_0 can be determined by comparing equation (2) with the empirical binding energy formula. We take it in the form given by Rosenfeld (1948, p. 24), which for the specifically nuclear part of the energy per particle gives

$$\left.\begin{aligned} &\bar{E}_v=\bar{E}_1\left[1-\gamma\left(\frac{N-Z}{A}\right)^2\right], \\ \text{where}\qquad &\bar{E}_1=-14{\cdot}66\ \text{MeV.};\ \gamma=1{\cdot}40. \end{aligned}\right\} \qquad \ldots\ldots(3)$$

In order to find P and ϵ_0 consider the energy per particle of a standard nucleus as a function of the average density

$$\bar{E}_v(n)=\frac{\epsilon_v(n)}{2n}=\epsilon_0/2n+P(n-n_0)/2n+Q(n-n_0)^2/4n. \qquad \ldots\ldots(4)$$

Now $(\bar{E}_v)_{n=n_0}=\bar{E}_1$, and $(\partial\bar{E}_v/\partial n)_{n=n_0}=0$ for equibrium. Hence

$$\epsilon_0=n_0P=2n_0\bar{E}_1\,. \qquad \ldots\ldots(4a)$$

To find S consider the energy per particle of a nucleus taken at $n=n_0$ and considered as a function of N and Z. Replacing n_n and n_p by their average values $2Nn_0/A$ and $2Zn_0/A$ respectively, we obtain from equation (2)

$$\bar{E}_v(N, Z)=\epsilon_0/2n_0+\tfrac{1}{4}Sn_0\left(\frac{N-Z}{A}\right)^2.$$

Comparing with equation (3) it follows that

$$S=-4\gamma\bar{E}_1/n_0. \qquad \ldots\ldots(4b)$$

The constant Q is related to the compressibility of nuclei and cannot be determined from the binding energy formula which refers to nuclei at nearly constant density. We shall therefore have recourse to a semi-empirical calculation.

§ 3. COMPRESSIBILITY FROM THE STATISTICAL MODEL

The compressibility coefficient E_v'' is usually defined as $R^2(\partial^2E_v/\partial R^2)$ taken at the equilibrium radius, E_v being the total energy of a standard nucleus. From equations (4) and (4*a*) $E_v=\frac{1}{2}P+\frac{1}{4}Q(n-n_0)^2/n$. Remembering that $4\pi R^3n/3=\frac{1}{2}A$, it follows on differentiation that $Q=(16\pi R_0^3/27A)E_v''$, where $R=R_0A^{1/3}$, $R_0=1{\cdot}42\times10^{-13}$ cm.

Existing estimates of E_v'' (see for instance Feenberg 1947) indicate values around $50-100\,A$ MeV. As this parameter is of importance in what follows we shall give some independent calculations of its value.

We assume a statistical model of the nucleus. For definiteness we first take a symmetrical type interaction between particles with a Gaussian distance dependence $J(r_{12})=C\exp(-r_{12}^2/a^2)$. The energy per particle can then be written explicitly as a function of the density. For a standard nucleus the first approxi- gives, as is well known,

$$\overline{E}_v = \frac{\hbar^2}{Ma^2}\left[\frac{3}{10}\kappa^2 - 0{\cdot}685\, bf(\kappa)\right], \qquad \ldots\ldots(5)$$

where M = nucleon mass, $b = \dfrac{C}{\hbar^2/Ma^2}$,

$$\kappa = \frac{3}{2}\left(\frac{\pi}{3}\right)^{1/3}\frac{a}{R_0} = (3\pi^2)^{1/3} a n^{1/3},$$

$$f(\kappa) = e^{-\kappa^2}\left(\frac{1}{\kappa} - \frac{2}{\kappa^3}\right) - \frac{3}{\kappa} + \frac{2}{\kappa^3} + \sqrt{\pi}\,\mathrm{erf}\,\kappa.$$

The parameters a and C are now chosen so that the minimum of $\overline{E}_v(\kappa)$ occurs at the observed density and the value of $(\overline{E}_v)_{\min}$ is the observed $-14{\cdot}66$ MeV. This gives $a = 2{\cdot}647 \times 10^{-13}$ cm., $C = 52{\cdot}60$ MeV., and, therefore,

$$\overline{E}_v(\kappa) = 1{\cdot}771\,\kappa^2 - 36{\cdot}03\, f(\kappa) \text{ MeV.} \qquad \ldots\ldots(6)$$

and

$$E_v'' = \frac{9\pi}{8}\left(\frac{a}{R_0}\right)^3 \frac{A}{\kappa_0}\left(\frac{d^2\overline{E}_v}{d\kappa^2}\right)_{\kappa_0} = 67{\cdot}2\,A \text{ MeV.},$$

where κ_0 is the value of κ at equilibrium.

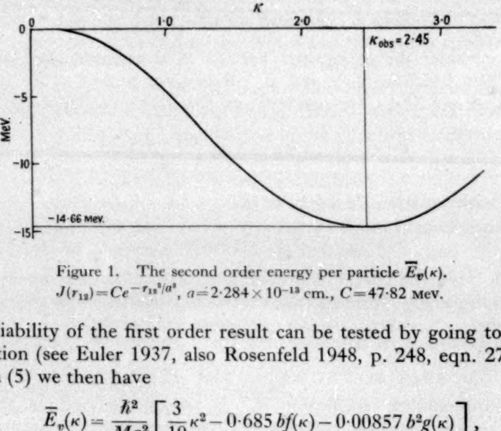

Figure 1. The second order energy per particle $\overline{E}_v(\kappa)$.
$J(r_{12}) = Ce^{-r_{12}^2/a^2}$, $a = 2{\cdot}284 \times 10^{-13}$ cm., $C = 47{\cdot}82$ MeV.

The reliability of the first order result can be tested by going to the second approximation (see Euler 1937, also Rosenfeld 1948, p. 248, eqn. 27). Instead of equation (5) we then have

$$\overline{E}_v(\kappa) = \frac{\hbar^2}{Ma^2}\left[\frac{3}{10}\kappa^2 - 0{\cdot}685\, bf(\kappa) - 0{\cdot}00857\, b^2 g(\kappa)\right],$$

where $g(\kappa) \simeq 10(1 - \log 2) - \dfrac{5}{2\kappa^2} + \dfrac{1}{2\kappa^4} + \dfrac{0{\cdot}16}{\kappa^6}$ for $\kappa > 1$ (a small second order exchange term $\sim 1\%$ has been omitted).

The parameters a and C are again adjusted to give the observed density and binding energy. The result is $a = 2{\cdot}284 \times 10^{-13}$ cm., $C = 47{\cdot}82$ MeV., and

$$\overline{E}_v(\kappa) = 2{\cdot}381\,\kappa^2 - 32{\cdot}75\, f(\kappa) - 2{\cdot}469\, g(\kappa),$$

$$E_v'' = 60{\cdot}62 A \text{ MeV.} \quad \text{(See Figure 1.)}$$

It is thus seen that E_v'' is not sensitive to the order of approximation provided a and C are adjusted at each stage. This is satisfactory, for it removes part of the uncertainty attached to the use of the statistical model which, for binding energy calculations, is quite inadequate. Thus with a and C derived from data on light nuclei, $1{\cdot}9 \times 10^{-13}$ cm. and 43·7 MEV. respectively, the first approximation gives 13% and the second 38% of the observed binding energy.*

In order to see how sensitive E_v'' is to the type of distance dependence $J(r_{12})$ assumed, the calculation was repeated with a meson interaction $J(r_{12}) = [Ca \exp(-r_{12}/a)]/r_{12}$.

The first approximation gives

$$E_v(\kappa) = \frac{\hbar^2}{Ma^2}\left[\frac{3}{10}\kappa^2 - 0{\cdot}676\, bf(\kappa)\right],$$

where $f(\kappa) = \dfrac{3}{4\sqrt{\pi}}\left\{2\left[\dfrac{1}{2\kappa} + \dfrac{1}{3(2\kappa)^3}\right]\log[1+(2\kappa)^2] + \left(2\kappa - \dfrac{1}{3\kappa}\right) - \dfrac{8}{3}\tan^{-1} 2\kappa\right\}$.

The attempt to fit a and C in the usual way gave a surprising result, namely that the form of $f(\kappa)$ is such that there is no choice of a and C which will give the right binding and density simultaneously. Going to the second approximation (see Huby 1949) does not improve the situation.† (Were it not for the inherent inadequacy of the statistical treatment this result would be important in disproving certain kinds of nuclear interactions.)

Naturally this suggests that the value of E_v'' will depend sensitively on the $J(r_{12})$ assumed. Thus, although we shall eventually adopt the value $E_v'' = 60{\cdot}62A$ MEV. for the compressibility coefficient, it must be understood that the reliability of this figure is unknown. We shall make our final conclusions independent of this figure and rely on a lower limit for E_v'' which is imposed by the empirical fact that average nuclear densities are, after all, approximately constant.

Subject to this uncertainty, the coefficients in equation (2) are

$$\left.\begin{aligned} \frac{\epsilon_0}{n_0} &= P = -29{\cdot}32\,\text{MEV.} && \pm\ 5\%, \\ S &= 87{\cdot}81\, r_0^3\,\text{MEV.} && \pm 10\%, \\ Q &= 14{\cdot}41\, r_0^3\,\text{MEV.} && \pm\ ? \end{aligned}\right\} \qquad \ldots\ldots(7)$$

where $r_0 = \mathbf{e}^2/\boldsymbol{mc}^2$ = classical electron radius.

§ 4. DENSITY DISTRIBUTION INSIDE A NUCLEUS

We ask the following question: If nuclear matter whose properties are described by equation (2) is confined in a sphere of radius R, how does the particle density adjust itself under the influence of the electrostatic forces? The solution is given by the functions $n_n(r)$, $n_p(r)$, which satisfy the variational equation

$$\delta \int \epsilon(n_n, n_p)\,d\tau = 0, \qquad \ldots\ldots(8)$$

---

* It is interesting to note that a guess at E_v'' can be made without the use of any nuclear model. Thus whatever the form of $\bar{E}_v(\kappa)$ we know it must have a minimum at $\kappa = \kappa_{\text{obs}}$, $\bar{E}_v = (\bar{E}_v)_{\text{obs}}$. Also it must pass through the origin. Fitting a parabola to these conditions, we obtain at once $E_v'' = -2(\bar{E}_v)_{\text{obs}} A = 29{\cdot}3A$ MEV. This is in effect a slightly refined dimensional argument.

† The author is indebted to Mr. Huby for a table of the second order function required for these calculations.

where the integration is carried out over the volume of the nucleus and δ implies small variations in n_n and n_p. The total number of particles

$$\int (n_n + n_p)d\tau = A$$

is kept constant.

Using the variables ϕ and ψ and Lagrange's variation procedure we can write equation (1) as

$$\delta \int [\epsilon_0 + P\phi + \tfrac{1}{2}Q\phi^2 + \tfrac{1}{2}S\psi^2 + k\phi + \tfrac{1}{2}ev(\phi - \psi + n_0)]d\tau, \quad \ldots\ldots\ldots(8\,a)$$

where k is a constant and the variations $\delta\phi$, $\delta\psi$ are arbitrary.

Remembering that from electrostatics

$$\delta \int \tfrac{1}{2}evn_p d\tau = \int ev\delta n_p d\tau \quad \text{and} \quad \nabla^2 v = -4\pi e n_p,$$

and taking independent variations $\delta\phi$ and $\delta\psi$, we easily obtain from equation (8 *a*) the equations

$$P + Q\phi + k + ev = 0, \quad \ldots\ldots(9\,a)$$

$$S\psi - ev = 0, \quad \ldots\ldots(9\,b)$$

$$\nabla^2 v = -4\pi e(\phi - \psi + n_0). \quad \ldots\ldots(9\,c)$$

Substituting for ϕ and ψ from (9 *a*) and (9 *b*), (9 *c*) becomes a simple second order differential equation for v. Together with k there are three arbitrary constants in the solutions, which are determined from the conditions: (i) v finite at the centre, (ii) $v(R) = e\int n_p\, d\tau_1/R$, (iii) $\int(n_n + n_p)d\tau = A$.

Having found $v(r)$, we substitute in (9 *a*) and (9 *b*) to find the densities. The final solution is

$$\left.\begin{aligned} ev(r) &= \frac{QS}{Q+S}n_p(0)\left\{\cosh\omega R - \frac{\sinh\omega r}{\omega r}\right\}, \\ n_p(r) &= n_p(0)\frac{\sinh\omega r}{\omega r}, \\ n_n(r) &= n_p(0)\left\{\frac{S-Q}{S+Q}\,\frac{\sinh\omega r}{\omega r} + \frac{2Q}{Q+S}\cosh\omega R\right\}, \end{aligned}\right\} \quad \ldots\ldots(10)$$

where

$$n_p(0) = \frac{n_0(1 + S/Q)\operatorname{sech}\omega R}{1 + 3S(\omega R - \tanh\omega R)/Q(\omega R)^3},$$

$$\omega = \left(\frac{4\pi e^2(Q+S)}{QS}\right)^{1/2}, \quad R = R_0 A^{1/3}, \quad n_0 = \frac{3}{8\pi R_0^3}.$$

With S and Q given by equation (7) the density distributions are plotted in Figure 2 for the three cases $A = 40, 100, 240$.

As expected, the size of the central depression grows with increasing A. The neutron distribution is found to follow the protons, but in an attenuated degree. The shape of the depression is seen to be rather flat; there is no sudden drop of density near the centre. The densities in Figure 2, however, drop abruptly to zero at the edge of the nucleus. This is due to the absence of any surface terms in equation (1). For this reason the graphs given are still rather bad representations of the true nuclear density function, which would have no sharp corners. A refinement of the method to take into account surface effects is given in §7.

To study the effect of the compressibility on the non-uniformity in density we define a factor k_p by

$$k_p = \frac{\text{mean proton density in the region } \frac{1}{2}R<r<R}{\text{mean proton density in the region } 0<r<\frac{1}{2}R},$$

and similarly for the neutrons.

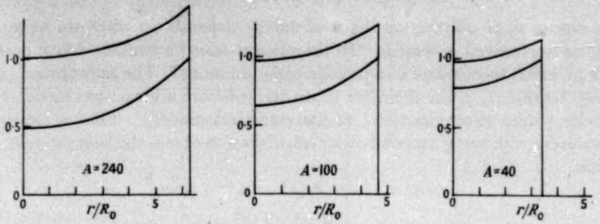

Figure 2. Neutron and proton densities without surface energy. The functions plotted are $\frac{n_n}{n_0}$ (upper curve) and $\frac{n_p}{n_0}$ (lower curve). $n_0 = \frac{3}{8\pi R_0^3}$, $R_0 = 1{\cdot}42\times10^{-13}$ cm., $Q = 14{\cdot}41 r_0^3$ MeV., $S = 87{\cdot}81\, r_0^3$ MeV.

Table 1 gives k_p and k_n as functions of Q for $A = 240$. It is seen that at the estimated $Q = 14{\cdot}41\, r_0^3$ MeV., $k_p = 1{\cdot}48$ and $k_n = 1{\cdot}18$.

Table 1

Q/r_0^3 (MeV.)	5	10	15	20	25	30
k_p	2·35	1·68	1·46	1·35	1·30	1·25
k_n	1·52	1·27	1·17	1·12	1·09	1·07
$\Delta R/R$ (%)	17·1	8·6	5·7	4·3	3·4	2·9

So far we have been varying the densities inside a fixed spherical boundary. In fact the nucleus would expand as a whole under the action of the electrostatic repulsion. The minimization with respect to R could easily be included in the variation calculation, but as far as the shape of the density function is concerned the results would not be materially affected. The magnitude of the expansion of the nucleus (in the absence of surface energy) is easily found. The relative change in radius turns out to be $\Delta R/R = E_c/E_v''$, where E_c is the electrostatic energy.

Taking E_c as $3Z^2e^2/5R^2$, we obtain

$$\frac{\Delta R}{R} = \frac{16\pi}{45}\frac{Z^2e^2}{A^{4/3}}\frac{R_0^3 r_0}{Q}.$$

The percentage change in R is given as a function of Q in Table 1. For values of Q of the order of or less than $10 r_0^3$ MeV. the change is greater than 10%. Assuming that changes of much more than 10% would show up as departures from the $A^{1/3}$ law of nuclear radii, we may place a lower limit on Q at between 5 and $10 r_0^3$ MeV. The approximation that the density deviations from n_0 are small also ceases to hold for $Q \lesssim 10\, r_0^3$ MeV. in the case of large A. For these cases the calculated densities have a comparative significance only.

§5. EFFECTIVE NUCLEAR POTENTIALS

The densities derived in the previous sections enable us to calculate the effective one-particle potential wells for neutrons and protons. In order to do this we must split the total energy density into a potential energy density w and a kinetic energy density t :

$$\epsilon_v(n_{\rm n}, n_{\rm p}) = w(n_{\rm n}, n_{\rm p}) + t_{\rm n} + t_{\rm p} + \tfrac{1}{2} evn_{\rm p}.$$

The exact way of splitting up the total energy depends on what use we want to make of the derived potentials. In the present case we wish to derive potential wells in which to calculate one-particle eigenfunctions. The appropriate kinetic energy densities $t_{\rm n}$, $t_{\rm p}$ are therefore those derived from a Fermi-gas model of free particles (' zero approximation ' of the statistical model). This is clearly not inconsistent with using a second order calculation to obtain the best estimate of Q. Hence

$$w(n_{\rm n}, n_{\rm p}) = \epsilon_v - \theta n_{\rm n}{}^{5/3} - \theta n_{\rm p}{}^{5/3} + \tfrac{1}{2} evn_{\rm p},$$

where

$$\theta = \frac{h^2}{M}\frac{3}{40}\left(\frac{3}{\pi}\right)^{2/3}.$$

The effective neutron well is now found by imagining a neutron added to the nucleus and calculating the change in the potential energy density. The effective potential well is therefore

$$U_{\rm n} = \frac{\partial w}{\partial n_{\rm n}} = \frac{\partial \epsilon_v}{\partial n_{\rm n}} - \frac{5}{3}\theta n_{\rm n}{}^{2/3}.$$

Now $\partial\epsilon_v/\partial n_{\rm n}$ = constant, from the minimization equation (8). (For protons it is best to calculate the contribution to the well from nuclear interactions first and then to add the electrostatic potential as given by equation (10).) It turns out that the wells for neutrons and protons, including electrostatic interaction, are

$$U_{\rm n} = B - \frac{5}{3}\theta n_{\rm n}{}^{2/3}, \quad U_{\rm p} = B - \frac{5}{3}\theta n_{\rm p}{}^{2/3}, \qquad \ldots\ldots(11)$$

with the same constant B. (Since $\frac{5}{3}\theta n^{2/3}$ is the kinetic energy of the most energetic particle in a Fermi-gas, the meaning of this is that the highest occupied eigenvalue for the neutrons in $U_{\rm n}$ is at approximately the same energy as that for the protons in $U_{\rm p}$.) The potentials given by equation (11) are plotted in Figure 3 for $A = 240$.

§6. APPLICATION TO THE DETERMINATION OF CLOSED SHELLS

As was mentioned at the beginning, the central elevation in the potential well can be made to account qualitatively for some of the observed closed shells. We shall now apply the results of § 5 to test the explanation of closed shells in terms of a wine-bottle potential.

Well-pronounced shells are known to occur at N or $Z = 2, 4, 8, 20, 50, 82$. The shells up to 20 are easily accounted for. The shell at 50 can be explained by assuming that by the time the 5g shell is full, the 2s, 3p, 4d family of levels has been pushed up and crossed it, and that in fact the lowest of these levels is already far enough above the 5g level to make the closing of the latter a pronounced event. To account for the shell at 82, Feenberg assumes that the order of the 2s, 3p, 4d levels is inverted to 4d, 3p, 2s, so that by the time the number 82 is reached the 4d and 6h levels have become filled and the 3p and 2s levels have moved up sufficiently high to make this a noticeable event.

It is easily shown that an inversion of levels within a family cannot be produced by a central elevation of any size, and so a wine-bottle potential by itself is in any case inadequate to explain all the shells. We shall now show that even the shell

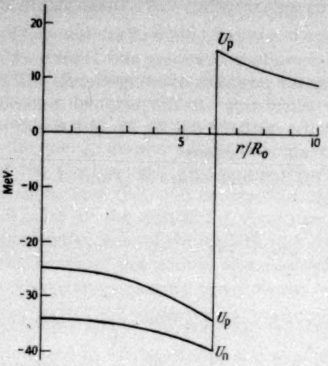

Figure 3. Equivalent one-particle potential wells for neutrons and protons.

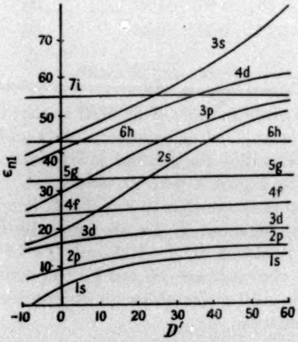

Figure 4. Behaviour of energy levels with increase of potential elevation D' in well of infinite depth and radius R. The elevation covers the range $0<r<\frac{1}{2}R$. ϵ_{nl} and D' in units $\hbar^2/MR^2$. (*Reproduced from* Feenberg and Hammack 1949.)

at 50 cannot be attributed to a wine-bottle potential caused by the electrostatic repulsion.

In order to achieve this we must estimate the positions of one-particle eigenvalues in the potentials of § 5. The inaccuracies in those potentials (especially near the edge of the nucleus) would make exact eigenvalue calculations futile. In any case we only wish to test the hypothesis that the electrostatic repulsion would lead to closed shells as revealed by experiment, and for this purpose a rough upper limit on the relative shift of the 2s, 3p, 4d family of levels is sufficient. A very crude approximation turns out to be adequate.

We replace the calculated potential by a square well of infinite depth with a suitably defined central elevation $\overline{\Delta U}$ in the region $0<r<\frac{1}{2}R$:

$$\overline{\Delta U} = \text{mean depth of well in } \tfrac{1}{2}R<r<R - \text{mean depth of well in } 0<r<\tfrac{1}{2}R.$$

The positions of energy levels in such a well are known (Feenberg and Hammack 1949, Figure 2). We reproduce Feenberg and Hammack's diagram in Figure 4. This way of estimating the positions of energy levels will certainly not reproduce an exact eigenvalue calculation in the original potential, but the order of magnitude of the relative shift of the 2s, 3p, 4d family of levels will be given correctly, and this is all we require.

Table 2 gives $\overline{\Delta U}$ for different values of Q and A.

Table 2

Q/r_0^3 (Mev.)	A	240	100	40	A	240	100	40
5	$\overline{\Delta U}_p$ (Mev.)	9·80	6·92	4·34	D_p'	18·44	13·02	8·17
	$\overline{\Delta U}_n$ (Mev.)	7·34	5·57	3·66	D_n'	13·81	10·47	6·89
14·41	$\overline{\Delta U}_p$ (Mev.)	4·79	3·10	1·85	D_p'	9·01	5·84	3·48
	$\overline{\Delta U}_n$ (Mev.)	2·92	2·02	1·25	D_n'	5·48	3·80	2·36
30	$\overline{\Delta U}_p$ (Mev.)	2·88	1·81	1·05	D_p'	5·41	3·40	1·98
	$\overline{\Delta U}_n$ (Mev.)	1·20	0·81	0·49	D_n'	2·26	1·53	0·93

$$D' = \overline{\Delta U}/(\hbar^2/MR^2).$$

The elevations are also given in units of $\hbar^2/MR^2$ so that they can be used directly in conjunction with Figure 4. For example, for $Q = 14{\cdot}41\, r_0^3$ Mev. and $A = 100$ the effective potential elevation for protons is 3·10 Mev. and the order of proton energy levels is given by Figure 4 with $D' = 5{\cdot}84$.

Inspection of Figure 4 shows that to put the 2s level well above the 5g level at N or $Z \sim 50$, D' has to be about 35, i.e. six times the D' calculated for protons or 9·2 times that for neutrons at $A = 100$ and $Q = 14{\cdot}41\, r_0^3$ Mev. Taking the extreme, $Q = 5\, r_0^3$ Mev., the ratios are 2·6 and 3·3 respectively.

This shows that the shell at 50, although qualitatively possible, is disproved by a quantitative calculation.

§7. POSSIBLE SOURCES OF ERROR

A disproof of Feenberg's hypothesis is of some importance regarding our ideas on nuclear structure, and so it is essential to examine the reliability of the above conclusions. The two most important errors committed in deriving the densities are that (*a*) we have neglected surface terms, and (*b*) for large A and small Q the density deviations cannot be regarded as small. We shall examine these errors in turn.

(*a*) The surface energy in a nucleus is usually considered as consisting of two parts : the kinetic surface energy and the potential surface energy. The former is a pure quantum-mechanical effect due to the fact that in a region where the density varies rapidly the wave functions have Fourier components of high frequency and consequently high kinetic energy. The potential surface energy is analogous to the classical surface energy. Particles near a surface are attracted on one side only and are therefore less strongly bound. Both effects will in general lead to an increase of energy. For not too large density gradients one might attempt to expand the additional energy density in a series whose leading term is a function of n and grad n only. We assume as an illustration an additional energy density in the very simple form $\epsilon_s = 2\sigma(\mathrm{grad}\, n)^2$, where σ is a constant.

We do not wish to give the impression that this form of ϵ_s has any serious theoretical basis. Taking σ as independent of n is certainly wrong; using $(\mathrm{grad}\ n)^2$ for small gradients may be right or wrong. We can however expect that a surface term in the energy density which will remove the sudden drop in density at the edge of the nucleus will also oppose the formation of density gradients inside the nucleus, and this will be true for the expression chosen. Let us see what type of solution the assumed ϵ_s gives rise to, without attaching much weight to the quantitative side of the results.

In what follows, the neutron and proton densities will be taken as equal, $n_n = n_p = n$, so that the total energy density is written as

$$\epsilon(n_n, n_p) = Pn + \tfrac{1}{2}Q(n - n_0)^2 + \tfrac{1}{2}evn_p + 2\sigma(\mathrm{grad}\, n)^2. \qquad \ldots\ldots(12)$$

The variation calculation can again be carried out explicitly, giving a density distribution $n(r)$ which is plotted in Figure 5 for three different values of A.

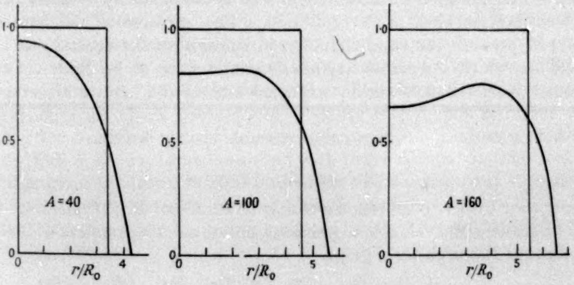

Figure 5. Average nuclear density $\dfrac{n}{n_0}$ with surface energy. $Q = 10{\cdot}2\, r_0{}^3$ Mev., $\sigma = 1{\cdot}013\, r_0{}^5$ Mev.

The value of σ was chosen so as to make the total energy increase due to ϵ_s of the order of magnitude of the observed surface energy. The qualitative behaviour of the density is as expected. For small A the nucleus consists entirely of a 'surface'. For medium A a constant density region develops, and for large A a central depression appears. It will be seen that the effect of the surface term on the central depression is, in this instance at least, very considerable. In how far this is due to the particular form of ϵ_s chosen remains uncertain.*

* It will be noted that the nucleus has, on this model, a well-defined radius. No importance should, however, be attached to $n(r)$ in this region. For small densities an equation of the type (12) can have no physical meaning. The model defined by equation (12) may become useful as a starting point for more accurate treatments. Its solution being elementary, moderate deviations arising from more adequate expressions for ϵ could, in principle, be treated as correction terms.

(*b*) The most important consequence of large deviations of n from n_0 is the inadequacy of a quadratic form for $\epsilon(n_n, n_p)$. In particular an inspection of Figure 1 tells us that for regions where the density is small, a smaller effective value of Q would be appropriate. This would result in a further density decrease in those regions. The theoretical possibility exists that an unstable point would be reached at which the density in the central region would drop to zero even though Q remained moderate over the remaining part of the nucleus. This possibility would be very difficult to treat quantitatively were it not for the fact that in this case we can regard the nucleus as a hollow shell so that the energy of the central region is describable by a surface energy, for which we have adequate experimental information. The sudden formation of a hollow centre is an effect which would take place even for an incompressible nucleus, and is in fact most easily studied in that case. Assuming an energy η per unit area, an elementary calculation shows that a hollow centre would form when the ratio Z^2/A exceeded the value $92{\cdot}7\ R_0^3\eta/e^2$. Now the critical value for spontaneous fission depends on the same combination of R_0, η and e, and is in fact $10(4\pi/3)R_0^3\eta/e^2$ (Bohr and Wheeler 1939), which is about one half of the previous figure. We conclude that, independently of the surface energy assumed, a nucleus would disintegrate well before the possibility of a hollow centre arose. The above two ratios are calculated on the assumption of an incompressible nucleus. There is no reason to believe that the relative magnitude would be materially affected if a reasonable compressibility were included.

The conclusion with regard to the hypothesis of a wine-bottle potential is that the central elevation in the potential well is too small by a factor of 5–10 to account for the shell at N or $Z=50$. The explanation of the shell at N or $Z=82$ presents the same difficulty, in addition to the necessity of a level inversion for which a separate hypothesis would have to be made. Further, quite apart from the theoretically expected size of the central elevation, the density reduction required to produce the observed shells corresponds to an almost hollow nucleus, a configuration unstable against fission.

ACKNOWLEDGMENTS

The author wishes to express his thanks to Professor R. E. Peierls for many helpful discussions and valuable suggestions, and to the Department of Scientific and Industrial Research for a grant.

REFERENCES

Bohr, N., and Wheeler, J., 1939, *Phys. Rev.*, **56**, 426.
Euler, H., 1937, *Z. Phys.*, **105**, 553.
Feenberg, E., 1941, *Phys. Rev.*, **59**, 593; 1947, *Rev. Mod. Phys.*, **19**, 239.
Feenberg, E., and Hammack, K. C., 1949, *Phys. Rev.*, **75**, 1877.
Huby, R., 1949, *Proc. Phys. Soc.* A, **62**, 62.
Rosenfeld, L., 1948, *Nuclear Forces* (Amsterdam : North-Holland Publishing Co.).

Spin Orbit Coupling in the Nuclear Shell Model

By J. HUGHES and K. J. Le COUTEUR
Department of Theoretical Physics, The University, Liverpool

Communicated by H. Fröhlich; MS. received 11th July 1950

ABSTRACT. It is shown that the magnitude of the doublet splitting postulated in Mayer's nuclear shell model is consistent with that observed in ^{5}He. The strength of the indicated spin orbital interaction between pairs of nucleons is worked out.

The occurrence of nuclear systems of particular stability and abundance has been interpreted as indicating the formation of closed shells of nucleons (Mayer 1948). The nucleus is treated, to a first approximation, as though each individual nucleon was moving in an average potential due to the other nucleons. Occupation numbers of levels in models, in which this potential is approximated by a spherically symmetrical well, do not provide the empirical ordering without level rearrangements (Feenberg and Hammack 1949, Nordheim 1949). A model has been proposed, in which the energetic order of the single particle orbits is that of a square well with strong spin orbit coupling giving rise to inverted doublets, which gives the empirical order directly (Mayer 1949). The theoretical basis of the spin orbit coupling is uncertain, for a simple calculation shows that the Thomas spin orbit coupling, which arises (cf. Rosenfeld 1948, § 15.22) as a relativistic correction to the motion of a particle in a central potential well, is too small by an order of magnitude to account for the observed doublet splitting. However, the vector theory of nuclear forces leads to a spin orbit coupling of the required form (Gaus 1949, Rosenfeld 1948, § 17.43). In the following the magnitude of the doublet splitting in heavy nuclei postulated by Mayer (1949) is shown to be consistent with that observed* in ^{5}He, both being derived from an additional nuclear interaction which is treated as a perturbation of the main effective potential well for a single particle.

Of the spin-dependent nuclear interactions listed by Rosenfeld (1948, § 15.22), only the interaction

$$M^{(12)} = -f(r_{12})\,(\boldsymbol{\sigma}^{(1)}+\boldsymbol{\sigma}^{(2)}).(\mathbf{r}^{(1)}-\mathbf{r}^{(2)})_{\wedge}(\mathbf{p}^{(1)}-\mathbf{p}^{(2)})/\hbar \qquad \ldots\ldots(1)$$

between nucleon (1) and nucleon (2) can, in first approximation, lead to the required spin orbit coupling. Here $r_{12}=|\mathbf{r}^{(1)}-\mathbf{r}^{(2)}|$ and $f(r_{12})$ describes the distance dependence and the strength of the potential.

If the nucleon (1) is outside a saturated core of nucleons (2) it experiences the resultant of the individual interactions $M^{(12)}$; this reduces to

$$\sum^{2} M^{(12)} = -\sum^{2} f(r_{12})\,\boldsymbol{\sigma}^{(1)}.(\mathbf{r}^{(1)}-\mathbf{r}^{(2)})_{\wedge}\mathbf{p}^{(1)}/\hbar \qquad \ldots\ldots(2)$$

since the other terms vanish as the core has no resultant spin or momentum. By writing

$$\sum^{2} f(r_{12})\,(\mathbf{r}^{(1)}-\mathbf{r}^{(2)}) = F(r_1)\mathbf{r}^{(1)}, \qquad \ldots\ldots(3)$$

---

* The evidence is not quite conclusive, see Rosenfeld 1948, § 17.42.

which is permissible since by symmetry the left-hand side must reduce to a vector in the direction $\mathbf{r}_1^{(1)}$, the resultant (2) is reduced to the form

$$\sum^{2} M^{(12)} = -F(r_1)\,\boldsymbol{\sigma}^{(1)}\,.\,\mathbf{r}^{(1)}{}_{\wedge}\mathbf{p}^{(1)}/\hbar = -F(r_1)\,\boldsymbol{\sigma}^{(1)}\,.\,\mathbf{L}^{(1)} \qquad \ldots\ldots(4)$$

representing the spin orbit interaction for the motion of (1) in the independent particle approximation. Equation (3) gives

$$\begin{aligned} F(r_1) &= \frac{1}{r_1{}^2}\sum^{2} f(r_{12})\,(\mathbf{r}^{(1)}-\mathbf{r}^{(2)})\,.\,\mathbf{r}^{(1)} \\ &= \frac{1}{r_1}\sum^{2} f(r_{12})\,r_{12}\,\frac{\partial r_{12}}{\partial r_1}\,. \qquad \ldots\ldots(5) \end{aligned}$$

To obtain definite results a form for $f(r_{12})$ which does not require a cut-off must be chosen. The most convenient choice is

$$f(r_{12}) = g\hbar c\,\frac{\exp(-\chi r_{12})}{r_{12}}\,, \qquad \ldots\ldots(6)$$

where g is a dimensionless coupling constant. This could, for example, arise from a form of meson theory recently proposed (Bhabha 1950). Then

$$\begin{aligned} F(r_1) &= \frac{g\hbar c}{r_1}\sum^{2}\exp(-\chi r_{12})\,\frac{\partial r_{12}}{\partial r_1} = -\frac{g\hbar c}{\chi r_1}\frac{\partial}{\partial r_1}\sum^{2}\exp(-\chi r_{12}) \\ &= \frac{g\hbar c}{\chi r_1}\frac{\partial}{\partial r_1}\frac{\partial}{\partial \chi}\,G(r_1,\chi), \qquad \ldots\ldots(7) \end{aligned}$$

where $$G = \sum^{2}\frac{\exp(-\chi r_{12})}{r_{12}}\,.$$

To perform this summation, the A core nucleons (2) are considered to be uniformly distributed throughout a sphere of radius a equal to the nuclear radius. Then by elementary integration one gets

$$G(r_1,\chi) = \frac{3A}{2a^3\chi^3}\left\{\begin{array}{ll} [e^{\chi a}(\chi a-1)+e^{-\chi a}(\chi a+1)]\{\exp(-\chi r_1)\}/r_1 & \text{for } r_1 > a \\ {[2\chi - e^{-\chi a}(\chi a+1)\{\exp(\chi r_1)-\exp(-\chi r_1)\}/r_1]} & \text{for } r_1 < a. \end{array}\right\} \qquad \ldots\ldots(8)$$

In heavy nuclei the last particle may be supposed to occupy an orbit of high angular momentum concentrated near the surface of the nucleus. Thus in this case it is sufficient to evaluate $F(r_1)$ for $r_1 = a$, and the result is

$$F(a) = g\hbar c\chi\left(\frac{3A}{2\chi^3a^3}\right)\{(\chi a)^{-1} - 3(\chi a)^{-3} + e^{-2\chi a}[2 + 5(\chi a)^{-1} + 6(\chi a)^{-2} + 3(\chi a)^{-3}]\}. \qquad \ldots\ldots(9)$$

The values of $F(a)/g\hbar c\chi$ plotted in the Figure assume $A^{-1/3}a = 1{\cdot}42 \times 10^{-13}$ cm. and $\chi^{-1} = 1{\cdot}5 \times 10^{-13}$ cm., which corresponds to a meson of 260 electron masses ; thus $3A/(2\chi^3a^3) = 1{\cdot}75$.

The case of ^{5}He is of special interest as, if the third neutron is assumed to occupy a p state in the field of an α-particle as core, the effects of the spin orbit coupling $M^{(12)}$ appear very directly without admixture of other effects. The level is virtual, so the neutron wave function extends far from the core and the previous approximation of a localized orbit is inadequate. Therefore for ^{5}He the average value of $F_1(r)$ has been calculated from (7) and (8) using the radial wave function

$$\left.\begin{aligned} R &= \frac{\pi}{a\sqrt{3}}(r)^{1/2}J_{3/2}\left(\frac{\pi r}{a}\right) \quad \text{for } r<a \\ R &= \left(\frac{2a}{3}\right)^{1/2}\frac{1}{r} \qquad\qquad\quad \text{for } r>a, \end{aligned}\right\} \quad \ldots\ldots(10)$$

appropriate to a particle in a p level of zero total energy in a square well of width a. The value $a=3\times10^{-13}$ cm. is used, giving $\chi a=2$ and $3A/(2\chi^3a^3)=0{\cdot}75$. The resulting average value 0·107 of $F(r)/g\hbar c\chi$ is plotted as an isolated point in the Figure.

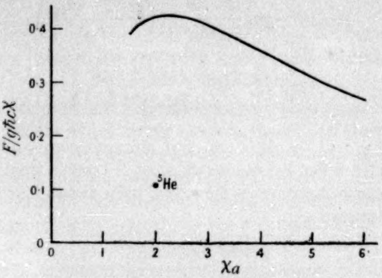

Effective potential F versus nuclear radius a.

The spin of the last particle may be aligned to give $j=l+\frac{1}{2}$ or $j=l-\frac{1}{2}$, and the corresponding values of $\boldsymbol{\sigma}.\mathbf{L}$ are $\frac{1}{2}l$ and $-\frac{1}{2}(l+1)$. Therefore, from (4), the splitting of the two energy levels is

$$\Delta E=E_{l+\frac{1}{2}}-E_{l-\frac{1}{2}}=-(l+\tfrac{1}{2})F(a). \qquad \ldots\ldots(11)$$

Values of the spin orbit splitting for a single particle outside a closed shell are tabulated. The figures are based on the interaction strength $g\hbar c\chi=2$ Mev., which corresponds to $g=2/133=1{\cdot}5\times10^{-2}$ and has been chosen to lead to the observed splitting for ^{5}He.

Nucleus	l	χa	ΔE (Mev.)
$^5_2$He	1	2	0·32
$^{91}_{40}$Zr	4	4·27	3·1
$^{181}_{51}$Sb	4	4·70	2·9
$^{143}_{60}$Nd	5	4·95	3·4
$^{209}_{83}$Bi	5	5·62	3·1

The calculated magnitude of the splitting is to be compared with a value of approximately 2 Mev. at $l=5$ estimated for the extra stability of the closed shell of 82 neutrons (Mayer 1948). The calculated splitting does not vary greatly with l, in accord with the empirical evidence (Mayer 1950). It is satisfactory that the level splittings in heavy nuclei calculated from the extreme assumption of pure single particle states are perhaps a little high. For two orbital momentum states $l=j+\frac{1}{2}$ and $l=j-\frac{1}{2}$ are available to the odd particle in a nucleus of spin j, and any contamination of the predominant state by a small admixture of the other will reduce the level splitting. A small contamination is suggested (Feenberg 1950) by the deviations of the experimental values of the magnetic moments from the Schmidt limits (Schmidt 1937).

Although some modification of the above results might be expected if a more precise calculation was possible, it may be concluded that the various data on doublet level splittings are self-consistent and can be attributed to an additional interaction of the form considered.

Note added in proof: At a conference held at Harwell in September 1951 Pais announced that the high energy nuclear scattering experiments indicate a potential of the form $M^{(12)}$ with the radial dependence

$$f(r_{12}) = -g\hbar c \frac{1}{r_{12}} \frac{\partial}{\partial(\chi r_{12})} \left(\frac{\exp(-\chi r_{12})}{r_{12}} \right).$$

This gives, in place of (7),

$$F(r_1) = -\frac{g\hbar c}{\chi r_1} \frac{\partial}{\partial(\chi r_1)} G(r, \chi).$$

With Pais's value $\chi^{-1} = 1{\cdot}1 \times 10^{-13}$ cm. and strength $g\hbar c\chi = 6$ MeV. the splittings of the heavy nuclei differ by not more than 0·1 MeV. from the results given above. This strength constant is, however, only about half that indicated by the scattering experiments.

REFERENCES

Bhabha, H. J., 1950, *Phys. Rev.*, **77**, 665.
Feenberg, E., 1950, *Phys. Rev.*, **77**, 771.
Feenberg, E., and Hammack, K. C., 1949, *Phys. Rev.*, **75**, 1877.
Gaus, H., 1949, Z. *Naturforsch.*, **4a**, 721.
Mayer, M. G., 1948, *Phys. Rev.*, **74**, 235; 1949, *Ibid.*, **75**, 1969; 1950, *Ibid.*, **78**, 16.
Nordheim, L. W., 1949, *Phys. Rev.*, **75**, 1894.
Rosenfeld, L., 1948, *Nuclear Forces* (Amsterdam : North Holland Publishing Co.).
Schmidt, T., 1937, Z. *Phys.*, **106**, 358.

Coherent Scattering of Light by an Atom and Negative Energy States

By K. J. Le COUTEUR and S. ZIENAU
Department of Theoretical Physics, The University, Liverpool

Communicated by H. Fröhlich; MS. received 26th June 1950

ABSTRACT. It is proved that the difference between the single electron theory and the positron theory for the coherent scattering of light by an atom represents the scattering of light by the atomic potential. In the practical cases the effect is negligible. The gauge invariance of the perturbation formulae for this effect is discussed.

---

§ 1. RELATIONSHIP OF THE SINGLE ELECTRON AND POSITRON THEORIES

Recently, Halpern and Hall (1949) have raised again the question of the equivalence of the Dirac single electron theory and the positron theory for the calculation of the cross section for the scattering of light by atoms. These authors remark that the proof usually advanced (cf. Heitler 1944) to show that the matrix element for this process is identical in both versions of the theory is erroneous when bound states are involved and coherent scattering is considered. In this case the exclusion principle appears to destroy the equivalence between the two theories as the final state of the electron is the same as its initial state.

One may restrict attention to a single electron held in a fixed potential V which can be thought due to a nucleus or to the combined action of a nucleus and the mean field of the other atomic electrons (Arnous 1950). We understand that Professor Waller is at present investigating more closely the definition of the mean field V in positron theory. In this fixed potential V, which cannot be more singular than a Coulomb field, the energy eigenstates form two clearly separated sets : (a) states of negative energy $E(a) < -mc^2$ all belonging to the continuous spectrum; (b) states of positive energy $E(b) > 0$ partly in the discrete spectrum (bound states). Thus a vacuum may be defined unambiguously even in the presence of the potential V.

In single electron theory the compound matrix element for the coherent scattering of a quantum λ on an atom with N non-interacting electrons occupying the discrete levels $B_i\,(E(B_i) > 0)$ is, in a customary notation,

$$\begin{aligned}
&\sum_{b^+}^{\text{empty}} \sum_{i=1}^{N} \frac{\langle B_i,\lambda'|\mathscr{H}|b,0\rangle\langle b,0|\mathscr{H}|B_i,\lambda\rangle}{E(B_i)+k_0-E(b)} \\
&\quad+\sum_{a^-} \sum_{i=1}^{N} \frac{\langle B_i,\lambda'|\mathscr{H}|a,0\rangle\langle a,0|\mathscr{H}|B_i,\lambda\rangle}{E(B_i)+k_0-E(a)} \\
&\quad+\sum_{b^+}^{\text{empty}} \sum_{i=1}^{N} \frac{\langle B_i,0|\mathscr{H}|b,\lambda\rangle\langle b,\lambda'|\mathscr{H}|B_i,0\rangle}{E(B_i)-k_0'-E(b)} \\
&\quad+\sum_{a^-} \sum_{i=1}^{N} \frac{\langle B_i,0|\mathscr{H}|a,\lambda\rangle\langle a,\lambda'|\mathscr{H}|B_i,0\rangle}{E(B_i)-k_0'-E(a)}, \qquad \ldots\ldots(1)
\end{aligned}$$

where $\lambda(\mathbf{k},k_0)$ denotes the incident, $\lambda'(\mathbf{k}',k_0')$ the scattered quantum, and where the summations over positive and negative energy states have been separated for convenience, matrix elements being labelled only by quantities that change. Waller (1929) has shown that in a non-relativistic approximation (1) leads to the usual cross section of the non-relativistic theory

$$d\phi = r_0^2\, d\Omega \left[\frac{1}{mc^2} \sum_{b^+}^{\text{empty}} \sum_{i=1}^{N} \left\{ \frac{\langle B_i | p_\lambda | b \rangle \langle b | p_{\lambda'} | B_i \rangle}{E(B_i) + k_0 - E(b)} + \frac{\langle B_i | p_{\lambda'} | b \rangle \langle b | p_\lambda | B_i \rangle}{E(B_i) - k_0 - E(b)} \right\} + \cos\Theta \right]^2 \qquad \ldots\ldots(2)$$

for coherent scattering ($k_0' = k_0$) (cf. Heitler 1944). Here Θ is the angle between the directions of polarization of the quanta λ and λ' and the term $\cos\Theta$ (Rayleigh scattering) results from the reduction of the summations in (1) which involve negative energy intermediate states a^-.

In positron theory, where the negative energy levels must be thought of as filled by electrons obeying the Pauli principle, the second order compound matrix element for the same coherent scattering process is

$$\sum_{b^+}^{\text{empty}} \sum_{i=1}^{N} \frac{\rangle B_i, \lambda' | \mathscr{H} | b, 0 \rangle \langle b, 0 | \mathscr{H} | B_i, \lambda \rangle}{E(B_i) + k_0 - E(b)} + \sum_{a^-} \sum_{b^+}^{\text{empty}} \frac{\langle a, \lambda' | \mathscr{H} | b, 0 \rangle \langle b, 0 | \mathscr{H} | a, \lambda \rangle}{E(a) + k_0 - E(b)} + \sum_{b^+}^{\text{empty}} \sum_{i=1}^{N} \frac{\langle B_i, 0 | \mathscr{H} | b, \lambda \rangle \langle b, \lambda' | \mathscr{H} | B_i, 0 \rangle}{E(B_i) - k_0' - E(b)} + \sum_{a^-} \sum_{b^+}^{\text{empty}} \frac{\langle a, 0 | \mathscr{H} | b, \lambda \rangle \langle b, \lambda' | \mathscr{H} | a, 0 \rangle}{E(a) - k_0' - E(b)}. \qquad \ldots\ldots(3)$$

In writing down this matrix element the exclusion principle is explicitly taken into account. The first and third terms in (3) agree with the first and third terms of (1), but the second and fourth terms of (3) look quite different from the corresponding terms of (1). A modification of the Rayleigh cross section might thus be expected. The second and fourth terms in (3) may, however, be rewritten as

$$\sum_{a^-} \sum_{b^+} \left\{ \frac{\langle a, \lambda' | \mathscr{H} | b, 0 \rangle \langle b, 0 | \mathscr{H} | a, \lambda \rangle}{E(a) + k_0 - E(b)} + \frac{\langle a, 0 | \mathscr{H} | b, \lambda \rangle \langle b, \lambda' | \mathscr{H} | a, 0 \rangle}{E(a) - k_0' - E(b)} \right\} - \sum_{a^-} \sum_{i=1}^{N} \left\{ \frac{\langle a, \lambda' | \mathscr{H} | B_i, 0 \rangle \langle B_i, 0 | \mathscr{H} | a, \lambda \rangle}{E(a) + k_0 - E(B_i)} + \frac{\langle a, 0 | \mathscr{H} | B_i, \lambda \rangle \langle B_i, \lambda' | \mathscr{H} | a, 0 \rangle}{E(a) - k_0' - E(B_i)} \right\}. \qquad \ldots\ldots(4)$$

Since $k_0 = k_0'$ (energy conservation in coherent scattering, as line breadth is ignored here) it is easily seen that the second summation in (4) is identical with the sum of the second and fourth terms in (1), the negative signs being compensated by the difference of signs of the energy denominators. The first sum in (4) therefore represents the difference between the compound matrix elements for coherent scattering in the two theories. The double summation is to be extended over all positive and negative energy states in the potential V and thus represents a vacuum effect. Physically, the term represents the scattering of light on the potential V. For a Coulomb field the resulting cross section has been considered by Kemmer (1937), who worked directly from the first sum in (4) using Born approximation and estimated the cross section to be of order

$r_0^2(Zr_0/\Lambda)^4$, where Λ is the wavelength of the incident light. A term of order $(Zr_0/\Lambda)^2$ should therefore be added into the square bracket in (2), but will be negligible in the non-relativistic region. It does, however, represent a physical effect which might become measurable for extremely high energy γ-ray scattering on heavy atoms.

§2. GAUGE INVARIANCE OF THE PERTURBATION FORMULAE

The vacuum terms in (4) involve, of course, divergent integrals which must be subtracted or more consistently regularized by the method of Pauli and Villars (1949). We do not wish to discuss this here, but only to show that if, as is often convenient, the longitudinal and transverse components of the electromagnetic potentials are not treated separately, the matrix element (4) is still formally consistent with the requirement of gauge invariance.

Explicitly, the vacuum part of the compound matrix element (4) reads (cf. Heitler 1944, p. 95)

$$\frac{2\pi e^2\hbar^2c^2}{k_0}\sum_{b^+}\sum_{a^-}\left\{\frac{\int\psi_a{}^*\alpha_\nu e^{-i\mathbf{k}'\mathbf{r}}\psi_b dv\int\psi_b{}^*\alpha_\mu e^{i\mathbf{k}\mathbf{r}}\psi_a dv}{E(a)+k_0-E(b)}\right.$$
$$\left.+\frac{\int\psi_a{}^*\alpha_\mu e^{i\mathbf{k}\mathbf{r}}\psi_b dv\int\psi_b{}^*\alpha_\nu e^{-i\mathbf{k}'\mathbf{r}}\psi_a dv}{E(a)-k_0{}'-E(b)}\right\}=J_{\nu\mu}(\mathbf{k},\mathbf{k}')\text{ say,}\qquad\ldots\ldots(5)$$

where $\mu, \mathbf{k}, k_0$ specifies the incident, $\nu, \mathbf{k}', k_0'$ the scattered light; also $k_0=k_0'$, and $\alpha_0=1$. Gauge invariance requires (cf. Pauli and Villars 1949) $k'^\nu J_{\nu\mu}=0$ and $J_{\nu\mu}k^\mu=0$. To show for instance the latter condition, one proceeds to cancel the energy denominators in (5) using

$$\int\psi_b{}^*k^\mu\alpha_\mu e^{i\mathbf{k}\mathbf{r}}\psi_a\,dv=\int\psi_b{}^*(k_0+\boldsymbol{\alpha}i\nabla e^{i\mathbf{k}\mathbf{r}})\psi_a\,dv$$
$$=\int\psi_b{}^*(k_0-\boldsymbol{\alpha}i\overleftarrow{\nabla})e^{i\mathbf{k}\mathbf{r}}\psi_a\,dv-\int\psi_b{}^*e^{i\mathbf{k}\mathbf{r}}(\boldsymbol{\alpha}i\overrightarrow{\nabla})\psi_a\,dv$$

which, together with the wave equations for ψ_a, $\psi_b{}^*$, gives

$$\int\psi_b{}^*k^\mu\alpha_\mu e^{i\mathbf{k}\mathbf{r}}\psi_a\,dv=\int\psi_b{}^*\{E(a)-E(b)+k_0\}e^{i\mathbf{k}\mathbf{r}}\psi_a\,dv.\qquad\ldots\ldots(6)$$

Hence

$$J_{\nu\mu}k^\mu=\frac{2\pi e^2\hbar^2c^2}{k_0}\sum_{a^-}\sum_{b^+}\left\{\int\psi_a{}^*\alpha_\nu e^{-i\mathbf{k}'\mathbf{r}}\psi_b\,dv\int\psi_b{}^*e^{i\mathbf{k}\mathbf{r}}\psi_a\,dv\right.$$
$$\left.-\int\psi_a{}^*e^{i\mathbf{k}\mathbf{r}}\psi_b\,dv\int\psi_b{}^*\alpha_\nu e^{-i\mathbf{k}'\mathbf{r}}\psi_a\,dv\right\}.\qquad\ldots\ldots.(7)$$

Assuming the completeness of the set of eigenfunctions a, b belonging to V, we can use the projection operators $\frac{1}{2}(1+\mathscr{H}_0/|\mathscr{H}_0|)$, $\frac{1}{2}(1-\mathscr{H}_0/|\mathscr{H}_0|)$ to convert (7) into a double summation over all eigenstates (a and b remaining in use only as convenient labels),

$$J_{\nu\mu}k^\mu=\frac{\pi e^2\hbar^2c^2}{2k_0}\sum_a\sum_b\left\{\int\psi_a{}^*\alpha_\nu e^{-i\mathbf{k}'\mathbf{r}}\left(1+\frac{\mathscr{H}_0}{|\mathscr{H}_0|}\right)\psi_b\,dv\int\psi_b{}^*e^{i\mathbf{k}\mathbf{r}}\left(1-\frac{\mathscr{H}_0}{|\mathscr{H}_0|}\right)\psi_a\,dv\right.$$
$$\left.-\int\psi_a{}^*e^{i\mathbf{k}\mathbf{r}}\left(1+\frac{\mathscr{H}_0}{|\mathscr{H}_0|}\right)\psi_b\,dv\int\psi_b{}^*\alpha_\nu e^{-i\mathbf{k}'\mathbf{r}}\left(1-\frac{\mathscr{H}_0}{|\mathscr{H}_0|}\right)\psi_a\,dv\right\}.\qquad\ldots\ldots(8)$$

Interchanging the dummy suffixes in the second factor one is left with

$$\frac{\pi e^2\hbar^2c^2}{k_0}\sum_a\sum_b\left\{\int\psi_a{}^*\alpha_\nu e^{-i\mathbf{k}'\mathbf{r}}\frac{\mathscr{H}_0}{|\mathscr{H}_0|}\psi_b\,dv\int\psi_b{}^*e^{i\mathbf{k}\mathbf{r}}\psi_a\,dv\right.$$
$$\left.-\int\psi_a{}^*\alpha_\nu e^{-i\mathbf{k}'\mathbf{r}}\psi_b\,dv\int\psi_b{}^*e^{i\mathbf{k}\mathbf{r}}\frac{\mathscr{H}_0}{|\mathscr{H}_0|}\psi_a\,dv\right\} \qquad \ldots\ldots(9)$$

or, in terms of generalized matrices,

$$J_{\nu\mu}k^\mu=\frac{\pi e^2\hbar^2c^2}{k_0}\left\{\mathrm{Sp}\left(\alpha_\nu e^{-i\mathbf{k}'\mathbf{r}}\frac{\mathscr{H}_0}{|\mathscr{H}_0|}e^{i\mathbf{k}\mathbf{r}}\right)-\mathrm{Sp}\left(\alpha_\nu e^{-i\mathbf{k}'\mathbf{r}}e^{i\mathbf{k}\mathbf{r}}\frac{\mathscr{H}_0}{|\mathscr{H}_0|}\right)\right\}. \qquad \ldots\ldots(10)$$

Since α_ν, $e^{i\mathbf{k}\mathbf{r}}$ and $e^{-i\mathbf{k}'\mathbf{r}}$ commute, cyclic permutation now shows that the spurs cancel formally.

In the absence of a potential V, the expression (5) for $J_{\nu\mu}$ takes a particularly simple form in the energy–momentum representation and becomes essentially identical with one investigated by Ma (1949 equation 98) who has shown, by explicit calculation, that the regularization procedure of Pauli and Villars leads to a finite and gauge-invariant expression for $J_{\nu\mu}$. In this special case our own formal proof of gauge invariance becomes very simple.

In the presence of a potential V, the explicit calculation of $J_{\nu\mu}$ is difficult. However one can, in principle, follow the procedure of the field free case and use a parameter m^i, in place of the electron mass m, to form $J_{\nu\mu}(m^i, V)$ by substituting in (5) wave functions ψ and energy levels E appropriate to the mass m^i. Then, with regularization parameters C_i, one defines

$$J_{\nu\mu}(m, V)=\sum_i C_iJ_{\nu\mu}(m^i, V) \qquad \ldots\ldots(11)$$

and $J_{\nu\mu}(m, V)$ is formally gauge invariant since each term of the sum has this property. Thus one can obtain finite gauge invariant results by proper choice of the parameters C_i. Since the divergence of $J_{\nu\mu}$ is associated with the summation over highly excited intermediate states, for which the wave functions may be approximated by plane waves, the regularization conditions

$$\Sigma C_i=0, \qquad \Sigma C_i(m^i)^2=0, \qquad \Sigma C_i\log(m^i)^2=0$$

for the free field case should be sufficient. Indeed, if one treats V by Born approximation, Kemmer's (1937) discussion shows that the divergent term in our problem is the same as for $V=0$. We have not been able to verify this more precisely because of the difficulty of working with the correct relativistic Coulomb wave functions.

REFERENCES

ARNOUS, E., 1950, *Phys. Rev.*, **77,** 149.
HALPERN, O., and HALL, H., 1949, *Phys. Rev.*, **75,** 1322.
HEITLER, W., 1944, *The Quantum Theory of Radiation* (Oxford : University Press).
KEMMER, N., 1937, *Helv. Phys. Acta,* **10,** 112, 182.
MA, T. S., 1949, *Phil. Mag.*, **40,** 1112.
PAULI, W., and VILLARS, F., 1949, *Rev. Mod. Phys.*, **21,** 434.
WALLER, I., 1929, *Z. Phys.*, **58,** 75.

The Determination of X-Ray Wavelength Distributions from Absorption Data

By J. R. GREENING
Radiotherapy Department, St. George's Hospital, London S.W.1

Communicated by H. T. Flint; MS. received 1*st February* 1950, *and in amended form* 17*th May* 1950

ABSTRACT. An existing empirical method which may be used, in limited cases, to determine x-ray wavelength distributions from absorption data is given some theoretical foundation. It is shown that the absorption curve function and the wavelength distribution function have the same relationship as a Laplace pair, the absorption curve function being the Laplace transform of the wavelength distribution function. The theory leads to the suggestion of Laplace pairs other than the one previously suggested, thus widening the scope of the method. By using the additive property of Laplace transforms the absorption method of determining spectral distributions is made of general application. The experimental requirements are discussed and examples of wavelength distributions determined by the absorption method are given.

---

§ 1. INTRODUCTION

In an endeavour to obtain the wavelength distribution of x-rays in the continuous x-ray spectrum with quite simple apparatus, a number of workers (Silberstein 1932, 1933, Bell 1936, Jones 1940, Greening 1947) have made use of the variation with wavelength of the linear x-ray absorption coefficient of elements such as aluminium, copper and tin. The apparatus consists solely of an instrument for measuring ionization current, and a number of metal foils which may be interposed between the ionization chamber and the x-ray tube. Thus the relative complexity of a crystal spectrometer is avoided together with those difficulties, including reflections of orders higher than the first, which are encountered when using crystal spectrometers at short wavelengths.

In the past the absorption method of determining x-ray wavelength distributions has been limited to those cases in which the absorption measurements could be fitted to an empirical equation first suggested by Silberstein (1933) and later extended by Jones (1940). It is thought that the additional methods of analysis to be given in this paper will make it possible to calculate the continuous x-ray spectrum corresponding to any set of absorption measurements, and that the paper will, to a rather limited extent, remove the empiricism of earlier methods of analysis.

§ 2. THE WAVE-BAND METHOD

Silberstein (1932) supposed an x-ray beam to consist of n wavelength bands to each of which a mean wavelength was attributed. By measuring the fraction of the radiation transmitted by n thicknesses of absorber he obtained n equations the solution of which gave the intensities of the n wave-bands. However, it will be found that as n increases or as the widths of the wave-bands decrease, the equations become increasingly ill-conditioned, small errors in the transmission measurements producing large errors in the calculated wave-band intensities. It would seem that a more complete use must be made of the relevant physics if a useful mathematical analysis of absorption data is to be achieved.

§3. THE SINGLE LAPLACE TRANSFORM METHOD

In the method of analysis referred to above no use was made of our knowledge that the X-ray spectrum is a continuous function (neglecting characteristic radiation for the moment) which is never negative. The general shape of the continuous X-ray spectrum is known from crystal spectrometer measurements. If, therefore, we can find a function of the same general shape as the continuous X-ray spectrum which has a known relationship with another function which can be fitted to the absorption measurements, it will be possible to proceed from these measurements to the corresponding X-ray distribution. Or, since the general shape of an absorption (or transmission) curve for X-rays passing through various thicknesses of absorber is known, we may first seek a function of this general shape and proceed from it to another function representing the X-ray spectral distribution. The relationship between the absorption curve function and the distribution curve function will be shown below to be provided by the Laplace transform equation. The problem then reduces to fitting a Laplace transform to the absorption data and calculating the X-ray spectral distribution using the other member of the Laplace pair.

If I_0 is the original intensity of an X-ray beam and I_x is its intensity after passing through x cm. of absorber,

$$I_x = I_0 \int_{\lambda_0}^{\infty} e^{-\mu(\lambda)x} f(\lambda) d\lambda, \qquad \ldots\ldots(1)$$

where $\mu(\lambda)$ is the linear absorption coefficient of the absorber for a wavelength λ, $f(\lambda)d\lambda$ is the fraction of I_0 lying between λ and $\lambda + d\lambda$, and λ_0 is the short wavelength limit of the X-ray spectrum given by the Duane–Hunt Law, viz. $\lambda_0 = \boldsymbol{hc}/\mathrm{V}\boldsymbol{e} = 12{\cdot}4/\mathrm{kv}$.A.

Since μ is a function of the wavelength we may write

$$f(\lambda) d\lambda = \phi(\mu) d\mu \qquad \ldots\ldots(2)$$

and using (2) in (1) we have

$$I_x = I_0 \int_{\mu_0}^{\infty} e^{-\mu x} \phi(\mu) d\mu \qquad \ldots\ldots(3)$$

as shown by Silberstein (1933). But

$$f(x) = \int_0^{\infty} e^{-\mu x} \psi(\mu) d\mu \qquad \ldots\ldots(4)$$

is one form of the Laplace transform equation, $f(x)$ being the Laplace transform of $\psi(\mu)$, i.e. $f(x) \subset \psi(\mu)$ (see, for example, McLachlan 1948). It is a general property of Laplace transforms that if $f(x) \subset \psi(\mu)$ then $e^{-ax} f(x) \subset \phi(\mu)$, where $\phi(\mu) = 0$ when $0 < \mu < a$, and $\phi(\mu) = \psi(\mu - a)$ when $\mu > a$. If for a we write μ_0, the absorption coefficient of radiation of wavelength λ_0, we have

$$\exp(-\mu_0 x) f(x) = \int_0^{\infty} e^{-\mu x} \phi(\mu) d\mu = \int_{\mu_0}^{\infty} e^{-\mu x} \psi(\mu - \mu_0) d\mu \qquad \ldots\ldots(5)$$

since $\int_0^{\mu_0} e^{-\mu x} \phi(\mu) d\mu$ is zero.

Thus (5) based on the Laplace transform equation has the form of (3) which is derived from physical considerations.

Therefore, if it is possible to find a Laplace transform $f(x)$ such that $\exp(-\mu_0 x)f(x)$ gives the experimentally determined values of I_x/I_0, then $\psi(\mu-\mu_0)$ may be calculated and $f(\lambda)$ derived from it as $f(\lambda)=\phi(\mu)d\mu/d\lambda=\psi(\mu-\mu_0)d\mu/d\lambda$ for $\mu>\mu_0$.

(i) *The Form of the Function* $f(x)$

In view of the exponential absorption of monochromatic x-radiation let us assume $I_x/I_0=e^{-\psi(x)}$. On physical grounds it is apparent that as x tends to infinity the absorption coefficient will tend to μ_0, the more readily absorbed radiation having been filtered out. Thus

$$\ln(I_x/I_0)=-\psi(x)=-\{\mu_0 x+g(x)\},$$

where $g(x)$ is much less than $\mu_0 x$ when x is large and, therefore, the powers of x in $g(x)$ are less than 1. As $I_x/I_0=1$ when $x=0$, $\mu_0 x+g(x)=0$ when $x=0$, i.e. $g(0)=0$. Thus the powers of x in $g(x)$ cannot be less than zero. Therefore if $g(x)$ contains terms such as x^n, $1>n>0$. Also as $g(0)=0$ any constants in $g(x)$ must appear (i) as coefficients of powers of x or (ii) twice, once positive and once negative.

As $1>n>0$ and as Laplace transforms involving $\exp(-x^{1/2})$ are known, it is convenient to assume $n=\frac{1}{2}$ and to see if this leads to expressions which may be made to fit experimental results. Thus we may assume $g(x)=x^{1/2}$ or, more generally, adding the constant allowed by (i) above, $g(x)=Bx^{1/2}$. Therefore,

$$I_x/I_0=\exp(-\mu_0 x-Bx^{1/2}) \qquad \ldots\ldots(6)$$

which is Bell's (1936) modification of the expression arbitrarily suggested by Silberstein (1933).

If, further, we add the constant allowed by (ii) above, $g(x)=B\{(x+d)^{1/2}-d^{1/2}\}$ and therefore

$$I_x/I_0=\exp[-\mu_0 x-B\{(x+d)^{1/2}-d^{1/2}\}] \qquad \ldots\ldots(7)$$

which is the expression arrived at empirically by Jones (1940).

Instead of assuming as in the previous section that $I_x/I_0=\exp\{-\mu_0 x-g(x)\}$, we could assume more generally that

$$I_x/I_0=e^{-\mu_0 x}h(x) \qquad \ldots\ldots(8)$$

Then

$$\ln(I_x/I_0)=-\mu_0 x+\ln h(x) \qquad \ldots\ldots(9)$$

and

$$\frac{d}{dx}\ln\frac{I_x}{I_0}=-\mu_0+\frac{h'(x)}{h(x)}. \qquad \ldots\ldots(10)$$

As before we know on physical grounds that $(d/dx)(I_x/I_0)$ tends to $-\mu_0$ as x tends to infinity. Therefore $h'(x)/h(x)$ tends to zero as x tends to infinity. Also as $I_x/I_0=1$ when $x=0$, $h(x)=1$ when $x=0$.

The essential shape of a transmission curve for heterogeneous radiation is shown in Figure 1, and in the same figure the straight line indicates the form the transmission curve would have if *all* the radiation were of wavelength λ_0, the short-wave limit of the spectrum. As x tends to infinity the curve will become parallel to the straight line. From (9) and Figure 1 it will be seen that $-\ln h(x)$ is proportional to lengths such as PQ, i.e. $\ln\{1/h(x)\}\propto$ PQ. It can be seen that as x increases PQ increases and therefore $h(x)$ decreases.

Summarizing:

(i) $h(x) = 1$ when $x = 0$,
(ii) $h(x)$ decreases as x increases,
(iii) $h'(x)/h(x) \rightarrow$ zero as $x \rightarrow \infty$.

Further, it may be deduced that $h'(x)$ increases as x increases but is never positive, and in physical grounds it is very unlikely that $h(x)$ will be a periodic function. We require therefore some simple functions that satisfy the above conditions. (There is little point in seeking more complicated functions because of the difficulty of fitting them to observed values of I_x/I_0.) As in the case considered earlier we find that $\exp(-x^n)$ is suitable, where n is greater than zero since $h(x)$ decreases as x increases, and is less than one since $h'(x)/h(x)$ tends to zero as x tends to infinity. As before, we may assume $\exp(-x^{1/2})$ to be a suitable function, or more generally, $\exp[-B\{(x+d)^{1/2} - d^{1/2}\}]$.

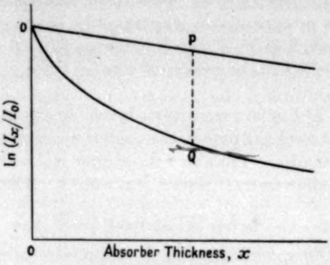

Figure 1. Typical transmission curve.

Another simple function that satisfies conditions (ii) and (iii) is $h(x) = 1/x^n$ where $n > 0$. This will also satisfy condition (i) if a constant is added making

$$h(x) = d^n/(x+d)^n . \qquad \ldots\ldots(11)$$

Further, $h(x)$ may be the product of the two functions suggested, i.e.

$$h(x) = \exp[-B\{(x+d)^{1/2} - d^{1/2}\}]\, d^n/(x+d)^n \qquad \ldots\ldots(12)$$

or

$$h(x) = C\exp\{-B(x+d)^{1/2}\}/(x+d)^n, \qquad \ldots\ldots(13)$$

where $C = d^n \exp(Bd^{1/2})$.

Thus from considerations of the physical conditions of the problem we have arrived at a number of expressions which it may be possible to fit to experimental values of I_x/I_0.

One other function we may mention is $K_0(x)$, the modified Bessel function of the second kind. Except in the vicinity of $x = 0$ where it becomes infinite, this function is very similar in form to e^{-x}, actually decaying slightly more rapidly than e^{-x}. It is probable, therefore, that $K_0\{B(x+d)^{1/2}\}$ could be fitted to experimental values of I_x/I_0. As $K_0\{B(x+d)^{1/2}\} = 1$ when $x = 0$, B and d are not independently variable. More freedom is obtained by assuming

$$I_x/I_0 = \exp(-\mu_0 x)\, C\, K_0\{B(x+d)^{1/2}\}, \qquad \ldots\ldots(14)$$

where C is another constant.

However, this function was not first obtained in the manner indicated above, but rather by considering the form of the function $\psi(\mu - \mu_0)$, which we now proceed to do.

(ii) *The Form of the Function* $\psi(\mu-\mu_0)$

As $f(\lambda)$ the wavelength distribution function is equal to $\psi(\mu-\mu_0)d\mu/d\lambda$ and as the absorber used must be chosen so that $d\mu/d\lambda$ increases smoothly in the wavelength range of the x-ray spectrum under investigation (Greening 1947), we may consider $f(\lambda)$ instead of $\psi(\mu-\mu_0)$.

From crystal spectrometer measurements it is known that $f(\lambda)=0$ when $\lambda=\lambda_0$ and $f(\lambda)$ tends to zero as λ tends to infinity. As λ increases from λ_0, $f(\lambda)$ increases rapidly to a maximum and then falls more slowly to zero at long wavelengths. It seems probable that the rapid rise would be provided by an exponential term.

Reference was made to a list of Laplace pairs (Pipes 1946) and those were selected which made $\psi(\mu-\mu_0)$ zero when $\mu=\mu_0$, and when $\mu=\infty$. Not surprisingly the corresponding transforms were of the forms suggested by (7), (11), (13), and (14). It is a general property of Laplace transforms that if $f(x) \leftharpoondown \psi(\mu-\mu_0)$ then $f(x+d) \leftharpoondown \exp\{-(\mu-\mu_0)d\}\psi(\mu-\mu_0)$. Using this we obtain the following list of Laplace pairs which satisfy the requirements for both $f(x)$ and $\psi(\mu-\mu_0)$.

No.	$f(x)$	$\psi(\mu-\mu_0)$
I	$\exp[-B\{(x+d)^{1/2}-d^{1/2}\}]$	$\dfrac{B\exp B\sqrt{d}}{2\sqrt{\pi}}\,\dfrac{\exp\{-(\mu-\mu_0)d\}\exp\{-B^2/4(\mu-\mu_0)\}}{(\mu-\mu_0)^{3/2}}$
II	$CK_0\{B(x+d)^{1/2}\}$	$\dfrac{C}{2}\,\dfrac{\exp\{-(\mu-\mu_0)d\}\exp\{-B^2/4(\mu-\mu_0)\}}{(\mu-\mu_0)}$
III	$\dfrac{\sqrt{d}\exp[-B\{(x+d)^{1/2}-d^{1/2}\}]}{(x+d)^{1/2}}$	$\dfrac{\sqrt{d}\exp B\sqrt{d}}{\sqrt{\pi}}\,\dfrac{\exp\{-(\mu-\mu_0)d\}\exp\{-B^2/4(\mu-\mu_0)\}}{(\mu-\mu_0)^{1/3}}$
IV	$\dfrac{d^{3/2}}{(x+d)^{3/2}}$	$\dfrac{2d^{3/2}}{\sqrt{\pi}}\exp\{-(\mu-\mu_0)d\}(\mu-\mu_0)^{1/2}$

In cases I, II and III $\psi(\mu-\mu_0)$ contains the term $\exp\{-B^2/4(\mu-\mu_0)\}$ and this will produce a rapid rise in $\psi(\mu-\mu_0)$ as μ increases from μ_0. It has been found by Jones (1940) and also by the present writer (Greening 1947), that expression I is often satisfactory for heavily filtered 200 kv. radiation. We have found expressions II and III more suitable for lightly filtered and lower voltage radiation, but expression IV does not appear to be very satisfactory for present purposes.

(iii) *Determination of* $f(\lambda)$, *the Wavelength Distribution Function*

If we can find the constants in any of the above expressions for $f(x)$ which will make $I_x/I_0=\exp(-\mu_0x)f(x)$ then $f(\lambda)$ can be computed if μ and $d\mu/d\lambda$ are known for the wavelength range under investigation. Jones (1940) has given a direct graphical method of finding B and d for expression I. However, to determine the constants in II and III recourse must be had to a more laborious process of trial and error.

In Figures 2 and 3 examples are given of wavelength distributions calculated after fitting expressions I and III respectively to the experimental values of I_x/I_0. As the x-rays were measured by the air ionization they produced, Figures 2 and 3 do not give strictly the energy distributions. These can be derived by dividing the ordinates by the real absorption coefficient of air, $(\tau+\sigma_a)$, at the corresponding wavelengths. Values of $(\tau+\sigma_a)$ for air are given by Greening (1948).

§ 4. THE MULTIPLE LAPLACE TRANSFORM METHOD

Although we now have two more expressions for $f(x)$, viz. II and III, than have been suggested previously, it may be found that none of the expressions I, II or III can be fitted to the complete range of values of x for which I_x/I_0 has been measured. The wavelength distribution function may still be determined, however, by using the fact that Laplace transforms are additive. Thus we may write

$$I_x/I_0 = \exp(-\mu_0 x)(a T_1 + b T_2 + c T_3 + \ldots) \qquad \ldots\ldots(15)$$

where T_1, T_2, T_3 etc. are Laplace transforms. The procedure is to fit aT_1 to values of $I_x/I_0 \exp(-\mu_0 x)$ so that agreement is obtained for the largest values of x and over as great a range of x as possible. bT_2 is then fitted to $I_x/I_0 \exp(-\mu_0 x) - aT_1$ in a similar manner, and so on until the whole range of x has been covered. Although any transforms may be used the most tractable mathematically is I with $d=0$, i.e. $f(x) = \exp(-Bx^{1/2})$, as B and the constant such as a, b, c, of equation (15) are easily determined by plotting $\ln\{I_x/I_0 \exp(-\mu_0 x)\}$ as a function of $x^{1/2}$.

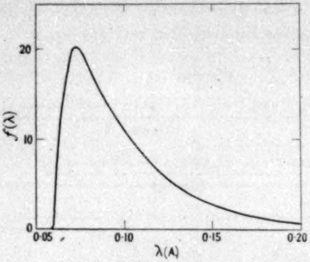

Figure 2. Wavelength distribution for radiation produced at 220 kv. with a filter of 0·66 mm. Sn + 0·5 mm. Cu + 1 mm. Al.

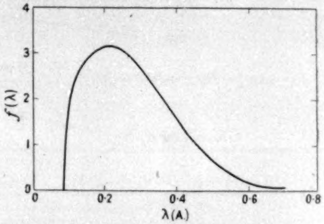

Figure 3. Wavelength distribution for radiation produced at 150 kv. with a filter of 1 mm. Al.

If other transforms can be made to fit a greater range of x it is an advantage to use them. Two or three terms are usually quite sufficient, the second and third terms being, in effect, small corrections to the first.

This method of using Laplace transforms has been employed by Macey (1948) for the stress–strain analysis of viscous elastic materials.

§ 5. EXPERIMENTAL REQUIREMENTS

Although the experimental work is small the following requirements must be met:

(*a*) I_x/I_0 must be accurately measured. In view of the difficulty in holding the output from an X-ray tube constant it is suggested that the ratio I_x/I_0 be measured directly using an apparatus such as that described by Kemp (1945, 1946).

(*b*) The absorber used must not have an absorption edge in the wavelength range under investigation, but the greater $d\mu/d\lambda$ the better. Suitable values of μ and $d\mu/d\lambda$ for aluminium, copper and tin have been tabulated by Greening (1947).

(*c*) A minimum of radiation scattered by the absorber should reach the measuring chamber.

(*d*) The measuring chamber must have a known variation of sensitivity with wavelength, e.g. if it is made of 'air-equivalent' material its sensitivity will vary as the real absorption coefficient $(\tau + \sigma_a)$ of air.

§ 6. DISCUSSION

The methods of analysing absorption data which have been described above should make it possible to derive the spectral energy distribution of a beam of x-rays from any set of absorption measurements. If accurate distributions are to be obtained using the 'wave-band method' of analysis the absorption data need to be of an accuracy at present unobtainable. However, in the Laplace transform methods of analysis the use of functions which are known on physical grounds to be of the correct general form allows good use to be made of absorption data of an accuracy which may be attained with reasonable care. On a previous occasion (Greening 1947), we examined the self-consistency of the Laplace transform method by deriving the wavelength distribution of an x-ray beam from absorption measurements using two different materials as absorbers. In all cases examined the wavelength distribution obtained was sensibly independent of the absorber used.

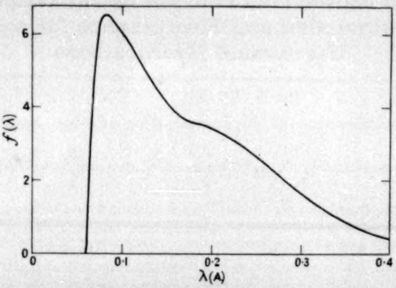

Figure 4. Wavelength distribution for radiation produced at 220 kv. with a filter of 0·25 mm. Cu + 1 mm. Al.

Throughout the Laplace transform methods of analysis, continuous functions have been used with the result that discontinuities such as characteristic radiation cannot be shown as the sharp peaks they really are. However it has been found that when conditions are such that a considerable amount of characteristic radiation might be expected to be present, e.g. 220 kvp, 0·25 mm. Cu + 1 mm. Al filter, analysis based on (15) gives a small hump on the distribution curve in the region of the tungsten K lines (see Figure 4). In the case of 150 kvp radiation with 1 mm. Al filter (Figure 3) the characteristic radiation would be included in the main peak of the distribution curve with which the characteristic radiation coincides. Thus such characteristic radiation as may be present in any x-ray beam, instead of appearing as a line or lines, is spread over a small wave-band in the region of the lines by the Laplace transform methods of analysis.

If the fraction of the total radiation that appeared in the K lines of the target material of the x-ray tube were known in a particular case, it would be a simple matter to compute the transmission of the characteristic radiation through the absorber and, by subtraction, to obtain the transmission of the continuous radiation alone. This could then be analysed by one of the methods shown above. However, the literature seems to be singularly devoid of such information.

REFERENCES

Bell, G. E., 1936, *Brit. J. Radiol.*, **9**, 680.

Greening, J. R., 1947, *Brit. J. Radiol.*, **20**, 71; 1948, *Ibid.*, **21**, 75.

Jones, D. E. A., 1940, *Brit. J. Radiol.*, **13**, 95.

Kemp, L. A. W., 1945, *Brit. J. Radiol.*, **18**, 107; 1946, *Ibid.*, **19**, 233.

Macey, H. H., 1948, *J. Sci. Instrum.*, **25**, 251.

McLachlan, N. W., 1948, *Modern Operational Calculus* (Macmillan : London).

Pipes, L. A., 1946, *Applied Mathematics for Engineers and Physicists* (New York : McGraw-Hill).

Silberstein, L., 1932, *J. Opt. Soc. Amer.*, **22**, 265; 1933, *Phil. Mag.*, **15**, 375.

Relation between the Franck-Condon Frequencies of Absorption and Fluorescence for some Unsaturated Hydrocarbons

By S. L. ALTMANN

Wheatstone Physics Department, King's College, London

Communicated by C. A. Coulson; *MS. received 20th March* 1950

ABSTRACT. Differences between the Franck–Condon frequencies for emission and absorption are calculated for butadiene, naphthalene and anthracene. The molecular-orbital method is used and its validity in the present case is discussed. A correlation with the experimental data has been attempted for anthracene and appears to be satisfactory. It is shown that the calculated values may be correlated qualitatively with the fluorescence efficiencies of the molecules.

§1. INTRODUCTION

It is well known that the electronic energy of a diatomic molecule may be expressed as a function of the internuclear distance by means of the so-called Morse curve. This is shown in Figure 1, where G refers to the ground state and E to the first excited level.

It was pointed out by Franck and further developed by Condon that the most probable electronic transition is that in which both the positions and the momenta of the nuclei are not changed. The first condition imposes the movement of the state of the molecule, as represented in Figure 1, on a vertical line, the second, that the vertical distances from the point representing the state of the molecule to the potential curve be kept constant during excitation. Further considerations show that the actual transitions during absorption and fluorescence are those represented by AA″ and F′ F″ respectively in the figure, where A^0A and F^0F' are equal to A′A″ and FF″ respectively. The energy differences corresponding to AA″ and F′ F″ are the Franck–Condon (F–C) frequencies, which are related to the maxima of absorption and fluorescence respectively. It must be borne in mind however, that on account of the existence of vibrational structure they may not correspond to an actual transition, that is, to a peak. In other words, the points A″ or F″ do not correspond to states that the excited molecule is able to occupy ; their meaning, and that of the F–C principle in this case, is that the more probable transitions are those to the nearest vibrational levels. For instance, if the situation were that which is depicted in Figure 1, two peaks would appear in the absorption spectrum with almost the same intensity and symmetrically placed with respect to the position of the F–C frequency.

All this is well known for diatomic molecules. It can be extended to polyatomic molecules, hyper-surfaces and normal modes of vibration being substituted for the Morse curves and vibrational states respectively. But for polyatomic molecules the experimental analysis is not yet good enough ; therefore some theoretical discussion and calculation are desirable. This will be provided in this paper, in which estimates are made of the difference between the F–C frequencies of absorption and fluorescence. Since the existence of a non-zero value for this difference depends upon the change in the geometrical structure of the molecule (such as bond lengths and angles), which takes place as a result of electronic excitation, our calculation requires that we should determine these quantities in both the ground and excited states. Molecular orbital (m.o.) theory offers a simple method of making these calculations. In what follows we shall make the usual assumption for conjugated and aromatic molecules, that in transitions among the π-electrons, the valence angles are substantially unaltered.

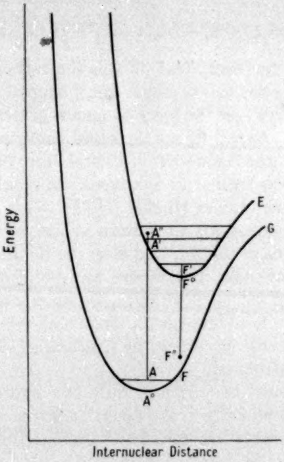

Figure 1.

§ 2. METHOD OF CALCULATION

As the m.o. theory has been fully discussed by several investigators (Hückel 1931, Lennard-Jones 1937, Coulson and Longuet-Higgins 1947) only a short account will be given here.

In the usual m.o. theory each π-electron is assigned to a certain orbital, extending over the whole nuclear framework and having an energy depending on the various Coulomb terms α_i and resonance integrals β_{ij}. We shall make the usual approximation of supposing that all the α_i are equivalent, that all overlap integrals between distinct atomic orbitals are zero and that all β_{ij} are zero except between neighbouring atoms. But we must not, as is often done, treat all the non-vanishing β_{ij} as equal, for the whole significance of the F–C principle depends upon changes of bond lengths on excitation, and this necessarily involves changes in the β_{ij}. The symmetry of the molecule will, of course, tell us that certain pairs of bonds are equal, so that the number of independent β_{ij} is much less than the number of bonds. In order to estimate the variation of each β_{ij} with internuclear distance, we use the Lennard-Jones (1937) formula:

$$2\beta = E_{\mathrm{d}}^0 - E_{\mathrm{s}}^0 + \tfrac{1}{2}k_{\mathrm{d}}(x-d)^2 - \tfrac{1}{2}k_{\mathrm{s}}(x-s)^2,$$

where x is the length of the bond, $d = 1{\cdot}33$ A. is the carbon–carbon (C – C) double bond length, $s = 1{\cdot}54$ A. is the C – C single bond length ; $k_{\mathrm{d}} = 9{\cdot}8 \times 10^5$ dyne/cm. and $k_{\mathrm{s}} = 5{\cdot}96 \times 10^5$ dyne/cm., are the force constants of the C – C bonds in ethylene and ethane respectively. E_{d}^0 and E_{s}^0 are the bond energies of a double and single bond respectively, and the value of -65 kcal. for the difference $E_{\mathrm{d}}^0 - E_{\mathrm{s}}^0$ as given by Pitzer (1948) was used; as a comparison results are quoted calculated with the value $-55{\cdot}7$ kcal., due to Hückel (1935).

Solving the secular equations we obtain values of the binding energies ϵ_{r} of the orbitals as functions of the β_{ij}, that is of the bond lengths. The lower half of the ϵ_{r} are bonding orbitals, the others anti-bonding. The energy of our electronic state will be $E = \Sigma_{\mathrm{r}} \nu_{\mathrm{r}} \epsilon_{\mathrm{r}}$, where ν_{r} is the number of electrons in each occupied level. Also, each ϵ_{r} determines the details of the corresponding m.o., and hence the bond orders from which, by Coulson's (1939) method, the various bond-lengths may be calculated.

The calculation must be carried out by successive approximations: (i) initially all the non-vanishing β are taken as being equal and values of ϵ are calculated; (ii) bond orders are calculated and preliminary bond lengths are deduced from them; (iii) two sets of improved values of the β integrals, for the ground and excited states respectively, are estimated from these bond lengths ; (iv) these new values of β integrals are put into the secular equations and improved values of $\epsilon_{\mathrm{r,g}}$ and $\epsilon_{\mathrm{r,e}}$ are obtained, where g and e denote whether the configuration of the nuclei corresponds to the ground or excited state; with these values the electronic energies E_{g}, E_{g}', E_{e} and E_{e}' are calculated, the dashes denoting that one electron is in an anti-bonding orbital ; the four values would therefore correspond respectively to the points A^0, A′, F and F^0 of Figure 1; (v) for a second approximation the steps (ii)–(iv) are repeated and final values of the energies are obtained.

The values in which we are interested are the differences $E_{\mathrm{a}} = E_{\mathrm{g}} - E_{\mathrm{g}}'$ and $E_{\mathrm{f}} = E_{\mathrm{e}} - E_{\mathrm{e}}'$ corresponding to absorption and emission respectively.

§ 3. RESULTS

The calculation was carried out for butadiene, naphthalene and anthracene. The second cycle of approximations was calculated only for naphthalene and the values obtained are quoted in brackets in Table 1, where the calculated bond lengths for the ground and excited states and the energies are shown. The nomenclature for the bonds is explained in Figure 2.

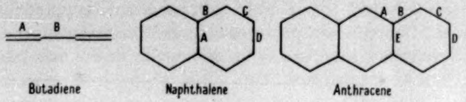

Figure 2.

Table 1

(1)		(2)					(3)			(4)		
	(5)	*A*	*B*	*C*	*D*	*E*	E_a	E_f	E_a-E_f	E_a	E_f	E_a-E_f
Butadiene	(6)	1·34	1·43				48·3	29·8	18·5	54·0	35·6	18·4
	(7)	1·43	1·38									
Naphthalene	(6)	$1{\cdot}41_7$ $(1{\cdot}41_4)$	$1{\cdot}41_0$ $(1{\cdot}41_2)$	$1{\cdot}37_7$ $(1{\cdot}38_0)$	$1{\cdot}40_0$ $(1{\cdot}41_2)$		40·6 (40·8)	31·1 (31·1)	9·1 (9·7)	46·4	37·1	9·3
	(7)	1·42 (1·41)	1·41 (1·40)	1·42 (1·43)	1·38 (1·38)							
Anthracene	(6)	1·40	1·42	1·41	1·38	1·40				32·0	27·0	5·0
	(7)	1·42	1·42	1·40	1·40	1·38						

(1) Molecule; (2) Bond lengths (A.); (3) Transition π-energies (kcal.) calculated with Hückel values; (4) Transition π-energies (kcal.) calculated with Pitzer values; (5) Nature of electronic state; (6) Ground state; (7) Excited state. The values quoted in brackets correspond to the second approximation.

§ 4. DISCUSSION

Before attempting a correlation of the calculated with the experimental data, it seems desirable to discuss the actual meaning of our calculations.

As we have not taken into account electron spin, except implicitly by not allotting more than two electrons to any m.o., the values E_g' and E_e' that we have employed in calculating E_a and E_f are really averages between singlet and triplet states. Furthermore, we have neglected configurational interaction (Jacobs 1949). It seems likely however that both effects produce a shift in the values E_g' and E_e' of approximately the same amount, introducing therefore an additive error in E_a and E_f that would cancel by subtraction. The very good coincidence between values of $E_a - E_f$ calculated with Hückel's and Pitzer's values for the bond energies offers a good example of a cancellation of errors of this kind, thus showing that the rather great indeterminacy in the values of β integrals is unimportant in our case. Even in the case of $E_a - E_f$, which is considerably smaller than either E_a or E_f separately, neglect of the second approximation (revised β-values) introduces an error of the order of only 6%. This is certainly less than the reliability of the whole scheme of calculation and justifies us in using only a first approximation for anthracene.

On the other hand, the values E_a and E_f that we have calculated correspond to the distances A^0A' and F^0F of Figure 1. But it is clear, from the considerations of § 1, that they are equal to AA'' and $F'F''$ respectively. That is, E_a and E_f are actually the F–C frequencies and are not affected by possible variations of the zero point energy.

The experimental check of our calculation has been attempted for anthracene only. In fact, the fluorescence spectrum of butadiene has not yet been studied and for naphthalene it turned out to be difficult to find a safe estimate of the position of the F–C frequencies, thus making any interpretation somewhat doubtful.

The fluorescence spectrum of anthracene has been measured quantitatively between 18,000 and 28,000 cm^{-1} by Kortüm and Finckh (1942) and the absorption spectrum was studied by v. Halban, Kortüm and Szigeti (1936) between 24,000 and 35,000 cm^{-1}. The vibrational structure of this band shows a very clear mirror-image symmetry. This is the first band in the ultra-violet spectrum and it seems likely that it corresponds to the electronic transition to the first excited level which has been calculated here (cf. Klevens and Platt 1949).

Both in the fluorescence and absorption spectra of anthracene in the vapour state or in solution in dioxane, the first two vibrational peaks are the most intense and have almost the same intensity. In the fluorescence spectra of crystals, however, the first peak is greatly weakened, thus departing from the mirror symmetry. The effect has been assigned to absorption of the fluorescent light (see Kortüm and Finckh 1942, Bowen and Lawley 1949).

We need now to find an estimate of the position of the experimental F–C frequencies. The equality of the intensity of the first two peaks, both in the absorption and fluorescence spectra of anthracene, makes it plausible in accord with the considerations of § 1 to assign the F–C frequencies, to the mid-point between the two peaks. With this tentative assumption we get the values quoted in Table 2.

Table 2

State	Absorption (cm^{-1})			Fluorescence (cm^{-1})			
	(1)	(2)	(3)	(1)	(2)	(3)	(4)
Vapour	27550	29000	28300	27300	26000	26700	1600
Sol. in dioxane	26500	27950	27200	26150	24800	25500	1600
Crystal	25550	27000	26300	24800	23750	24300	2000

(1) First peak; (2) Second peak; (3) Mid-point between the two; (4) Difference between the two mid-points.

The theoretical value of the F–C difference, corresponding to $E_a - E_f = 5{\cdot}0$ kcal., is 1,750 cm^{-1}. Without giving too much weight to the rather striking coincidence between this and the values quoted in the last column of Table 2, we think that the present interpretation is further supported by the fact that these values appear to be sensibly constant for the vapour, solution and solid phases, whilst the actual position of the peaks is shifted by more than 2,000 cm^{-1}, as may be seen from the quoted data. Even the fact that for the crystal there is a larger value for the difference between the two estimates of the F–C frequencies agrees with the view that here the first fluorescence peak is weakened by absorption, and is consequently shifted towards the red.

We will show now that our results may be useful in obtaining some insight into the conditions that determine the fluorescence efficiency of a molecule. As was pointed out by Norrish *et al.* (1934) a molecule may give up its electronic energy as vibrational energy. In this case no emission occurs. This phenomenon, called ‘ internal conversion ’, has been studied in greater detail by Franck and Livingston (1941) and is reviewed by Franck and Sponer (1947). It depends on the crossing of the potential curve of the excited level with that of the ground state. This effect is particularly important with polyatomic molecules because here vibrations may destroy the initial symmetry and therefore the intersection of levels forbidden by the non-crossing rule becomes allowed.

It seems reasonable that the value of the difference between the F–C frequencies of the absorption and fluorescence spectra (that is, the vertical distances between the potential surfaces of the ground and excited states) may be taken as indicating how much the potential surface of the excited state is shifted with respect to that of the ground state.

Further, this shift may be correlated with the distortion of the molecule. A good index for this distortion is the root-mean-square of the bond length differences from the ground to the excited states. This is shown in Table 3. The result for benzene is quoted for the sake of completeness and the necessary data have been taken from Garforth, Ingold and Poole (1948).

Table 3

σ (A.)	Butadiene	Benzene	Naphthalene	Anthracene
	$7{\cdot}9\times10^{-2}$	4×10^{-2}	$2{\cdot}9\times10^{-2}$	$1{\cdot}7\times10^{-2}$

The data quoted follow closely the same relationship that holds for the difference between the F–C frequencies and show, as might be expected, that the larger the molecule the smaller the distortion during excitation, and in consequence the smaller the shift of the potential curves. Now, these are clearly more likely to cross each other the more they are shifted. This being assumed, the greater the difference between the two F–C frequencies, the lower the stability of the excited state. In accordance with this, our data would show that anthracene is a better fluorescent molecule than naphthalene. This is in agreement with the results of Bowen and Sawtell (1937), who show that the percentage fluorescence efficiencies of naphthalene and anthracene in ethyl alcohol solutions are respectively 2·54 and 1·70 with 2650 A. as incident radiation. Later work by Bowen (unpublished) indicates, however, that the actual numerical value for naphthalene is considerably larger. On the other hand, for crystals, Bowen, Mikiewicz and Smith (1949) have shown that at ordinary temperatures the efficiency of naphthalene is 70% and of anthracene 90%. Naphthacene and pentacene, besides, fluoresce fairly well only as vapours. This would indicate that at least in condensed phases the importance of internal conversion, as a factor determining fluorescence efficiencies, must not be over-estimated, since intermolecular forces may sometimes be more important.*

Finally, our results would indicate that the larger the conjugated molecule, the closer together we may expect to find the maxima of absorption and fluorescence.

---

* The author is indebted to Mr. E. J. Bowen for this observation.

ACKNOWLEDGMENTS

This work has been suggested by Professor C. A. Coulson, and the author is grateful for his sympathetic guidance and criticism, during both the prosecution of the work and the preparation of the manuscript. It is a pleasure also to acknowledge a British Council scholarship which made this work possible.

REFERENCES

Bowen, E. J., and Lawley, P. D., 1949, *Nature, Lond.*, **164,** 572.
Bowen, E. J., Mikiewicz, E., and Smith, F., 1949, *Proc. Phys. Soc.* A, **62,** 26.
Bowen, E. J., and Sawtell, J. W., 1937, *Trans. Faraday Soc.*, **37,** 1425.
Coulson, C. A., 1939, *Proc. Roy. Soc.* A, **169,** 143.
Coulson, C. A., and Longuet-Higgins, H. C., 1947, *Proc. Roy. Soc.* A, **191,** 39; **192,** 16.
Franck, J., and Livingston, R., 1941, *J, Chem. Phys.*, **9,** 184.
Franck, J., and Sponer, H., 1947–48, *Contribution a l'Étude de la Structure Moléculaire,* Volume Commémoratif V. Henri (Liège : Desoer), p. 169.
Garforth, F. M., Ingold, C. K., and Poole, H. G., 1948, *J. Chem. Soc.*, 508.
v. Halban, H., Kortüm, G., and Szigeti, B., 1936, *Z. Elektrochem.*, **42,** 628.
Hückel, E., 1931, *Z. Phys.*, **70,** 240; 1935, *International Conference on Physics* (London : Physical Society), p. 25.
Jacobs, J., 1949, *Proc. Phys. Soc.* A, **62,** 710.
Klevens, H. B., and Platt, J. R., 1949, *J. Chem. Phys.*, **17,** 470.
Kortüm, G., and Finckh, B., 1942, *Z. phys. Chem.*, 8, **52,** 263.
Lennard-Jones, J. E., 1937, *Proc. Roy. Soc.* A, **158,** 280.
Norrish, R. G. W., Crone, H. G., and Saltmarsh, O. D., 1934, *J. Chem. Soc.*, 1456.
Pitzer, K. S., 1948, *J. Amer. Chem. Soc.*, **70,** 2140.

Penetrating Particles in Air Showers

By C. B. A. McCUSKER
Dublin Institute for Advanced Studies

Communicated by L. Jánossy; MS. received 11*th April* 1950

ABSTRACT. The penetrating particles in extensive air showers are compared directly with the penetrating particles in the main cosmic-ray beam. It is found that not more than 70±3% of the air-shower particles are single μ-mesons, whilst the remainder are strongly interacting particles. The barometer coefficient of extensive penetrating showers is determined.

§1. INTRODUCTION

It is now well established that extensive air showers contain about 2% of particles more penetrating than electrons. It has been shown by Broadbent and Jánossy (1948), Salvini and Tagliaferri (1949) and others (Ise and Fretter 1949, Brown and McKay 1949) that some of the penetrating particles occur in groups. Other observers (Cocconi, Cocconi-Tongiorgi and Greisen 1949, Sitte, private communication) have demonstrated the presence of single penetrating particles, probably μ-mesons, coming from the air, and have shown, contrary to the supposition of Broadbent and Jánossy, that these make up the greater part of the penetrating component. The other component, which may be termed the interacting component (cf. Sitte), produces locally in the absorber small groups of particles which are themselves fairly penetrating. The present experiment was undertaken to determine the proportion in which these types of events occur and to investigate the nature of the interacting component.* When investigating the interacting component it is important to distinguish between the truly interacting events, in which a group of penetrating particles is produced locally in the absorber and events caused by two or more μ-mesons striking the apparatus simultaneously.

§2. THE EXPERIMENTAL ARRANGEMENT

The apparatus consisted of two unshielded trays S_1 and S_2 originally of area 750 cm^2 and later of area 1,500 cm^2, an unshielded anti-coincidence tray A of area 300 cm^2, and a penetrating shower set to record penetrating particles associated with air showers (Figure 1). The anti-coincidence tray was used as a bias against dense air showers. Such a bias is desirable, as in a dense region random association of two or more penetrating particles over the area of the penetrating shower set is to be expected frequently.

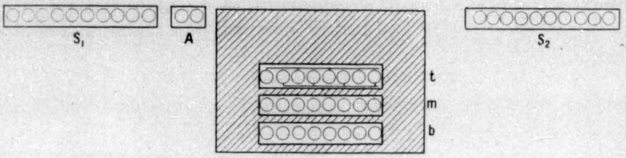

Figure 1. The counter arrangement.

Table 1

S_1, S_2–A accompanied by
(1) t_1 or t_2, m_1 or m_2, and b_1 or b_2, single event
(2) t_1 and t_2, m_1 or m_2, and b_1 or b_2
(3) t_1 or t_2, m_1 and m_2, and b_1 or b_2 } single ‘ knock-on ’ type
(4) t_1 or t_2, m_1 or m_2, and b_1 and b_2
(5) t_1 and t_2, m_1 and m_2, and b_1 or b_2
(6) t_1 and t_2, m_1 or m_2, and b_1 and b_2 } double ‘ knock-on ’ type
(7) t_1 or t_2, m_1 and m_2, and b_1 and b_2
(8) t_1 and t_2, m_1 and m_2, and b_1 and b_2, treble ‘ knock-on ’ type

The penetrating shower set consisted of three trays (t, m and b) each of area 1,200 cm^2. The trays were placed above each other with 2·5 cm. of lead between the trays, 20 cm. of lead above the top tray, 2·5 cm. below the bottom tray and 15 cm. on all sides (Figure 1). A master pulse consisted of a coincidence (S_1, S_2, t, m, b, – A), i.e. a fivefold coincidence between the two unshielded trays and the three trays of the penetrating shower set not accompanied by a pulse from the anti coincidence tray. That is to say, a master pulse required particles to strike each of the unshielded trays and at least one penetrating particle to traverse all three of the trays of the penetrating shower set. To distinguish between μ-mesons and the interacting component each of the trays t, m and b was arranged so as to be able to detect secondaries. For this purpose these trays were split into halves (t_1 and t_2, m_1 and m_2, b_1 and b_2). Each half consisted of four counters, the counters in the two sections alternating (Figure 1). When a master pulse occurred, coincidences between the two parts of each tray were accepted and recorded. The simultaneous occurrence of secondaries in any two of the trays, or in all three of the trays, was also recorded, thus giving the eight types of events shown in Table 1.

---

* I learned of Professor Sitte's work after having completed the present experiment. I am indebted to Professor Sitte for communicating his results.

The apparatus could be arranged in either of two positions. In the first, the two unshielded trays were placed vertically above the penetrating shower set and close to it (see Figure 2 (*b*)). In this position most of the master pulses were produced by single μ-mesons of the main cosmic-ray beam at a high counting rate ($\simeq$100/min.). In the second position the two unshielded trays were separated horizontally by 2 metres from the penetrating shower set and each other (Figure 2 (*a*)). By this arrangement extensive penetrating showers were detected.

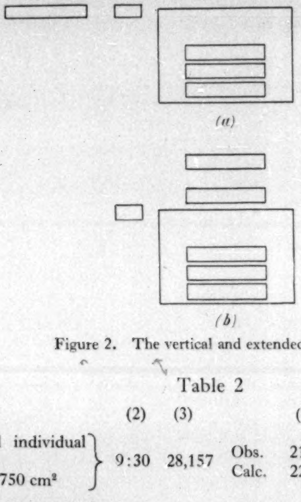

Figure 2. The vertical and extended positions.

Table 2

(1)	(2)	(3)		(4)	(5)	(6)	(7)
No lead round individual counters $S_1 = S_2 = 750\ \text{cm}^2$	9:30	28,157	Obs.	2108	141	28	$0{\cdot}075 \pm 0{\cdot}001$
			Calc.	2212	63	1	
0·25 cm. Pb round individual counters of penetrating shower set $S_1 = S_2 = 1{,}500\ \text{cm}^2$	27:30	109,862	Obs.	2817	225	52	$0{\cdot}026 \pm 0{\cdot}0005$
			Calc.	2991	29	1	

(1) Arrangement; (2) time; (3) total no. of events; (4) no. of single knock-on type events; (5) no. of double knock-on type events; (6) no. of treble knock-on type events; (7) ratio of no. of single knock-on type events to total no. of events.

§ 3. KNOCK-ON EVENTS PRODUCED BY THE MAIN COSMIC-RAY BEAM

The actual measurements with the first of the above arrangements (Figure 2 (*b*)) were spread over the period of the main experiment. Such runs, taken daily, also acted as a test of the apparatus. The results are given in Table 2.

It was found that wrapping individual counters of the penetrating shower set in lead foil 0·25 cm. thick greatly reduced the number of single knock-on type events. This reduction is easily understood assuming these events to be due to knock-on showers produced by μ-mesons, as these are predominantly of low energy. The probabilities for a μ-meson to produce respectively no detected secondaries, a single knock-on event, a double knock-on event, a treble knock-on event are $(1-p)^3$, $3p(1-p)^2$, $3p^2(1-p)$ and p^3, where p is the probability of the particle producing a detected secondary in any one tray. Assuming that the particles are all μ-mesons, and calculating p from the rate of single knock-ons, the expected numbers of double and treble knock-ons are given in Table 2.

It will be seen that the rate of single events is as expected but that the actual number of double and treble events is considerably greater than those expected on the knock-on hypothesis. Also the rate per penetrating particle of events not caused by multiple knock-ons is not greatly altered by wrapping the counters in lead. This rate is $0{\cdot}0037 \pm 0{\cdot}0004$ in the first case and $0{\cdot}0025 \pm 0{\cdot}0005$ in the second case. These events are probably either local penetrating showers or knock-on showers started by a single electron which are sufficiently energetic to penetrate the 2·5 cm. of lead between the trays. The gradual predominance of the local penetrating showers as the multiplicity of the coincidence is increased is in excellent agreement with the results of Jánossy (1942).

§ 4. EXTENSIVE AIR SHOWERS

In Table 3 the results for the extended arrangement are collected together.

Table 3

(1)	(2)	(3)	(4)	(5)	(6)	(7)	(8)	(9)
None	466:45	1006·4	207	0·46	31	16	12	$0{\cdot}15 \pm 0{\cdot}03$
0·25 cm.	629:10	1013·4	528	0·84	78	49	44	$0{\cdot}15 \pm 0{\cdot}02$

(1) Thickness of lead round individual counters of penetrating shower set; (2) time; (3) average barometric pressure (mb.); (4) no. of penetrating events; (5) rate per hour; (6) no. of single knock-on type events; (7) no. of double knock-on type events; (8) no. of treble knock-on type events; (9) ratio of single knock-on type events to total no. of events.

It can be seen from the above table that multiple discharges are much more frequent for penetrating particles from air showers than for ordinary μ-mesons. Tables 2 and 3 are, however, not directly comparable. The arrangement used to obtain the results of Table 2 selected single penetrating particles and, apart from an insignificant admixture, the groups can be attributed to the secondary effects of one particle. The shower arrangement, on the other hand, recorded events caused by a single particle and also events caused by the random association of several penetrating particles above the penetrating shower set. It is therefore necessary to assess the importance of random association before discussing the values of Table 3 directly.

§ 5. DISCUSSION OF RANDOM ASSOCIATION

Using well-known integrals (Auger and Daudin 1945, Broadbent and Jánossy 1948) it is possible to calculate many of the rates involved in the experiment, in particular the expected rate of showers containing two or more randomly associated mesons over the penetrating shower set. The calculated and observed values for the relevant rates are given in Table 4. The observed values are corrected to a barometric pressure of 1,000 mb. and the calculated values are normalized to a value 3·0 for coincidences S_1, S_2, t. The units are counts per hour. For the fraction of penetrating particles the value $k=1/40$ was assumed.

In making the calculation it was necessary to take into account the fact that the penetrating shower set required the particle to pass through three trays vertically arranged. It was assumed that this condition reduced the effective area of the set by a factor of two, and the calculations were made on this assumption. To confirm this assumption the apparatus was run in the extended position for a few days with the lower trays of the penetrating set and the anti-coincidence disconnected (S_1, S_2, t).

It will be seen from the table that the calculated rates for coincidences S_1, S_2, t; S_1, S_2, t, m, b and S_1, S_2, t, m, b–A are in very good agreement with the observed rates. This makes it likely that the calculated rate (S_1, S_2, t, m, b, s–A) for the incidence of two or more mesons in the penetrating shower set will be an accurate prediction of the actual rate. It is not possible to check this directly by experiment since the penetrating shower set is unable to distinguish between a coincidence caused by two or more mesons coming from the air and, say, a coincidence caused by a penetrating shower produced in the absorber by a single nucleon. However, the rate at which two or more randomly associated mesons strike the two halves of any one tray (t, m or b) is identical with the rate at which two such mesons strike one-half of a tray and another separately shielded tray S placed near to the penetrating shower set. Such a tray, of area 800 cm², and shielded similarly to the penetrating shower set, was constructed and the rate (S_1, S_2, t, m, b, s–A) determined. This rate is given in Table 4. The agreement between all the calculated and measured rates is excellent, and from both it follows that with the selection used for the main experiment (S_1, S_2, t, m, b–A) only 3% (the ratio of S_1, S_2, t, m, b, s–A to S_1, S_2, t, m, b–A) of the events recorded were due to two or more mesons striking the penetrating shower set simultaneously.

Table 4

Type of coincidence	S_1, S_2, t	S_1, S_2, t, m, b	S_1, S_2, t, m, b–A	S_1, S_2, t, m, b, s–A
Calculated	3·0	1·60	0·82	0·018
Observed	3·0 ± 0·13	1·62 ± 0·06	0·96 ± 0·02	0·020 ± 0·007

§6. THE PENETRATING PARTICLES IN EXTENSIVE AIR SHOWERS

Since the number of events due to multiple mesons is so small it is possible to compare Tables 2 and 3 directly. It will be seen that, while wrapping the counters of the penetrating shower set in 0·25 cm. of lead reduces the knock-on rate for μ-mesons by a factor of three, it has no effect on the number of secondaries recorded for the penetrating particles in air showers. Also, since the knock-on probability for μ-mesons for this apparatus, with lead around the counters, is 0·9% per tray, the expected number of secondaries, if all the penetrating particles in extensive showers were μ-mesons, is 14; the number recorded is 308. It follows that at least 157 of the penetrating particles observed were not single μ-mesons and, therefore, that the maximum proportion of μ-mesons in the penetrating particles of extensive air showers is 70 ± 3%. This figure is in agreement with the rough estimate of

Cocconi, Tongiorgi and Greisen and with Sitte's more accurate determination. It has already been shown that 3% of the events are caused by two or more mesons striking the penetrating shower set. The remainder of the penetrating particles may be called the interacting component.

§7. THE INTERACTING COMPONENT

It follows from the above that the minimum proportion of the interacting component is 25%. In order to estimate the maximum proportion it is necessary to know the probability of an interacting particle falling on the penetrating set without producing a coincidence in the trays. This can happen (*a*) when the interacting particle does not produce a shower, and (*b*) when a shower is produced which only sets off one-half of each of the trays t, b and m.

Assuming that one-third of the area of each of the trays t, m and b is dead space, the probability that a shower of n particles which sets off one tray will also set off the other is

$$P=1-\frac{2^{n+1}-1}{3^n}.$$

The probability of such a shower producing a single knock-on event, a double knock-on type event and a treble knock-on type event is $3P(1-P)^2$, $3P^2(1-P)$ and P^3. These probabilities for $n=2, 3, 4, 5$ and 6 are given in Table 5.

Table 5

No. of particles	2	3	4	5	6
P	0·22	0·43	0·63	0·74	0·82
$1-P$	0·78	0·57	0·37	0·26	0·18
Probability of single event	0·49	0·18	0·06	0·04	0·01
Probability of single knock-on type event	0·40	0·42	0·26	0·14	0·08
Probability of double knock-on type event	0·10	0·32	0·44	0·42	0·36
Probability of treble knock-on type event	0·01	0·08	0·24	0·40	0·55

If a distribution of number of showers against number of particles per shower is assumed which produces a good fit for single, double and treble knock-on type events it is possible to estimate the number of showers which produce no coincidences between the halves of the trays. A suitable distribution is given in Table 6.

Table 6

No. of particles	2	3	4	5	6	>6
Relative no. of showers	30	15	8	6	4	8

This distribution is very similar to that found by Camerini *et al.* (1949) for penetrating showers in photographic plates. Assuming such a distribution, 51 showers which do not cause any coincidences in trays t, m and b are expected in 528 penetrating events, and therefore, according to this distribution, one is led to expect that the interacting component constitutes 35% of the particles. It is difficult to estimate the probable error of this figure. It must be remembered also that this figure has been calculated assuming that all interacting particles produce a shower in the absorber. Since this is probably not true, the actual percentage of interacting particles may be somewhat greater.

§ 8. ADDITIONAL EVIDENCE

The apparatus was run for 764 hours with the top 5 cm. of absorber of the penetrating shower set raised by 50 cm. The solid angle subtended by the absorber at the counters was maintained constant. This was done in an attempt to investigate the interacting component. The proportion of the total flux formed by the interacting component was not known at the time, and it was expected that raising the point at which the interaction occurred might have a considerable effect on the distribution of multiple events. No change outside the statistical fluctuations was however found but, considering the final results, none is in fact to be expected. These results, given in Table 7, may therefore be added to those in Table 3.

Table 7

(1)	(2)	(3)	(4)	(5)	(6)	(7)	(8)	(9)
0·25 cm.	764:45	1001·4	764	1·0±0·07	109	64	62	0·14±0·02

(1) Thickness of lead round each counter of penetrating set, top 5 cm. of absorber of penetrating set raised; (2) time; (3) average barometric pressure; (4) no. of penetrating events; (5) rate per hour; (6) no. of single knock-on type events; (7) no. of double knock-on type events; (8) no. of treble knock-on type events; (9) ratio of single knock-on type events to total no. of events.

§ 9. BAROMETRIC COEFFICIENT

The average barometric pressure was taken for each day when the apparatus was running and the barometric coefficient of extensive penetrating showers calculated from this. The value obtained was 9·5 ± 1·2% per cm. Hg, which is in good agreement with the value obtained in other experiments at sea level (Millar 1950, Jánossy and Rochester 1944).

§ 10. DISCUSSION

(*a*) *Comparison with Sitte's Results*

It is possible to compare these results with those of Sitte, obtained with a very different arrangement. He found the ratio of the interacting component to the μ-meson component to be 0·26 ± 0·03. However, he made no attempt to exclude events in which several particles fell on his hodoscope set. For μ-mesons he finds that 75 ± 2% were single particles and, for interacting particles, 62 events out of 90 were due to single particles; in 10 cases the primary was accompanied by another penetrating particle, and 18 events were too complex to be analysed. Thus according to Sitte the proportion of μ-mesons in the single events is 78 ± 5%.

The difference between this result and that of the present experiment (65 ± 8%) is not greater than the combined errors. A small difference might be expected because of the difference in selection, which in Sitte's case was more stringent for interacting particles, and also because of the difference in altitudes, sea level and 3,260 m., at which the experiments were carried out.

(*b*) *Comparison with the Results of Broadbent and Jánossy*

Broadbent and Jánossy (1948) concluded that the penetrating particles which they observed in extensive air showers could not be μ-mesons coming from the air. The results of the present experiment show that about 65% of the penetrating particles associated with extensive air showers are μ-mesons. These two results are due to the different type of selection used. The apparatus of Broadbent and

Jánossy would not respond to passage of a single μ-meson except in the unlikely case of a triple knock-on event, the probability of which the authors estimate at 10^{-6}. The penetrating particles detected by them were probably identical in nature with the interacting component of this experiment. The transition effect they found (Broadbent and Jánossy 1946) was, however, entirely different from that found for local penetrating showers. This may be due to the fact that in extensive showers the interacting particle will generally be associated with a large number of electrons which set off the top tray in their experiment. This would account for the increase in rate when 2 cm. of lead was placed on top of that tray. The transition curve obtained would be a mixture of the electron transition curve and that due to the interacting component.

§ 11. CONCLUSION

It has been shown that there are at least two types of penetrating particle in extensive showers. The upper limit for the proportion of μ-mesons is $70 \pm 3\%$. The actual proportion is probably in the region of 65%. The other component is strongly interacting and is probably composed of nucleons. The results are in reasonable agreement with other recent experiments.

ACKNOWLEDGMENTS

The author is greatly indebted to Professor Jánossy for many valuable discussions. He also wishes to thank Professor L. W. Pollak for making available his meteorological records and Dr. D. M. Ritson and Mr. D. D. Millar for help in building and running the apparatus.

REFERENCES

Auger, P., and Daudin, J., 1945, *J. Phys. Radium*, **6**, 233.

Broadbent, D., and Jánossy, L., 1946, *Proc. Roy. Soc.* A, **190**, 497; 1948, *Ibid.*, **192**, 364.

Brown, W. W., and McKay A. S., 1949, *Phys. Rev.*, **76**, 1034.

Camerini, U., Coor, T., Davies, J. H., Fowler, P. H., Lock, W. O., Muirhead, H., and Tobin, N., 1949, *Phil. Mag.*, **40**, 1073.

Cocconi, G., Cocconi-Tongiorgi, V., and Greisen, K., 1949, *Phys. Rev.*, **75**, 1063.

Ise, J., Jr., and Fretter, W. B., 1949, *Phys. Rev.*, **76**, 933.

Jánossy, L., 1942, *Proc. Roy. Soc.* A, **179**, 361.

Jánossy, L., and Rochester, G. D., 1944, *Proc. Roy. Soc.* A, **183**, 186.

Millar, D. D., 1950, *Proc. Irish. Acad.*, in the press.

Salvini, G., and Tagliaferri, G., 1949, *Nuovo Cim.*, VI, 108.

Observations of Cosmic-Ray Events in Nuclear Emulsions Exposed below Ground

By E. P. GEORGE and J. EVANS
Birkbeck College, University of London

MS. received 29*th March* 1950; *read on* 29*th September* 1950

ABSTRACT. Ilford Nuclear research plates were manufactured in a laboratory at an equivalent depth of 60 m. of water below ground. After having been stored at various depths, the plates were processed below ground. The observed frequencies of μ-mesons stopped in the plates are consistent with those expected from measurements on the energy-spectrum of cosmic rays. Several π-mesons stopping in the plates were observed, and reasons for believing these to have been locally produced in the matter near the plates are discussed.

Forty-two nuclear disintegrations have been observed, the frequency at a depth of 60 m. water equivalent being of the order of 5×10^{-3} stars/cm^3/day. Approximately one third of these are attributed to the electromagnetic interaction of μ-mesons on their passage through nuclei. The remainder are attributed in part to neutrons from this first group of stars, and in part to the photons of the soft component underground.

Four examples of stars accompanied by showers of particles at minimum ionization have been observed, and are discussed.

§ 1. INTRODUCTION

In the last few years, many studies have been made of the frequency of occurrence of nuclear disintegrations observed in nuclear emulsions exposed under absorbers of various thicknesses. The frequency had been determined at many points in the atmosphere by Addario and Tamburino, Powell, Page, Bernadini, George and Jason, Harding *et al.*, and many others. At mountain altitudes, several of these workers have determined the frequency of stars in plates exposed under ice, carbon, aluminium and lead. The absorption length of the radiation causing the stars has been found to vary from about 150 gm/cm^2 in air and other light materials to about 300 gm/cm^2 in lead. These results support the general view that most of the stars are produced by particles possessing a strong interaction with atomic nuclei, presumably the primary protons and the secondary nucleons to which they give rise in the atmosphere. The frequency of stars produced by these nucleons at a depth below ground equivalent to 60 m. of water would be undetectably small, of the order of $\exp(-40)$ per cm^3 per day.

On the other hand, evidence for the production of meson pairs at this depth has been reported by Braddick and Hensby (1939), and one would conclude that the processes leading to the production of these meson pairs would be likely to result in the disintegration of atomic nuclei also.

It therefore seemed worth while to determine whether stars could be detected underground, and if so to determine their frequency and general properties. In order to ensure that any stars observed were actually produced below ground, Ilford Nuclear research plates were prepared in our underground laboratory, and were brought to the surface only after they had been processed.

In the plates obtained in this way, a small but finite rate of production of stars was recorded, and the preliminary results were described in a note in *Nature*

(Evans and George 1949). A fuller account of the observations is given in the present paper. The statistical accuracy of the results is poor, but as it will take some time to improve this aspect of the investigation, it was thought that the present interim report would be of some interest.

§ 2. EXPERIMENTAL DETAILS

The coatings were performed in our underground laboratory on a disused part of Holborn Station, and at a depth equivalent to 60 m. of water. Up to the present, two separate batches of plates have been coated; for the first batch, Ilford type C2 emulsions were used, for the second, the Ilford 'electron sensitive' type, G5. The emulsion for both batches was brought molten from the factory and poured on to glass plates at Holborn. In each case emulsions 200 microns thick were used.

The C2 plates of the first batch were left at a depth of 60 m., while the G5 plates of the second batch were divided into three groups: one group was left in the laboratory at 60 m. water depth, one group was taken to another platform at a different depth at Holborn (34 m. water) and the remaining group was taken by Underground train and left at Arsenal Station which is at an equivalent depth of 20 m. water.

§ 3. THE FREQUENCY OF SLOW MESONS

In the examination of 144 cm^3 of emulsion, a total of 363 mesons have been observed to come to rest of which the greater part were μ-mesons. A few π-mesons have been observed also. We give our results for these mesons separately.

3.1. *μ-Mesons*

Table 1 shows the observed frequencies of occurrence of μ-mesons brought to rest in plates exposed at sea level and the three different depths underground.

Table 1

Depth (m. water)	0	20	34	60
μ-meson per cm^3/day	$0{\cdot}70 \pm 0{\cdot}05$	$0{\cdot}091 \pm 0{\cdot}009$	$0{\cdot}055 \pm 0{\cdot}004$	$0{\cdot}017 \pm 0{\cdot}002$

Rossi (1948) has given a curve showing the expected numbers of mesons stopping per gramme of air, per unit solid angle in the vertical direction, and our results are compared with his curve in Figure 1. In reducing our results to standard units, we have allowed for the mesons lost due to plate geometry (cf. Lattes, Occhialini and Powell 1947), and for the relative stopping powers of air and nuclear emulsion, and have assumed that the frequency of slow mesons travelling in a direction θ from the vertical varies as $\cos^3\theta$ (cf. Kraushaar 1949).

From Figure 1, it is seen that the observed numbers of slow mesons are in fair agreement with the expected values, the underground results being low by a mean value of $35 \pm 6\%$. Some part of the difference must be attributed to the fact that under the conditions of microscopic examination of the underground plates ($\times 10$ objective, $\times 6$ eyepieces), some of the mesons probably escaped observation. The question of the angular distribution of slow μ-mesons will be taken up later, when we have observed a sufficient number. If the distribution were proportional to $\cos^2\theta$ underground, the experimental points would have to be lowered by 25%.

Approximately one half of the plates were developed after 6 weeks exposure, and the rest after 12 weeks. Of the μ-mesons ending in G5 plates, $50 \pm 5\%$ were accompanied by the track of the characteristic decay-electron. Cosyns *et al.* (1949), using exposures of 6 and 12 days, have shown that $62 \pm 4\%$ of the mesons above ground decay in G5 emulsions, but that in plates 200 microns thick, 20% of the decay tracks would not be observed for reasons of geometry. Assuming the ratio of positive to negative μ-mesons to be the same below ground, we see that the observed number agrees well with the expected number of μ-mesons showing β-decay. From this we may conclude that the loss of minimum tracks even after three months was negligible under our conditions of exposure.

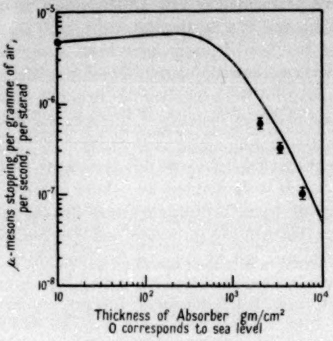

Figure 1. Slow μ-mesons as a function of depth below sea level.

Out of a total of 363 μ-mesons, 10 (i.e. $2{\cdot}7 \pm 0{\cdot}9\%$) were observed to enter the emulsion from below the horizontal.

3.2. π-*Mesons*

Eight π-mesons have been observed to come to rest in our underground emulsions, of which four were positive and four were negative. Figure 2 (Plate I) shows a mosaic of photographs in which a positive π-meson stops in one of the G5 plates and emits a μ-meson which also ends in the emulsion. The decay electron which originates from the end of the μ-meson can be clearly seen. The number observed is too small to enable us to determine the variation of slow π-mesons with depth below ground. We accordingly group the results together, and divide by the total exposure of all the underground plates ($=8{\cdot}8 \times 10^3\,\text{cm}^3 \times \text{days}$) and obtain a mean figure for the frequency of slow π-mesons at the mean depth of 34 m. water:

$$N_\pi' = (9{\cdot}1 \pm 3{\cdot}2) \times 10^{-4} \text{ per cm}^3 \text{ per day.} \qquad \ldots\ldots(1)$$

Since the plates were exposed at a mean distance of about three metres from the walls of the tunnel, and since we may take 10^{-8} sec. as the lifetime of the π-meson at rest, we may infer that, but for decay in the air gap between the tunnel walls and the plates, about three times as many π-mesons would have been observed:

$$\mathrm{N}_\pi \sim (2{\cdot}7 \pm 1{\cdot}0) \times 10^{-3} \text{ per cm}^3 \text{ per day.} \qquad \ldots\ldots(2)$$

In other words, 24 π-mesons were travelling with suitable values of direction and energy to come to rest in our plates, of which 16 decayed in flight in the air space. Of the eight that arrived, four entered the emulsion from above the horizontal and four from below. If we assume that the 16 decaying π-mesons were similarly distributed in direction, then we may infer that, during the sensitive time of the plates, about eight π-mesons travelling towards the plates from below decayed in flight, giving rise to μ-mesons. The actual number of upward travelling μ-mesons observed was 10 (see above), and therefore may be accounted for by the decay of the observed upward stream of π-mesons. A similar interpretation of the upward stream of μ-mesons observed at the Jungfraujoch was advanced by Camerini, Muirhead, Powell and Ritson (1948). The question of the origin of the π-mesons is discussed below.

§4. NUCLEAR DISINTEGRATIONS

Up to the present we have observed 42 nuclear disintegrations giving rise to 'stars' with three or more branches, which have been produced below ground, 18 in C2 plates and 24 in G5 plates. Of the 24 observed in the G5 plates, 10 were stars with charged primary particles and 14 stars with neutral primary particles. Four stars were associated with showers of fast electrons.

4.1. *The Size–Frequency Distribution*

In Figure 3 (*a*) is plotted a histogram showing the number of stars observed with a given number of heavy tracks, N_h, as a function of N_h. In Figure 3 (*b*) is plotted for comparison the corresponding histogram for about 10,000 stars observed in our laboratory in plates exposed at the Jungfraujoch. Within the rather wide limits of statistical error, the two size–frequency distributions appear to be similar.

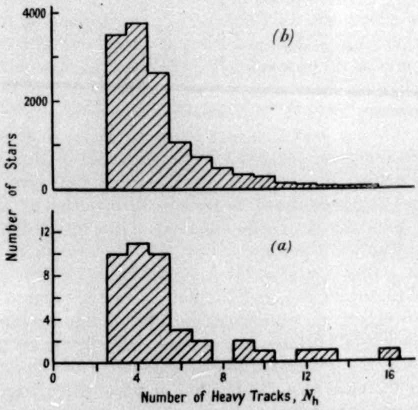

Figure 3. Distribution of the numbers of heavy tracks for stars observed (*a*) underground and (*b*) at the Jungfraujoch.

4.2. *The Frequency of Stars versus Depth below Ground*

In Table 2 are given the details of the star-frequencies observed at sea level and at the three different depths below ground at which the plates were exposed. The results from C2 and G5 type emulsions are included together.

Table 2

Depth below ground (m. H_2O)	No. of stars observed	Frequency of stars per cm^3 per day
0	383	1·46±0·07
20	7	0·0066±0·0025
34	13	0·0044±0·0012
60	22	0·0050±0·001

The statistical accuracy is poor, and is not likely to be greatly improved using nuclear emulsion techniques. It appears however that there is only a slow variation in the frequency of occurrence of stars with depth below ground. It is exceedingly unlikely, for example, that the frequency differs by as much as 4 : 1 between 20 and 60 m. water.

The star frequency varies by a factor of approximately 10^3 between the top and bottom of the atmosphere, equivalent to 10 m. water, and this would correspond to a variation of the order of 10^{12} for an absorber equivalent to 40 m. water. The particles responsible for the stars below ground may with confidence be assumed to be different from those responsible for the bulk of the stars observed above ground.

4.3. *Stars associated with Fast Particles*

Using the G5 plates, the grain density, g_{min}, corresponding to particles with minimum ionization was determined from the many straight tracks produced by cosmic-ray particles of great energy. The value so obtained was $g_{\text{min}} = 340$ grains/mm. Following Brown *et al.*, a 'fast' particle is defined as one producing a grain density less than $1{\cdot}5\, g_{\text{min}}$. A star was assumed to be produced by a charged primary particle if it was associated with a fast particle at an angle less than 90° to the vertical (cf. Brown *et al.* 1949 b). In the event of two or more tracks satisfying this condition, the track nearest the vertical was taken.

Of the 42 stars discussed above, 18 were in C2 emulsion in which the tracks of fast particles would not have been observed. The remainder were observed in G5 emulsion, and of these 24 stars, 10 (i.e. 42%) were produced by fast charged primary particles. Brown *et al.* (1949 a, b) and Page (1950) have reported that in plates exposed at the Jungfraujoch 17% of the stars are produced by fast charged particles. If this proportion were maintained in the underground events then, out of 24 stars, four would be expected to show charged primary particles. The probability of observing ten instead of four on account of a fluctuation is 0·013. It appears likely therefore that the fraction of stars with charged primaries is greater below ground than it is at mountain altitudes.

For each of these ten stars, we have measured the angle θ between the vertical and the projection in the plane of the emulsion of the track of the fast primary particle. The values thus obtained are 4, 10, 12, 18, 27, 31, 33, 36, 37 and 48 degrees respectively.

In five of these stars produced by fast charged particles, a single fast particle was observed on the lower side of the star. Two photo-micrographs of events

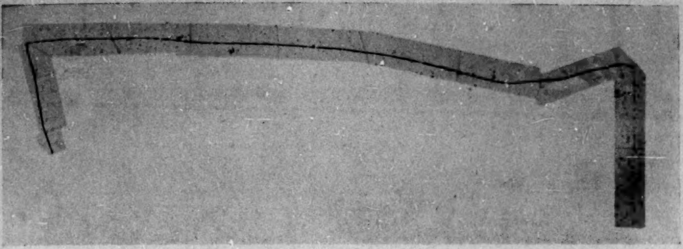

Figure 2. A positive π-meson, observed at a depth of 60 m. water, entered the emulsion from below the horizontal, showing the characteristic π–μ decay and also the β-decay of the μ-meson. Observer: J. Evans.

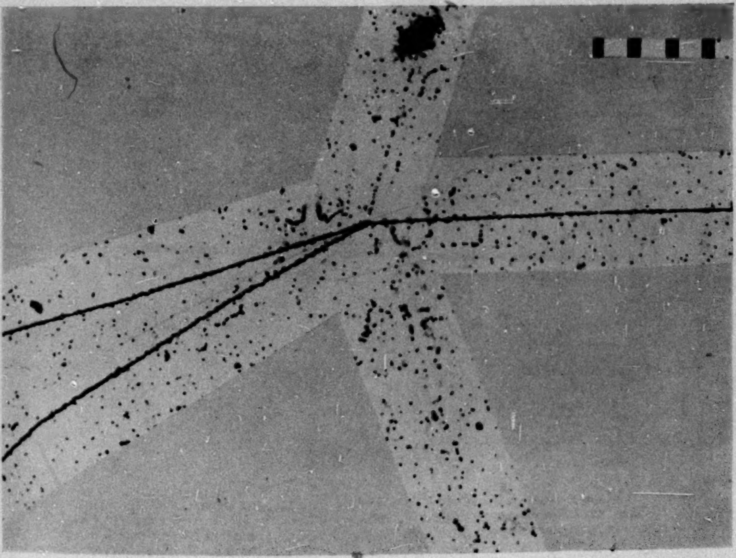

Figure 5. A disintegration produced by a fast charged particle at a depth of 20 m. water. The angle of deviation of the fast particle is 30°, the largest that has so far been observed in underground stars of this type. Observer: E. P. George.

Plate I.

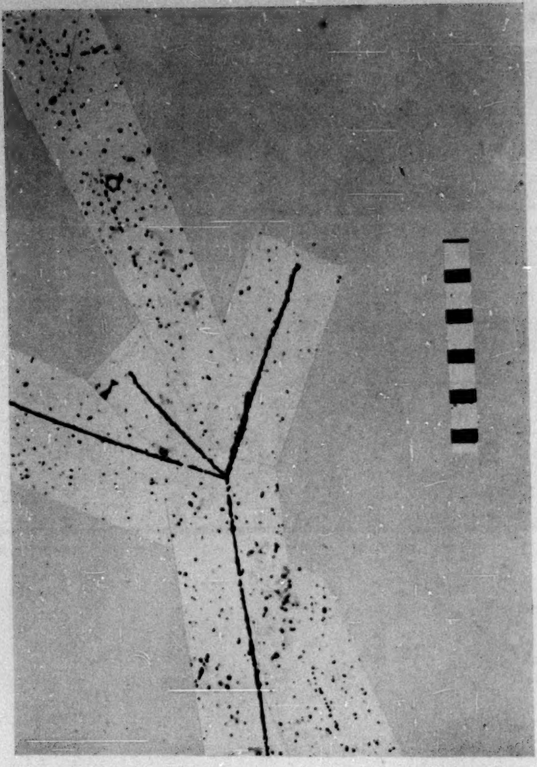

Figure 4. A disintegration produced by a fast charged particle at a depth of 60 m. water. We attribute this type of star to nuclear excitation produced by a fast μ-meson. The electromagnetic interaction between the charge of the μ-meson and neutrons and protons is probably sufficient to account for the observed frequency. In this, and Figure 5, the scale shows steps of 10 microns.
Observer: E. P. George.

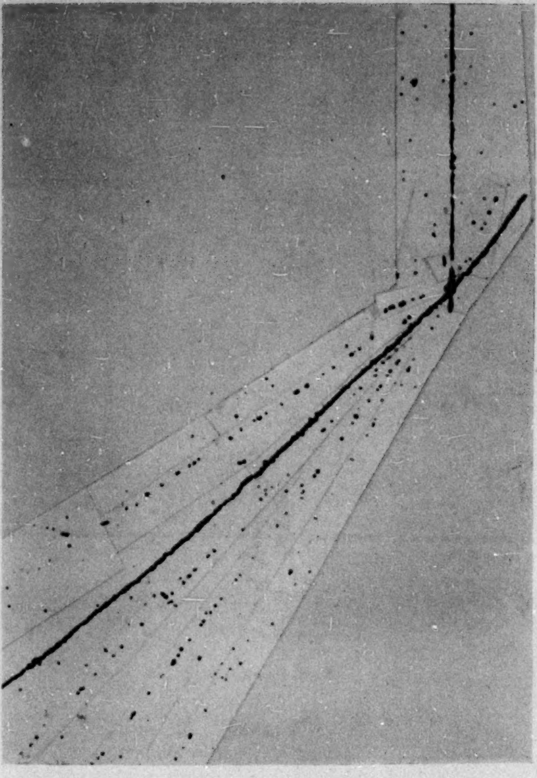

Figure 7. A disintegration produced by a fast charged particle at a depth of 34 m. water, and accompanied by a shower of 5 fast particles. The event occurred very near the surface of the emulsion, and the track of the primary particle, and one of the shower particles, are very short but may be clearly distinguished. Observer: Mrs. M. H. GEORGE.

PLATE III.

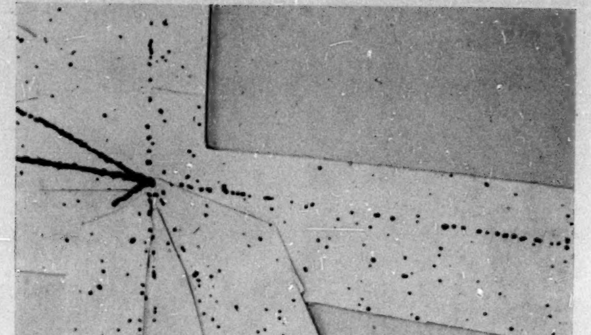

Figure 8. A disintegration, produced by a fast charged particle at a depth of 34 m. water and accompanied by a shower of 5 fast particles. Observer: Mrs. M. H. GEORGE.

of this type are shown in Figures 4 and 5 (Plates I and II). The simplest interpretation of this type of event is that the energetic fast particle is scattered by a nucleon inside an atomic nucleus. The recoil momentum of the scattered nucleon then leads to the disintegration of the nucleus. From the fact that the size–frequency distribution of the underground stars is similar to that for stars observed at mountain altitudes, we may make use of the analysis of Brown *et al.* (1949 b) in order to determine the mean energy of a star having a given number, N_h, of heavy tracks. These authors give the relation between energy and N_h:

$$E(\text{MeV.}) = 37N_h + 4N_h^2. \qquad \ldots\ldots(3)$$

Assuming a value for the mass of the fast particle, and that the collisions are elastic, then equation (3) combined with a knowledge of the angle of deflection

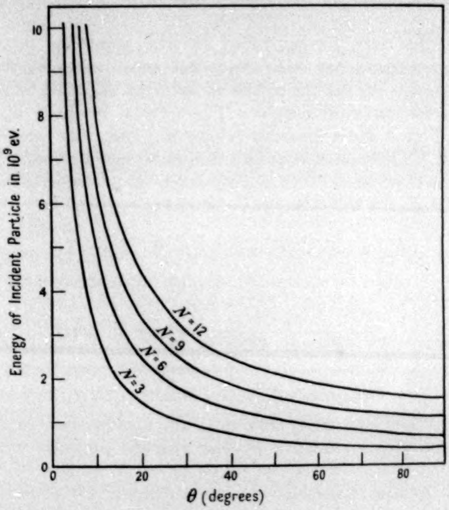

Figure 6. Relation between the angle of deflection and energy of the incident particle, for stars produced by the elastic scatter of μ-mesons. Plotted for various values of N, the number of tracks per star.

of the incident particle leads to an estimate of its energy from the conservation laws. For the angles of deflection observed, the energies of the fast particles calculated in this way depend very little on their assumed mass. By way of illustration, a series of curves showing the relation between the energy and angle of scatter for fast μ-mesons has been evaluated for various values of N_h, and is plotted in Figure 6. Using these curves, the energies of the initial particles, assumed therefore to be μ-mesons, are given in Table 3. Other assumptions concerning the nature of the initial particles will be discussed in §5. Event No. 5, in Table 3, occurred too near the emulsion surface to enable a reliable estimate of the deflection to be made. From Figure 6 it is seen that the deduced energies increase rapidly for small angles of deflection. The energies in the bottom line of Table 3 should therefore be treated with some reserve and taken merely as an indication of the order of magnitude. They are seen to lie in the region 10^9–10^{10} ev., values which are not unreasonable.

In one of these ten stars, produced by fast charged particles, no fast particles leaving the point of collision could be identified.

Table 3

Event No.	1	2	3	4	5
Depth below ground (m. H_2O)	20	34	60	60	60
Size of star N_h	3	4	5	4	10
Energy of star (Mev.)	147	212	285	212	770
Angle of deflection of fast particle (deg.)	30	5	12	2·5	—
Energy of fast particle (assumed μ-meson) (Mev.)	1000	7300	3500	15000	—

Assuming the stars are produced by the μ-mesons of the penetrating component, an estimate may be made of the cross section for the production of stars by μ-mesons. We use the results at the greatest depth, 60 m. water, as they have the greatest statistical weight. The vertical intensity at this depth was measured by Follett and Crawshaw (1936) and found by them to be 6% of the sea-level value. This corresponds to a flux of 80 fast μ-mesons per cm^2 per day. This figure has since been confirmed by many measurements in our laboratory. The frequency of stars with charged primaries is

$$2 \times 10^{-3}/\text{cm}^3/\text{day} = 5 \times 10^{-4}/\text{gm}/\text{day}.$$

Hence the cross section for star production by fast μ-mesons is given by

$$\sigma = \frac{5 \times 10^{-4}}{80 \times 6 \times 10^{23}} \simeq 10^{-29}\,\text{cm}^2/\text{nucleon}. \qquad \ldots\ldots(4)$$

4.4. *Stars associated with Showers of Fast Particles*

One of the more interesting features of the underground stars is that four of the ten disintegrations produced by fast charged particles were accompanied by the emission of showers of fast particles, while none of the disintegrations produced by neutral particles was accompanied by showers. Mosaics of photo-micrographs of two examples with five shower particles are shown in Figures 7 and 8 (Plates III and IV). The other two examples were associated with showers of three fast particles. The values of the grain density of the shower particles all lie between 0·93 and 1·14 $g_{\min}$. The angles ϕ in the plane of the emulsion, between the direction of the incident particle and the shower particles were measured, and a histogram showing the distribution in ϕ is given in Figure 9. A comparison with the angular distributions of Brown *et al.* (1949 b) for similar showers observed at the Jungfraujoch suggests that the angular distribution of the underground shower particles is rather similar to that in showers at mountain altitudes, though again it is recognized that our observations need to be extended before detailed comparisons can be made.

Of the stars observed with charged primaries at 70,000 ft. by Camerini *et al.* (1949) and at 11,000 ft. by Brown *et al.* (1949 b), 18% were accompanied by showers of three or more particles. If this fraction were the same below ground, then out of a total of ten events, the expected number of showers would be 1·8 and the probability of observing four instead due to fluctuation is 0·06.

The showers seem very similar in appearance and general properties to those observed in similar plates exposed above ground except for the fact that all those observed below ground are associated with charged primary particles.

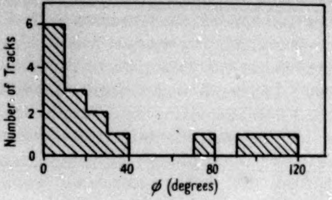

Figure 9. Distribution in the values of ϕ of the tracks of shower particles. ϕ is the angle in the plane of the emulsion, between the incident particle (produced) and a shower particle.

§ 5. DISCUSSION OF RESULTS

The frequency of slow μ-mesons underground is seen to be close to the expected value, and does not therefore call for further comment. The remaining features of our observations, for which an explanation is sought, may be summarized as follows:

(i) The frequency of slow π-mesons stopping in solid matter is approximately $2{\cdot}7 \times 10^{-3}$ per cm^3 per day (equation (2)).
(ii) The frequency of stars is approximately 5×10^{-3} per cm^3 per day at a depth of 60 m. water.
(iii) The variation of the star frequency between 20 m. and 60 m. water depth below ground is small.
(iv) The size–frequency distribution of the underground stars is not very different from that of the stars observed at sea level and mountain altitudes.
(v) About 40% of the underground stars are produced by charged particles.
(vi) Four out of ten stars produced by fast charged particles are associated with showers of fast particles.

We will discuss in the first place those stars produced by fast charged particles. There are two questions to be answered: what are the particles producing the stars? and what is the mechanism of the interaction?

As to the first question, we think the charged particles producing the underground stars must in nearly all cases be assumed to be the μ-mesons. This is suggested by the slow variation of star frequency with depth, and is justified in the following argument.

5.1. *The Charged Particles producing Underground Stars*

The grain density in the tracks of the fast particles is close to $g_{\min}$, and hence the particles possess charge $\boldsymbol{e}$ and kinetic energy greater than or equal to $2\boldsymbol{mc}^2$, where $\boldsymbol{m}$ is their rest mass. They might therefore be protons, π-mesons, μ-mesons or electrons.

From the fact that the general features of the underground stars are rather similar to those of the stars observed at mountain altitudes, except for a reduction in frequency of about 2,000, one might be tempted to assume that the particles causing the stars are the same in both places, i.e. principally cosmic-ray nucleons. On this viewpoint, the stars with fast charged primaries would be due to protons and possibly to some extent to π-mesons. However, this is completely at variance with the observed slow variation of star frequency with depth, the discrepancy being a factor of 10^{12}. It would be necessary to postulate some process leading to the generation underground of energetic protons by the μ-mesons forming the penetrating component. In general, such a process would lead to the simultaneous disintegration of the nucleus supplying these fast protons, i.e. to the production of stars by μ-mesons. This contradicts the premise from which we started, that the fast particles causing stars are protons. The only condition under which protons could be accepted as the primary agent would be that relativistic protons be generated by μ-mesons underground in a process not associated, in general, with a nuclear disintegration, and this seems a rather artificial assumption.

The possibility that the charged primary particles are π-mesons may be eliminated on two grounds. One of the arguments is the same as that used above against protons. The absorption length, L_A, of π-mesons in the energy interval 200–800 MEV., reported by Camerini *et al.* (private communication), is approximately 100 gm/cm² of nuclear emulsion, which corresponds to a cross section for absorption close to the nuclear geometric cross section. This figure is at variance with the figure $L_A > 1{,}200$ gm/cm² reported by Piccioni, who measured the absorption of penetrating shower particles with a system of counters. However, the former result, based on a more direct measurement seems much less open to doubt and is to be preferred. Accepting this figure of $L_A \sim 100$ gm/cm², all the arguments against identifying as protons the fast charged particles causing the stars may be taken as applying to π-mesons also. A further argument against π-mesons may be based on the observation of Camerini *et al.* that of 25 stars in which they were able to identify the fast primary particle as a π-meson, in 20 cases the incident particle was absorbed and no fast particle was detectable on the other side of the star (called by these authors O_p-type stars). In the remaining cases, one fast track was observed on the further side of the star (type I_p in their nomenclature). The situation is reversed in our stars. Out of a total of six, five were of type I_p (see Figures 4 and 5), and one was of type O_p. Hence we think it safe to assume that the charged particles producing stars underground are, in general, not π-mesons.

The ionization loss of particles penetrating to our deepest level is $1{\cdot}2 \times 10^{10}$ ev., and we have based part of our argument against π-mesons on the observation that the absorption length of these particles is of the order of 100 gm/cm² at lower energies. Heitler (1941) and Wilson (1941) have shown that taking radiation damping into account, the cross section for collision with nucleons is proportional to $1/E$, at high energies; this raises the possibility that π-mesons of sufficient energy to penetrate below ground may have a nuclear cross section sufficiently small that they may arrive in large enough numbers and yet sufficiently large that they can cause the observed stars. The situation at these high energies is by no means clear, as we have no direct evidence concerning the penetration of π-mesons in the energy range in which we are interested. Basing our argument on the theories of Heitler and Wilson, it is again concluded that π-mesons are unlikely to be responsible for the underground stars.

Electrons may be eliminated by referring to the estimated energies of the charged particles in Table 3. Here they were assumed to be μ-mesons, but the energies of the particles if assumed to be electrons would be comparable. Energetic electrons, arising from knock-on collisions with μ-mesons, are known to exist below ground, and it may be shown that the path length of the electrons with energies greater than 10^9 ev. is 3×10^{-4} times that of the μ-mesons. In order to account for the observed frequency of stars it would be necessary to assume a collison cross section of 3×10^{-26} cm^2 per nucleon for these electrons, i.e. a cross section of the same order of magnitude as that for nucleon–nucleon collisions. Hence, we need not consider electrons as the agents causing the stars with fast charged primary particles.

This leaves us as the only alternative the μ-mesons. There is no difficulty in accounting for the presence of these particles, since they are considered to constitute the main component of the cosmic-ray flux at sea level and below ground, and we have shown that the number stopping and identified as μ-mesons in the photographic emulsions is close to the number expected. The only objection that may be advanced is that μ-mesons are thought to have such a weak interaction with nuclear matter that they could not cause the observed frequency of occurrence of stars. In fact, from observations of the β-decay of μ-mesons in solid matter, it may be concluded that the cross section for the nuclear collision of μ-mesons is of the order of 10^{-39} cm^2 per nucleon, whereas in order to account for the observed star frequency we would need to assume a cross section of the order of 10^{-29} cm^2 per nucleon. However, the μ-mesons, being charged, experience an electromagnetic interaction with nucleons, and it is shown below that this mechanism leads to a cross section of the right order of magnitude.

5.2. *Nuclear Collisions of Fast Charged Particles by the Coulomb Interaction*

Consider a proton at rest which is passed at a distance a by a fast singly charged particle. Due to the Coulomb interaction, the proton recoils with momentum P, given by (cf. Jánossy 1948, p. 89):

$$P = \frac{2\mathbf{e}^2}{a\mathbf{c}}. \qquad \ldots\ldots(5)$$

Assuming the fast particle to be traversing an absorber, the effective cross section averaged over all collisions in which the proton recoils with momentum greater than P is $\sigma = 4\pi\mathbf{e}^4/P^2\mathbf{c}^2$.

Inserting for $P\mathbf{c}$ the value 430 Mev., corresponding to a minimum recoil energy of 100 Mev. sufficient to cause the stars observed, we obtain a cross section of the order of 10^{-30} cm^2. Allowing for the fact that there would be no such interaction with neutrons, this would give a cross section of about

$$4 \times 10^{-31} \text{ cm}^2 \text{ per nucleon.} \qquad \ldots\ldots(6)$$

Assuming this argument may be applied to the μ-meson component below ground, we see that this figure is much smaller than the observed figure of the order of 10^{-29} cm^2 per nucleon. However, this theoretical figure is likely to be an over-estimate as the distance of closest approach, a, from (5) is of the order of 5×10^{-16} cm., and the usual considerations of screening would suggest therefore that the Coulomb interaction hardly applies to impact parameters as small as this. Thus, at first, we were inclined to discount the possibility that the stars could be caused by the Coulomb interactions of fast μ-mesons below ground.

However, it was pointed out to us by Heisenberg, at the Como Conference, that the Coulomb cross section is likely to be greater than that given by equation (6) on account of the stronger interaction between the electromagnetic field and the nuclear meson fields.

This suggestion has recently received support from the observations of McMillan *et al.* (1949) of the production of π-mesons by the photons of the Berkeley electron synchrotron. These authors give a cross section for the production of π-mesons by photons of $5 \times 10^{-28}\,\text{cm}^2$ per carbon nucleus. Heitler and Peng (1943) have shown that the cross sections for the anomalous scatter of photons with or without the production of free mesons are expected to be about the same. Hence we may take as a probable figure for the total cross section for star production by photons:

$$\sigma_\nu = 10^{-28}\,\text{cm}^2 \text{ per nucleon} \qquad \ldots\ldots(7)$$

from the observations of McMillan *et al.* Following Williams (1933), a fast μ-meson of energy E is regarded as being accompanied by the following number of photons in the frequency interval $d\nu$ at ν:

$$N(\nu)d\nu = \frac{2\alpha}{\pi}\frac{d\nu}{\nu} \log \frac{E}{\boldsymbol{h}\nu}. \qquad \ldots\ldots(8)$$

The cross section for the production of stars by μ-mesons would be from (7) and (8)

$$\sigma_\mu = \frac{2\alpha}{\pi}\int_{E_{\min}}^{E} \frac{\sigma_\nu}{\nu}\, d\nu \, \log\left(\frac{E}{\boldsymbol{h}\nu}\right), \qquad \ldots\ldots(9)$$

where $E_{\min}$ is the minimum energy for star production, which we may conveniently take to be $m_\pi \mathbf{c}^2$. Substituting the observed value (7) for σ_ν, we get the following approximate expression for σ_μ:

$$\sigma_\mu = \frac{2\alpha}{\pi}\left[\log \frac{E}{m_\pi \mathbf{c}^2}\right]^2 \times 10^{-28}\,\text{cm}^2. \qquad \ldots\ldots(10)$$

At 60 m. water depth, the mean energy of the μ-mesons is approximately $1{\cdot}4 \times 10^{10}$ ev., and substituting this value in (10) we obtain the numerical value:

$$\sigma_\mu = 10^{-29}\,\text{cm}^2 \qquad \ldots\ldots(11)$$

which is quite close to the observed value.

In arriving at the expression (10) we have ignored the variation of σ_ν with ν. This is unlikely to introduce serious errors however, for the numerical value (7) is already a mean value averaged over the frequency interval which begins at the threshold for meson production, 150 Mev., and extends to the maximum energy of the particles produced by the synchrotron, viz. 335 Mev. Since the photon energy enters (10) in the logarithmic term, any variation of σ_ν above 335 Mev. will not make a great difference in the numerical value (11).

Basing our confidence in the numerical value (7), derived from the observations of McMillan *et al.*, we believe that the stars observed below ground which have charged primary particles may be ascribed to Coulomb interactions of fast μ-mesons. As the depth below ground is increased, the mean energy of the mesons increases also, and from (10) this would cause the star frequency to decrease less rapidly than the total meson flux. The results of § 4 although of poor statistical weight, indicate a trend in this direction as the variation in the total meson flux between the depths 20 and 60 m. water is about 4 : 1.

The above argument, based on the Williams–Weiszäcker method of replacing the Coulomb field of a fast particle by its equivalent photon spectrum would of course apply to any charged particle and not only to μ-mesons. But below ground, electrons form about 14 % of the total radiation, their energy is rather low, and their contribution to the star frequency may be safely ignored. Above ground, however, all the charged particles of the cosmic radiation may be considered as making a contribution to the star frequency by the Coulomb interaction discussed here. The magnitude of the contribution will be considered below.

The stars above ground are produced by particles with a strong interaction which leads to the well-known $A^{1/3}$ law connecting the range of the particles with atomic number. If the interaction is much weaker—as we believe it to be for the particles producing the underground stars—this law no longer holds and the collision length is independent of Z or A. This follows from the fact that if the collision cross section per nucleon, σ, is very much less than the geometric cross section, the individual nucleons of a given nucleus no longer screen each other to any appreciable extent, and the probability of a collision per gm/cm² is simply $N\sigma$. This justifies the procedure adopted in arriving at equation (4).

5.3. *Underground Stars produced by Neutral Particles*

For every star produced by a charged particle there are 1·4 produced by neutral particles.

A simple explanation of these stars with neutral primary particles is the assumption that they are produced mainly by neutrons and to a lesser extent by photons. The presence of these neutral particles below ground would be expected in any case, and it only remains to be seen whether they occur in sufficient numbers to account for the observed frequency of stars with neutral primaries.

(*a*) *Neutrons.*

Brown *et al.* (1949 b) and Page (1950) have given details of the energies of the protons emitted in stars observed at mountain altitudes. These authors report that the number of protons per star with energy greater than 70 MeV. is approximately 0·5. It is reasonable to assume that the energy distribution of the neutrons from stars is similar to that of the protons, and allowing for the neutron excess in atomic nuclei, we arrive at a figure of 0·6 neutron per star with energy greater than 70 MeV.

We have already seen that the size distributions of the underground stars and stars at mountain altitudes are similar, and it therefore seems reasonable to us to assume that for every star produced underground by a fast meson, there is 0·6 neutron with E greater than 70 MeV. These neutrons will be in equilibrium with the μ-mesons at great depths, and the disintegrations which they produce will be included in our category of stars. It follows therefore that for every star with a charged primary particle, there should be about $0{\cdot}6+0{\cdot}6^2+0{\cdot}6^3+\ldots=1{\cdot}5$ stars produced by locally generated secondary neutrons. In general, if r is the number of neutrons per star capable of producing further stars, the ratio of the numbers of stars with neutral and charged particles is given by

$$\frac{N_n}{N_p}=\frac{r}{r-1}. \qquad \ldots\ldots(12)$$

For $r=0{\cdot}5$ and $0{\cdot}7$ this gives 1 and 2·3 respectively for the ratio N_n/N_p. We do not know the value of r with any certainty. The value $r=0{\cdot}6$ is a reasonable estimate, and leads to the conclusion that most of the stars with neutral primaries are produced by neutrons.

(*b*) *Photons.*

From absorption measurements carried out in this same laboratory (George 1946), and elsewhere (Wilson 1938), it is known that the cosmic radiation below ground may be divided into the usual hard and soft components. The soft component at our depth of operation comprises about 14 % of the total radiation. The photons of sufficient energy in this soft component would be expected to produce stars with neutral primary particles, as discussed in § 5. 2. This contribution, however, will be rather small, on account of the small number of photons of sufficient energy.

The photons of the soft component underground can arise from the following processes: (*a*) cascade development of the knock-on electrons from μ-mesons; (*b*) bremsstrahlung by μ-mesons; (*c*) γ-rays from the nuclear disintegrations produced by μ-mesons. The contribution from (*b*) is negligible, and as we have no data concerning (*c*), this process will be ignored. A detailed calculation based on process (*a*) shows that the number of photons with energy above 100 MEV. (sufficient to cause a small star) is only about 2 % of the flux of fast mesons. This figure is consistent with the frequency of occurrence of electron pairs in our G 5 plates. Bearing in mind that the cross section for star production by photons is about ten times that for star production by μ-mesons (equations (7) and (11)), we see that the number of stars produced by photons is expected to be about 20% of the number produced by fast μ-mesons. In other words, of the 14 stars, observed in G5 plates, with neutral primary particles something like two might have been produced by photons. Thus most of the stars with neutral primaries may be attributed to the locally produced secondary neutrons, while some small contribution may be ascribed to the photons of the soft component.

One question that may be raised is as follows: if photons of sufficient energy do indeed produce stars with the cross section (7), then is this consistent with the well established observation in cloud chamber studies that stars are not usually associated with cascade showers? A simple calculation shows that there is no contradiction. Assume we have a cloud chamber containing a large number of separated lead plates in which the development of a cascade shower may be observed. The path length of the visible tracks in the gas is proportional to their path length in the lead. Assume an electron of energy E_0 falls on the top plate. The total path length of the cascade electrons in the lead is approximately (Rossi and Greisen 1941):

$$x_e = l_e \times 0{\cdot}5\,\frac{E_0}{E_c}\,\text{cm.}, \qquad \ldots\ldots(13)$$

where l_e and E_c are the cascade unit of length and the critical energy respectively. Let E_s be the threshold energy for the production of stars by photons. Then a similar formulr to (13) gives the photon path length, and the stars produced during the development of the cascade will be given by

$$\begin{aligned} n &= l_e \times \frac{0{\cdot}5E_0}{E_s}\,\rho N\sigma_\nu \qquad \ldots\ldots(14)\\ &= 1{\cdot}7 \times 10^{-4} E_0/E_s, \text{ using (7).}\end{aligned}$$

N is Avogadro's number.

We estimate that a reasonable figure for the total path length of the heavy fragments of the average star in lead would be about 0·6 cm., giving a total path length of heavy fragments per cascade shower:

$$x_s = l_e \times \frac{0{\cdot}5E_0}{E_s}\rho N\sigma_\nu \times 0{\cdot}6\,\text{cm}.$$

Hence

$$\frac{x_s}{x_e} = 0{\cdot}6\frac{E_e}{E_s}\rho N\sigma_\nu. \qquad \ldots\ldots(15)$$

Substituting $\sigma_\nu = 10^{-28}\,\text{cm}^2$, $E_s = 100$ MEV., we get

$$\frac{x_s}{x_e} = 2{\cdot}8 \times 10^{-5}. \qquad \ldots\ldots(16)$$

This number gives the relative probabilities of seeing the track of a cascade electron and a fragment of a star produced by one of the cascade photons, accepting the value (7) of σ_ν. It is seen to be very low, about 1 in 35,000 electron tracks for lead, a value, as far as we can tell, not inconsistent with the results of cloud chamber studies of cascade showers.

Thus there is no objection to accepting the cross section (7) in order to account for the underground stars.

5.4. *Showers of Fast Particles.*

From the arguments used already in § 5.1 we may assume that showers of fast particles are produced by μ-mesons. The cross section for the production of these showers by μ-mesons is then

$$\sigma_s = 4 \times 10^{-30}\,\text{cm}^2 \text{ per nucleon} \qquad \ldots\ldots(17)$$

(this is only an order of magnitude) for μ-mesons of mean energy of order 10^{10} ev.

Concerning the nature of the shower particles, we have to consider the following three features: (*a*) they have charge $\boldsymbol{e}$; (*b*) the values of their kinetic energy are all more than 50 MEV., and are probably much greater than this figure, which has been determined from rather limited measurements of the multiple scattering along the tracks of the shower particles; (*c*) the shower particles are frequently found at wide angles from the axis of the primary particle (Figure 9).

Considerations (*b*) and (*c*) taken together make it unlikely that the shower particles are electrons, as secondary electrons of energy E are usually found at an angle $\boldsymbol{m}_0\boldsymbol{c}^2/E$ from the axis of the initial particle. Thus, all electrons with E greater than 50 MEV. would be expected at angles less than 0·5 degree from the initial particle, whereas, of the 16 shower particles, one was at 3°, two were at 4° and the rest at greater angles.

We think it unlikely that the shower particles are protons for the following reason. In the 24 stars observed in electron sensitive plates, 133 slow tracks and 16 shower tracks were observed. Of the 133 slow tracks, 14 had a grain density between 3·5 and 7 times minimum, corresponding to energy limits for protons 40 MEV. and 100 MEV. (cf. Page 1950). The shower particles, if protons, would have energies greater than 1,000 MEV., and it seems unreasonable that the energy spectrum of the star particles should contain a number of particles with energy greater than 1,000 MEV. equal to those lying in the interval 40 to 100 MEV.

The underground shower particles are probably mesons, and we may assume they are π-mesons, as has been confirmed by Fowler (1950) for the showers observed in plates exposed at great heights in the atmosphere.

In § 3.2 we reported that eight π-mesons had been observed to come to rest in the plates, equation (1), and we multiplied this by three to account for the loss by decay in the air path from tunnel wall to the plates, equation (2). One half of the observed slow π-mesons entered the emulsion from below and one half from above. This strongly suggests that the π-mesons are created in the local material. The observed numbers are consistent with the assumption that the showers are in fact the process in which the underground slow π-mesons are generated.

A certain interest lies in the question of the multiplicity of meson production. The limiting viewpoints of Heisenberg (multiple meson emission) and Heitler (single meson emission) are well known. On the latter viewpoint showers are explained on the basis of a plurality of collisions inside an atomic nucleus. One hesitates to draw collisions concerning multiplicity of emission from observations on meson showers, as all the available experimental evidence has so far been adequately explained by both schools of thought (Heisenberg 1949, Heitler and Jánossy 1949). The plural theory depends on the fact that the cross section for meson production is comparable with the geometric cross section of nucleons ($\sim 6 \times 10^{-26}$ cm^2). However, if the showers are produced by the μ-mesons below ground, with a cross section not very different from (17), then the chance of a nuclear collision occurring in crossing a silver nucleus is only about 1 in 1,000, and thus the observed showers would be difficult to reconcile with the plural theory. The alternative would be to assume that some unknown process leads to the production of relativistic protons below ground, and then the interpretation of the showers would be as ambiguous as before.

§ 6. COMPARISON WITH OTHER OBSERVATIONS

Our results confirm the observations of Braddick and Hensby (1939) that nuclear interactions occur below ground, and it would seem possible that the showers we have reported are related to the meson pairs observed by them in a cloud chamber. A more quantitative comparison is not possible owing to the large differences in experimental conditions.

Attempts were made by George and Jason (1947) to record penetrating showers in the same laboratory, using a system of shielded Geiger counters similar to that used by Jánossy, with a negative result. From our present results we conclude that something like 200 showers of the type observed in nuclear emulsions were produced in their top absorber during the period of observation. From the fact that no penetrating showers were recorded, we may conclude that the counter system had a low efficiency for the detection of these underground showers. This might be due to the low mean energy of the shower particles, or to their low density.

Using a counter system less selective for high density penetrating showers, a positive result was reported by George and Trent (1949). The cross section reported by them for the production of groups of penetrating particles was 5×10^{-29} cm^2 per nucleon, and later measurements have shown that this must be reduced to 2×10^{-29} cm^2, as the effect of knock-on electron showers had not been sufficiently eliminated in the initial measurements. This cross section may be compared with our figure for shower production (17) of approximately 4×10^{-30} cm^2, and is seen to be of a similar order of magnitude. The nuclear emulsion measurements need to be extended before a more detailed quantitative comparison can be usefully made.

Fast μ-mesons at the Jungfraujoch are about 50 times more frequent than they are at 60 m. water depth, but from equation (10) we should expect their efficiency for star production by electromagnetic interaction to be reduced by a factor of about three on account of the difference in mean energy. Hence, if our interpretation of the underground stars is correct, one would expect approximately $50 \times 2 \times 10^{-3}/3 = 0{\cdot}033$ stars per cm^3 per day to be caused directly by them, due to their electromagnetic interactions with nuclei. Brown *et al.* (1949 b) report that the number of stars of type I_p, in their nomenclature (similar to our stars shown in Figures 4 and 5), is 0·45/cm^3/day at the Jungfraujoch. Thus it seems possible that an appreciable fraction of the stars of this type at altitude may be due to fast μ-mesons.

§ 7. CONCLUSIONS

The conclusions that have been reached are as follows :

(i) The frequency of slow μ-mesons observed to come to rest is close to the number expected from the μ-meson spectrum deduced from cloud chamber measurements and the depth–intensity curve.

(ii) Nuclear disintegrations occur at depths 20 to 60 m. water below ground with a frequency detectable in nuclear emulsions.

(iii) The slow variation of the frequency with depth suggests that they are produced by fast μ-mesons.

(iv) Assuming the primary agent producing the stars to be μ-mesons, the cross section per nucleon for star production is 10^{-29} cm^2.

(v) From the experiments on nuclear photo-disintegrations at high energies, a cross section of this magnitude may be understood in terms of the Coulomb interaction of the μ-mesons with nucleons.

(vi) Further stars, not caused directly by μ-mesons are thought to be due in part to neutrons, arising from the disintegrations due to μ-mesons, and in part to the photons of the underground soft component of cosmic rays.

(vii) Some showers have been observed associated with stars; these are thought to be showers of π-mesons also produced presumably by the Coulomb interaction of μ-mesons.

(viii) Slow π-mesons have been observed below ground, in number comparable to the number of observed shower particles, and are thought to be the end-points of similar showers occurring in the local material.

(ix) The cross section for shower production by photons must be similar to that for star-production, of the order of 10^{-28} cm^2 per nucleon.

ACKNOWLEDGMENTS

It is with pleasure that we express our thanks to Professor J. D. Bernal for providing us with laboratory facilities and for the interest he has taken in our experiments. We are grateful to the London Transport Executive for permission to expose the plates at various Underground stations.

The underground coatings were performed under the supervision of Mr. Vincent of Messrs. Ilford Ltd.; without this assistance we doubt if the experiments would have been successful, and we record with pleasure our great indebtedness. We are grateful for helpful criticism from Dr. J. G. Wilson. We must also thank Mrs. M. H. George for scanning the greater part of the nuclear plates. The earlier part of the work was supported by a grant from the Department of Scientific and Industrial Research, and the later part by a grant from the Central Research Fund of the University of London.

REFERENCES

BRADDICK, H. J. J., and HENSBY, G. S., 1939, *Nature, Lond.*, **144**, 1012.

BROWN, R., CAMERINI, U., FOWLER, P. H., MUIRHEAD, H., POWELL, C. F., and RITSON, D.M., 1949 a, *Nature, Lond.*, **163**, 47.

BROWN, R., CAMERINI, U., FOWLER, P. H., HEITLER, H., KING, D. T., and POWELL, C. F., 1949 b, *Phil. Mag.*, **40**, 862.

CAMERINI, U., MUIRHEAD, H., POWELL, C. F., and RITSON, D. M., 1948, *Nature, Lond.*, **162**, 433.

CAMERINI, U., COOR, T., DAVIES, J. H., FOWLER, P. H., LOCK, W. O., MUIRHEAD, H., and TOBIN, N., 1949, *Phil. Mag.*, **40**, 1073.

CAMERINI, U. FOWLER, P. H., LOCK, W. O., and MUIRHEAD, H., 1950, private communication.

COSYNS, M. G. E., DILWORTH, C. C., OCCHIALINI, G. P. S., SHOENBERG, M., and PAGE, N., 1949, *Proc. Phys. Soc.* A, **62**, 801.

EVANS, J., and GEORGE, E. P., 1949, *Nature, Lond.*, **164**, 20.

FOLLETT, D. H., and CRAWSHAW, J. D., 1936, *Proc. Roy. Soc.* A, **155**, 546.

FOWLER, P. H., 1950, *Phil. Mag.*, **41**, 169.

GEORGE, E. P., 1946, *Nature, Lond.*, **157**, 296.

GEORGE, E. P., and JASON, A. C., 1947, *Nature, Lond.*, **160**, 327.

GEORGE, E. P., and TRENT, P. T., 1949, *Nature, Lond.*, **164**, 838.

HEISENBERG, W., 1949, *Nature, Lond.*, **164**, 67.

HEITLER, W., 1941, *Proc. Camb. Phil. Soc.*, **37**, 291.

HEITLER, W., and JÁNOSSY, L., 1949, *Proc. Phys. Soc.* A, **62**, 669.

HEITLER, W., and PENG, H. W., 1943, *Proc. R. Irish Acad.*, **49**, A7.

JÁNOSSY, L., 1948, *Cosmic Rays* (Oxford : University Press), p. 89.

KRAUSHAAR, W. L., 1949, *Phys. Rev.*, **76**, 1045.

LATTES, C. M. G., OCCHIALINI, G. P. S., and POWELL, C. F., 1947, *Nature. Lond,*, **160,** 486.

MCMILLAN, E. M., PETERSON, J. M., and WHITE, R. D., 1949, *Science*, **110**, 579.

PAGE, N., 1950, *Proc. Phys. Soc.* A, **63**, 250.

PICCIONI, O., 1950, *Phys. Rev.*, **77**, 6.

ROSSI, B., 1948, *Rev. Mod. Phys.*, **20**, 537.

ROSSI, B., and GREISEN, K. I., 1941, *Rev. Mod. Phys.*, **13**, 240.

WILLIAMS, E. J., 1933, *Proc. Roy. Soc.* A, **139**, 163.

WILSON, A. H., 1941, *Proc. Camb. Phil. Soc.*, **37**, 301.

WILSON, V. C., 1938, *Phys. Rev.*, **53**, 337.

Note added in proof. Concerning the showers, Professors Marshak and Heitler have pointed out that if a single π-meson is produced it could itself generate a shower inside the same nucleus by the plural process. Thus the smallness of the cross section for shower production (17) does not necessarily imply a multiple production of π-mesons.

Heat Changes Accompanying Magnetization in Low and Moderate Fields: the Effects of Strain, and a Theoretical Interpretation

By L. F. BATES and J. H. DAVIS
University of Nottingham

MS. received 11*th April* 1950

ABSTRACT. The technique of Bates and his co-workers was used to measure the adiabatic temperature changes occurring during magnetization of nickel under conditions of progressively increased internal strain as a pure specimen was taken from the fully annealed state to the state of maximum strain, in absence of deforming force. A new technique enabled accurate thermal curves during virgin magnetization, and in cycles up to 400 oersteds, to be obtained; the induction effect previously reported was investigated and its origin determined. A new theoretical treatment is described in which account is taken of the energy changes associated with magnetostriction and which enables the thermal curves to be calculated from available data on magnetization and magnetostriction, and a general physical interpretation of the curves is given. Agreement is good for strained specimens and an explanation of the less satisfactory agreement for annealed specimens is offered.

§ 1. INTRODUCTION

THE most recent work on the thermal energy changes accompanying magnetization of ferromagnetic materials in low and moderate fields is that of Bates with Weston, Healey, Edmondson, Harrison and Davis severally (1941 to 1948). These workers examined the thermal changes in iron, nickel and cobalt in the annealed and hard-drawn states, as well as the changes in several alloys, when these substances were taken through normal hysteresis cycles, or subjected to virgin magnetization. The experimental methods are fully described in communications from the authors mentioned; the present work was carried out with the apparatus in the form used by Bates and Harrison, apart from certain interesting modifications described below.

The first object was to examine the transition in nickel from the results typical of the annealed state to those of the fully strained state as the internal strain of the specimen was gradually increased. The second was to find equations to fit the experimental curves and to give a theoretical interpretation of them. Finally, a thorough examination of the induction effect was made in order to determine its origin as definitely as possible.

§ 2. MODIFICATION OF APPARATUS

As it was intended to make frequent measurements at fields up to 400 oersteds, it was necessary to modify existing apparatus by improving the cooling arrangements to reduce galvanometer drift. A Stuart–Turner electric pump in a sound-proof, magnetically shielded box was installed to increase the flow of cooling water. The original reservoir capacity was doubled, and the water was continuously stirred, so that variations in the temperature of the water supply were smoothed out. Additional cooling was arranged by passing cold water through a thin rubber tube wound over the outside of the magnetizing solenoid.

The thermocouples were tied to the specimen with waxed thread, and considerable reduction of galvanometer drift was obtained by covering each thermocouple with a cotton-wool pad and by filling vacant spaces inside the solenoid with loose cotton-wool, which restricted the flow of air up and down the specimen.

§ 3. EXPERIMENTAL PROCEDURE

The specimen was a pure nickel rod, 40 cm. long and 4 mm. in diameter, kindly supplied by the Mond Nickel Company. Its composition was: Si 0·05, Mn 0·06, Cu 0·18, Fe 0·28, Mg 0·02, Co 0·07, Ni 99·34.

The rod was annealed by heating to a temperature of 930° c. *in vacuo* in three hours, maintaining at this temperature for one hour and then cooling at a constant rate of 10° c. in five minutes. As the specimen was too long for our furnace, it was turned end for end, and the annealing process was repeated. This procedure made the rod extremely soft.

The general experimental procedure was to take (I, H) and thermal curves (energy change in ergs/cm^3 against I or H) both on the annealed specimen and after stretching it under successively increasing tensions, i.e. curves were taken on the specimen in several states of increasing strain. Readings were taken, starting from the demagnetized state, in fields up to 400 oersteds, and also for cycles of magnetization with maximum fields of 122 and 400 oersteds. The (I, H) curves were all obtained by the ballistic method. The approximate mean temperature of the specimen at each step was recorded.

The specimen was stretched by means of a steelyard which could be screwed to the floor below the wooden frame carrying the solenoid. A chosen tension was applied for three hours and then removed, whereupon the specimen was allowed to recover for at least 24 hours before thermal measurements were taken. All curves were taken in the absence of applied force; in fact, the weight of the brass rod attached to the specimen to hold it in position was compensated by a simple lever arrangement. The strain was assessed by measurements of length and diameter of the rod, the length between two fine lines marked near the ends being measured in a comparator. Owing to the fracture of the rod during strain 7 the tension was not applied for the three hour period in this case.

In most of the earlier work on the magnetic effects of strain, measurements were taken while the stress was actually applied. Two separate conditions thus simultaneously affected the specimen, namely, the internal strain and the tension producing the strain. The magnetic effects due to internal strain alone are those observed in hard-drawn materials, and are considerably less than those produced by permanent application of the tension necessary to produce the same strain. This is apparent from a comparison of the magnetization data given by Bates and Weston (1941) with those of the present paper. Again, with external tension applied to the specimen, work is done on or by the specimen during its magnetostrictive movements, and this work, $F\,dl$, may reach 65,000 ergs/cm^3 with a tension of 33 kg/mm^2 and a longitudinal saturation magnetostriction of 20×10^{-6} cm/cm. Because of the magnitude of this external work, and because it was desired to study particularly internal strain such as occurs in all ferromagnetic materials below the Curie point, all the curves were taken as far as possible in absence of external constraint.

The general method of obtaining the thermal readings has been described in earlier papers. Modifications of the technique were necessary in the present work because of the larger hysteresis energy to be dissipated, and the increased heat generated in the solenoid by the use of higher fields and solenoid currents respectively. These modifications were as follows: First, an examination of galvanometer drifts having made it possible to know beforehand when a considerable time of stable zero could be expected, readings were taken only during these times. Secondly, whenever possible, two or three consecutive steps were taken one after the other, so that time wasted in waiting for the dissipation of the hysteresis heat was reduced to a minimum. Finally, in taking virgin curves, the method given below was adopted after an examination of the curves of Bates and Weston had shown a marked lack of consistency in shape.

The first virgin curves obtained in the present work varied greatly with the direction of the magnetizing current, and it was realized that this variation was due to the fact that the galvanometer deflections arose from very large induction effects rather than from thermal effects. As in previous work, inductive deflections were balanced in work on the closed cycles by means of a compensating coil placed in the solenoid field and connected to its own primary winding on the transformer, but accurate adjustment of the coil was not easy in work on the virgin curves because of the difficulty of repeating individual steps. An examination of the induction effect, described in the next section, showed that the effect could be much reduced by closely twinning the thermocouple leads. The virgin curves were then taken with current in both directions and with the compensating coil in a fixed position. At least one of the nineteen current-steps was then found to give a thermal deflection which was of the same sign for both senses of the current, and the compensating coil was thus adjudged to be nearly in the correct position for this step. Slight changes in position of the coil for adjacent steps when the curve was repeated then showed the correct direction of adjustment, and repetition enabled the compensation to be made more exact and to be extended over the whole curve.

The virgin curves obtained showed good consistency, and this fact and the values of individual readings indicated that the necessity for compensating inductive deflections large compared with the thermal deflections did not appreciably impair the accuracy of measurement of the latter.

§4. INVESTIGATION OF THE INDUCTION EFFECT

The induction effect usually manifests itself as a short, sudden deflection of variable sign and magnitude, immediately preceding the true thermal deflection. It was found by most earlier workers, and its peculiar nature prompted suggestions of a subtle origin such as thermal effects in the closure domains in the specimen, or variations in surface thermal conductivity or magnetization. Bates and Harrison obtained curves of an unusual shape by plotting $\Delta B_l/\Delta H$ against $1/x$ where x was the distance between compensating coil and solenoid, and B_l the longitudinal flux density.

In the present investigation the constantan used in the thermocouples was first shown to be effectively non-ferromagnetic by a susceptibility measurement. Inductive deflections were then observed in the nickel specimen. Thermal insulation of the thermocouples was found to eliminate the thermal deflections, leaving only the inductive ones. Removal of the specimen reduced the deflections to very small values. A length of twin wire with one end connected to the galvanometer and the other end short-circuited was then used as a search coil and, in spite of the twinning, inductive deflections were obtained with the twinned wire inside the solenoid and the specimen removed, and just outside it when the specimen was present.

It appeared, therefore, that the effect was purely inductive, and was principally due to 'pick-up' in those parts of the thermocouple leads inside the solenoid. As was expected, closer twinning of the leads reduced the effect very considerably, and thereafter adjustment of the compensating coil was much more rapid, less critical, and less frequently necessary.

§ 5. EXPERIMENTAL RESULTS

The several tensions applied and the resulting dimensional changes are given in Table 1. The length of the specimen was measured at about 17° c., the error being $\pm 0{\cdot}0015$ cm. before fracture; after fracture, following strain 7, the error was $\pm 0{\cdot}01$ cm.

Table 1. Stresses and Dimensional Changes

Tension (kg/mm^2)	Length (cm.)	Diameter (cm.)	Permanent elongation (%)	Remarks
0	36·925	0·4005	0	Annealed
0·90	—	—	—	Strain 1
2·0	—	—	—	Strain 2
5·0	37·008	0·3997	0·22	Strain 3
8·0	37·078	0·3992	0·41	Strain 4
15·2	38·110	0·3940	3·21	Strain 5
				Elastic limit exceeded
27·6	40·511	0·383	9·71	Strain 6
40·2	46·0	0·363	24·6	Strain 7
				Specimen fractured

Numerical data obtained with the annealed and fully strained specimens which enable the (I, H) curves for the virgin magnetization and the 400-oersted cycles to be plotted are given in Tables 2 to 5 inclusive, together with the relevant thermal data (ΔQ is the energy change).

Table 2. Annealed Nickel, Unstrained. Virgin $Q-H, I$ Data

H	I	ΔQ (erg/cm^3)	$\Sigma\Delta Q$
0·8	82	−238	−238
3·2	316	−287	−525
6·9	386	−673	−1198
13·0	419	−1157	−2355
19·6	433	−1080	−3435
25·6	445	−933	−4368
34·1	450	−1170	−5538
47·3	460	−1683	−7221
61·9	469	−1543	−8764
95·9	483	−3562	−12326
131·4	492	−1704	−14030
157·3	496	−771	−21731
185·3	498	−189	−21920
209·3	501	841	−21079
233·3	501·5	750	−20329
250·3	502	1781	−18548
303·3	503	3366	−15182
342·3	503·5	2888	−12294
386·3	505	4086	−8207

Table 3. Annealed Nickel, Strain 7. Virgin $Q-H, I$ Data

H	I	ΔQ (erg/cm^3)	$\Sigma\Delta Q$	H	I	ΔQ (erg/cm^3)	$\Sigma\Delta Q$
9·3	14·3	−255	−255	136	383	1418	8979
15·6	28	368	113	166·8	399	1050	10029
22·8	57	615	728	194·8	410	1155	11184
28·8	110	1185	1913	219·7	419·5	1110	12294
37	177·5	1561	3474	259·7	429·7	2055	14349
51·5	257	1702	5176	333·4	442	3563	17912
66·5	302	915	6091	395·4	449·1	3007	20919
101·6	357	1470	7561				

Table 4. Annealed Nickel, Unstrained. 400 oe. Cycle $Q-H, I$ Data

H	I	ΔQ (erg/cm^3)	$\Sigma\Delta Q$	H	I	ΔQ (erg/cm^3)	$\Sigma\Delta Q$
−398·4	−489	—	—	11·3	387	−1954	3216
−337·4	−488	−4419	−4419	23·2	420	−2145	1071
−261·4	−486	−4121	−8540	31·7	430	−1176	−105
−216·4	−484·5	−1388	−9928	45·0	441	−1876	−1981
−167·4	−481	−700	−10629	58·3	449·5	−1706	−3687
−135·2	−476·5	1006	−9623	91·5	465	−3073	−6760
−97·1	−467·5	1792	−7831	123·4	474	−2082	−8842
−64·7	−454	3024	−4807	179·4	482	−1289	−10131
−49·9	−446	1395	−3412	201·4	484	191	−9940
−20·7	−422·5	3526	114	223·4	485	580	−9360
−7·6	−380	2514	2628	246·4	486	871	−8489
−0·75	−245	2181	4809	301·4	487·5	2790	−5699
0·7	−136·5	0	4809	323·4	488	1523	−4176
1·45	−50	361	5170	388·4	488·5	4404	228
3·4	135	0	5170	398·4	489	878	1106

Table 5. Annealed Nickel, Strain 7. 400 oe. Cycle $Q-H, I$ Data

H	I	ΔQ (erg/cm^3)	$\Sigma\Delta Q$	H	I	ΔQ (erg/cm^3)	$\Sigma\Delta Q$
−401·5	−441·2	—	0	15·7	−198	1292	−12773
−338·4	−435	−3106	−3106	22·7	−150	1398	−11375
−289·7	−427·7	−2605	−5711	34·8	90	7962	−3413
−265·4	−424	−1340	−7051	62·3	287	7111	3698
−220·6	−415	−1904	−8955	129·4	374·5	4079	7777
−170·6	−404	−2244	−11199	187·6	402	2637	10414
−105·1	−376	−2457	−13656	252	420	3137	13551
−37·5	−317·5	−1164	−14820	326·3	433·5	3892	17443
−15·5	−284	154	−14666	389·3	441	3218	20661
1·3	−248	601	−14065				

Thermal curves obtained during virgin magnetization and in the 400-oersted cycle in all states of strain, plotted against both effective field H and intensity of magnetization I, are given in Figures 1 to 4. The 122-oersted cycle thermal curves are shown in Figure 5 plotted against intensity of magnetization only, no numerical data being tabulated here. The first two strains were purely exploratory, so that only the virgin thermal curves were taken. The coefficient

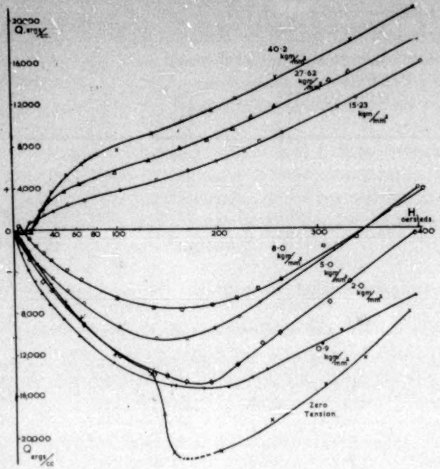

Figure 1. Annealed nickel. Virgin *Q–H* curves. Effect of internal strain.

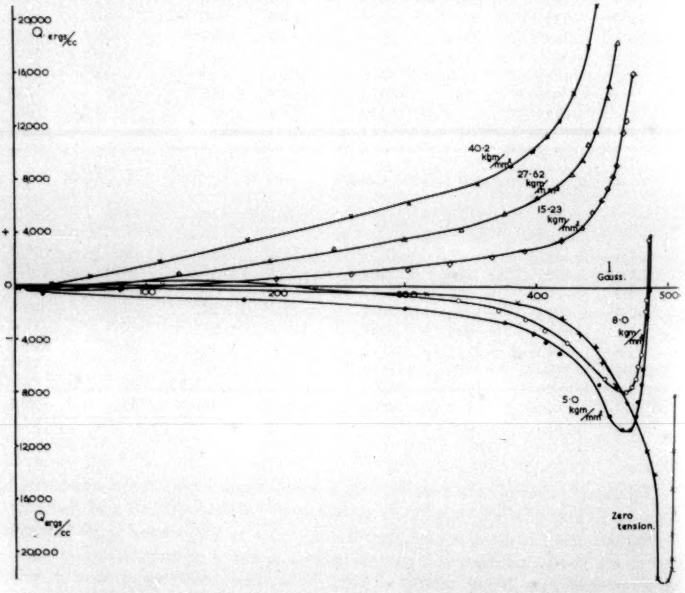

Figure 2. Annealed nickel. Virgin *Q–I* curves. Effect of internal strain.

of expansion used in the calibration was $12{\cdot}8 \times 10^{-6}$ per °c. (Guillaume 1920); this was used throughout the work as no measurements of the effect of strain on the coefficient of nickel appear to have been made.

The variation of the magnetic and thermal characteristics with strain is given in Table 6, in which I_{rem} is the remanent intensity of magnetization, H_c the coercive force, $\int H\,dI$ the hysteresis heat evolved per half-cycle, $\Sigma\,dQ$ the summation of thermal energy-changes per half-cycle, $\Sigma\,dQ - \int H\,dI$ the discrepancy per half-cycle, $\Sigma|dQ|$ the arithmetic sum of thermal deflections, and the percentage error $100(\Sigma\,dQ - \int H\,dI)/\Sigma|dQ|$.

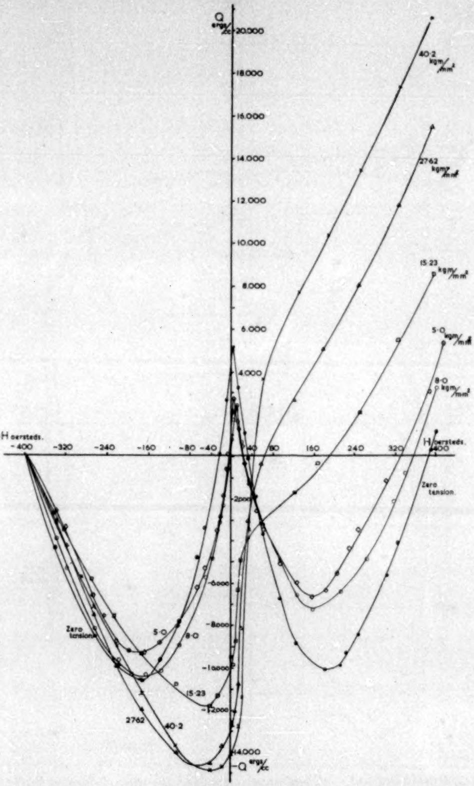

Figure 3. Annealed nickel. 404-oersted cycle Q–H curves. Effect of internal strain.

For use in the calculations based on the theory given later, the virgin and 400-oersted cycle longitudinal magnetostriction curves of the specimen were kindly measured by Mr. E. W. Lee after strain 7 and after re-annealing the specimen. Measurements could not be made on the specimen as originally annealed because the apparatus for magnetostriction measurements was not then available. The results are given in Figures 6 and 7.

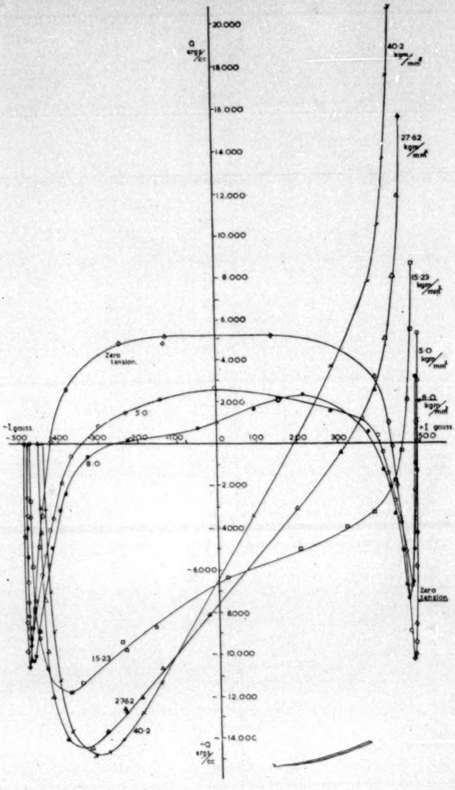

Figure 4. Annealed nickel. 404-oersted cycle Q–I curves. Effect of internal strain.

§ 6. DISCUSSION OF RESULTS

(i) *Errors.* As shown in Table 6, in the 400-oersted cycles there was never more than 3·9% discrepancy between the amounts of *overall* irreversible heat developed per cycle as indicated by integration of hysteresis-loop area, and by summation of measured thermal energy changes. This error is considered not excessive in view of the relatively large fields used. In the 122-oersted cycle much greater errors were found. The reason for this is obscure, but lies partly in the fact that these curves cover only the steep, central parts of the (Q, H) curves and the proportion of small galvanometer deflections was higher than in the 400-oersted cycle. An attempt to allow for the non-linearity of the galvanometer

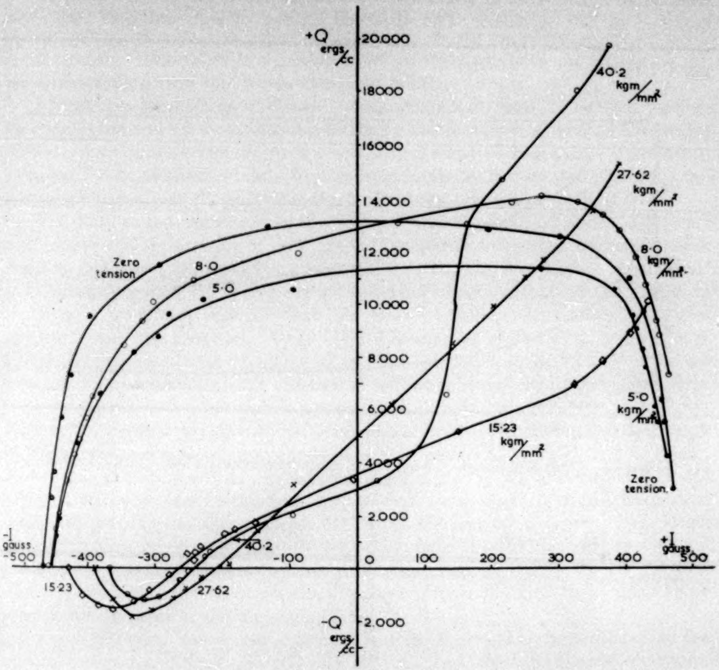

Figure 5. Annealed nickel. 121·7-oersted cycle *Q-I* curves. Effect of internal strain.

Table 6. Variation of Magnetic and Thermal Characteristics with Strain

Virgin curves				Strain		
State	Annealed	3	4	5	6	7
H_{max}	392·3	401·5	402·7	404·0	399·1	395·4
I_{max}	504·7	487·2	486·1	474·9	465·2	449·1
400-*oersted cycles*						
H_{max}	401·4	401·4	401·4	401·3	401·4	401·5
I_{max}	488·8	487·7	484·8	478·6	456·2	441·4
I_{rem}	200	300	270	265	248	252
H_c	2·5	3·8	5·3	12·7	21·8	31
$\int H\,dI$ (erg/cm³)	2003	4580	4320	9905	16490	21758
ΣdQ (erg/cm³)	1106	5270	3215	8595	15580	20660
$\Sigma\, dQ - \int H\,dI$	−897	690	−1105	−1310	−910	−1098
$\Sigma\, \lvert dQ \rvert$	52970	42560	43090	32960	44940	50400
% error	1·7	1·62	2·56	3·9	2·0	2·1

sensitivity, which was appreciable at very small deflections only, produced no significant improvement. It is interesting that the errors in the 400- and 122-oersted cycles were, with one exception, of opposite signs, and that the errors were small in the work of Bates and Weston, in which the cycles were normally confined to 200 oersteds. The observed change of sign indicates that eddy-current effects were very small. The sensitivity varied between 50 and 70 erg/cm^3 per 0·1 mm.

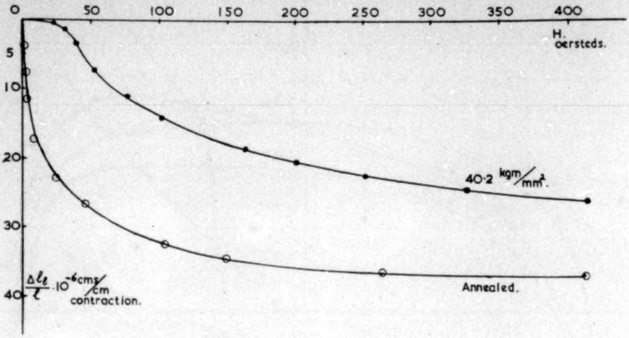

Figure 6. Annealed nickel. Longitudinal magnetostriction curves. Virgin curves. Effect of strain.

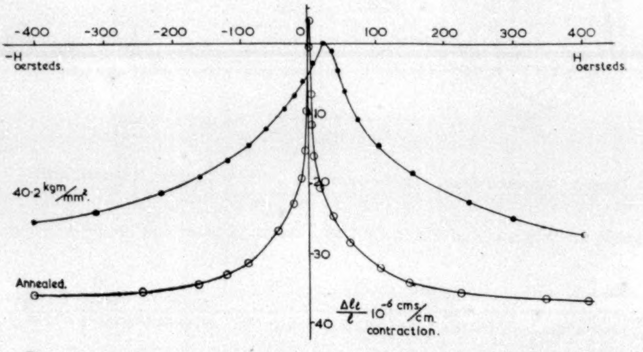

Figure 7. Annealed nickel. Longitudinal magnetostriction curves. 400-oersted cycle. Effect of strain.

(ii) (I, H) *curves*. The changes produced by strain in the (I, H) curves were small, particularly before application of the yield-point tension; they may be compared with the large changes found by Bates and Weston and others, when the load was maintained during measurements. Considerable changes in remanent intensity and coercive force were found in the present work but the values of these quantities were not determined separately and were therefore not of good accuracy.

(iii) ***Thermal curves.*** In contrast to the (I, H) curves, the thermal curves were found to be extemely strain-sensitive. This is particularly noticeable in such features as the steep fall seen at about 140 oersteds in the virgin (Q, H) curves for the annealed state only, and not found after the first strain. The most striking point about the curves, however, is that they fall into two sharply divided classes, namely those taken before and those taken after application of the yield-point tension. But there is a gradation of curve-shape with increasing strain, the change being very rapid near the yield point.

The curves themselves will now be considered in detail. Turning first to the curves obtained before application of the yield-point tension, several differences between the virgin curves, Figures 1 and 2, and those of Bates and Weston may be noted. The method of obtaining the later curves is described in § 3 above, and the steady transitions they show indicate that they are substantially correct.

The 400-oersted cycle curves for the less severely strained states, Figures 3 and 4, have the appearance of two virgin curves joined together, as may be seen from the figures. They may be compared with the curve of Figure 16 of Bates' and Weston's paper, but the more pronounced characteristics of the curves in the present work may indicate that the present specimen was softer, as is also apparent from the magnetic data. The 122-oersted cycle curve, Figure 5, is practically identical with the central parts of the 400-oersted curve although numerical agreement between the two is not close except in particular regions.

Considering next the curves obtained after application of the yield-point tension, the virgin curves show that increasing internal strain obliterates the trough in the curves and that in the heavily strained specimen the final, almost linear, rise of temperature starts at much lower fields, i.e. at about 50 oersteds. In the 400-oersted cycle curves the first trough has been broadened and deepened, while the second has disappeared. The (Q, H) and (Q, I) curves now show greater similarity. In the 122-oersted cycle curve, Figure 5, again the central parts of the 400-oersted curve are seen, but the range is more restricted because of the greater reduction of maximum intensity of magnetization by strain in these curves than in those at the higher field.

The small variations in the curves at low fields are, as indicated later by the theory, due to the interplay of the various quantities which fix the curve-shapes. In low fields these quantities are all small but increasing at different rates, and their summation thus varies irregularly. The movement of the region of zero magnetostriction outwards from $H = 0$ as the strain increases is particularly important in this respect.

The fact that the 122-oersted cycle curves show only the central sections of the 400-oersted curves and not the whole in miniature, is interesting. Agreement is not exact but the implication is that there is a direct relationship between the value of $H_{\max}$ used and the proportion of the boundary movement and rotational processes involved in a change of intensity from the negative to the positive maximum values.

§ 7. THEORY

It is curious that in nearly all the early papers, the theoretical work was merely put forward to enable the variations in magnetic energy to be calculated from the measured variations of thermal energy. No attempt was made to calculate the shape of the thermal curves from fundamentals. The first attempt to base a theory on fundamental concepts was that of Stoner and Rhodes (1949), whose theory was directed to the interpretation of the thermal curves, and was tested by the constancy, or otherwise, of a particular calculated coefficient b''. Stoner and Rhodes did not consider in detail the work done in magnetostrictive processes, but the treatment given below indicates that this work is not negligible.

The present theory is an attempt to calculate the actual thermal curves. It is not intended to derive the curves from any particular fundamental concepts, for example those of the domain theory, but to produce an equation enabling the curves to be calculated from independent measured quantities. These quantities are the data of the (I, H) curve, the magnetostriction data, and the rate of change of intrinsic magnetization with temperature, i.e. the data of the ordinary magneto-caloric effect. This procedure avoids the well-known difficulties met in attempts to calculate (I, H) curves from basic concepts, but success gained subsequently in this matter will necessarily enable calculation of the thermal curves from fundamentals to be carried out.

The principle of the present theory is first to calculate for each change of solenoid current the total amount of energy put into or abstracted from the system consisting of solenoid and specimen; from this energy change the work done on or by the specimen in all conceivable ways is subtracted. The residue or deficit of energy then appears as an increase or decrease of thermal energy and hence of the temperature of the specimen.

We will consider the total energy of the specimen to consist of magnetic, thermal, magneto-crystalline, and strain-energy components, whose sum must be a minimum when the solenoid current is constant. Now, a change of solenoid current will produce a field change which may lead to a change in each of these energies. The thermal energy change is what is measured by the thermocouples.

Let us now calculate the energy changes as far as possible, first dealing with energy changes due to work done in magnetization. Let the intensity of magnetization of the specimen in a field H be I. It is easily shown that a small change in field to $(H+dH)$ with which is associated a change in intensity from I to $(I+dI)$, produces a total energy change of

$$\Delta E = \frac{H\,dH}{4\pi} + H\,dI = \frac{H\,dB}{4\pi}. \qquad \ldots\ldots(1)$$

This energy is supplied by or received by the battery supplying the solenoid according to the sign of the change.

Integrating over the range from $H=0$ to $H=H_{\max}$ we have

$$E = \frac{H^2}{8\pi} + \int_{H=0}^{H=H_{\max}} H\,dI.$$

Over a complete cycle,

$$\oint \frac{H\,dH}{4\pi} = 0, \qquad \text{and therefore} \qquad E = \oint H\,dI,$$

a result in accordance with Warburg's law.

In addition to the above energy change there will also be a change of energy due to the ordinary magneto-caloric effect, the actual quantity being given by equation (2) below. This change is a direct transference from magnetic to thermal energy, or the reverse, according to the sign of H. We have

$$\Delta Q_0 = S_H \Delta T = -T\left(\frac{\partial I_0}{\partial T}\right)_H \Delta H, \qquad \ldots\ldots(2)$$

where ΔQ_0 is the thermal energy change due to this effect for a small, finite field change ΔH, S_H is the specific heat of the material at constant field, and $(\partial I_0/\partial T)_H$ is the rate of change of intrinsic magnetization with temperature at constant field.

This effect produces a heating or cooling of the specimen when the field is increased or reduced respectively. The effect has been thoroughly investigated at fields beyond those used in the present work and it can only be assumed to persist at low fields. The effect will not be completely linear in an unsaturated specimen because of the non-alignment of all the domain vectors. There is plainly, in our opinion, no reliable way of correcting for this departure from linearity in the calculations.

We now come to energy changes due to work done against internal stresses during the magnetostrictive changes of dimensions. Under adiabatic conditions the energy to perform this work comes from the magnetic energy change $H\,dB/4\pi$. With increasing field, energy is transferred from magnetic energy to potential energy of the magnetostrictive strain. During subsequent reduction of the field the energy change $H\,dB/4\pi$ will be partly off-set by the transfer back to the magnetic energy of some of the magnetostrictive strain energy.

Let the internal strain be assumed isotropic, as is usual in the case of nickel, so that we may take the mean internal stress as σ_i dyne/cm^2 acting parallel and perpendicular to the axis of the specimen. Then the work done in a length change of, say, $\Delta l_1/l_1$ will be $\sigma_i \Delta l_1/l_1$ erg/cm^3. This work is independent of the sense of the magnetization and sign of the magnetostriction, but is zero at zero magnetostrictive deformation, and positive during increasing change in dimensions. The work done in the changes in diameter due to the transverse magnetostriction will, similarly, be $\sigma_i 2\Delta l_n/l_n$ where $\Delta l_n/l_n$ is the change in diameter.

The mean internal stress, σ_i, may be calculated by three methods due to Kersten (1932), based respectively on values of initial permeability, of remanent intensity, and of reversible work during magnetization. All three methods give comparable results but the last mentioned is used here because the values obtained for initial permeability and remanent intensity are not regarded as sufficiently accurate. Kersten assumes that the reversible work done against strain forces is $\int_{H_{\max}}^{H=0} H\,dI$. If the saturation longitudinal magnetostriction is λ_{sat}, he states that

$$\int_{H_{\max}}^{H=0} H\,dI = \sigma_i \lambda_{\text{sat}}, \qquad \text{so that} \qquad \sigma_i = \left(\int_{H_{\max}}^{H=0} H\,dI\right)\Big/\lambda_{\text{sat}},$$

giving values of about 6·5 kg/mm^2 in nickel.

In the present paper it is hoped to obtain a more accurate value for σ_i by taking into account both longitudinal and transverse magnetostriction, the equation being then

$$\sigma_i = \int_{-H_{\max}}^{H=0} H\,dI \Big/ \left\{\frac{\Delta l_1}{l_1} + 2\left(\frac{\Delta l_n}{l_n}\right)\right\}.$$

The work done over one step of the cycle is then

$$\partial W = \sigma_1 \left\{ \delta\left(\frac{\Delta l_1}{l_1}\right) + 2\delta\left(\frac{\Delta l_n}{l_n}\right) \right\}. \qquad \ldots\ldots(3)$$

Volume changes as such are neglected since Esau (1931) showed that they can be calculated accurately from the length and diameter changes. Thus volume changes are implicitly accounted for in the foregoing calculation.

We will now briefly consider energy changes due to crystal anisotropy. Local directions of easy magnetization are determined in annealed materials by the crystal anisotropy and in heavily strained materials by the internal strain. In each case, during magnetization work is done in rotating domain vectors out of the easy directions into the direction of the applied field. This work is stored as potential energy and is to be abstracted from the energy put into the system during magnetization, i.e. from $H\,dB/4\pi$. On reduction of the field this energy becomes available again as kinetic (thermal) energy. The process is analogous to that of the preceding section.

It is considered that the crystal anisotropy effects can be neglected in the heavily strained states of the specimen, the calculation of the preceding section accounting adequately for the strain anisotropy. The results given later show this to be the case. In the annealed states the effects of crystal anisotropy are large and at present there appears to exist no exact method of calculating the work done during re-orientation in these states in polycrystalline materials, but work on this point is being continued. For the present, the effects will be neglected.

To complete the above description, let us now consider what occurs during, say, an increase of H. Let the zero energy level be so chosen that an increase of H may be taken as increasing the energy of the system. An increase of solenoid current will increase the energy of the system by $H\,dB/4\pi$, and an increase of thermal energy, ΔQ_0 will result from the ordinary magneto-caloric effect, this energy originating in the change of intrinsic magnetization of the specimen on application of the field.

If a change of dimensions due to magnetostriction occurs, a transfer of some of the energy change, $H\,dB/4\pi$, to potential energy of the magnetostrictive strain will take place. If the effects of crystal anisotropy are appreciable there will also be a transfer of energy which will be stored as potential energy in the rotation of domain vectors with respect to the easy directions of the crystals. The quantities of energy transferred in these last two processes are, therefore, to be subtracted from $(H\,dB/4\pi + \Delta Q_0)$ in calculating the curves; as stated above, crystal energy effects are negligible in the heavily strained states, and, at present, are not calculable with accuracy in other states and must be omitted here.

Two other quantities of transferred energy ought to be subtracted, but may in practice be neglected. These are (i) the work done against atmospheric pressure during magnetostrictive deformations, which amounts only to about 60 erg/cm^3 between $I=0$ and $I=I_{\text{sat}}$, and (ii) the work done in raising and lowering the lower parts of the specimen and thermocouple leads. This work cannot be calculated, but it was partly compensated by counterbalancing the weight by the lever arrangement mentioned in § 3; in any case it is small.

If we have, in the above, calculated the total thermal energy increase of the system, and have subtracted from it the quantities of energy required for the performance of all the internal and external work done by the specimen, then the residue or deficit will appear as a rise or fall of temperature of the specimen, and this will be measured by the thermocouples.

Finally, if the total thermal energy change for a field change from $-H_{\max}$ to H is $\sum_{-H_{\max}}^{H} dE$, we have

$$\sum_{-H_{\max}}^{H} dE = \int_{-H_{\max}}^{H} \frac{H\,dH}{4\pi} + \int_{-I_{\max}}^{I} H\,dI + \sum_{-H_{\max}}^{H} \Delta Q_0 - \sigma_i \left\{ \sum_{-\lambda_{l_{\rm sat}}}^{\lambda_l} \delta\left(\frac{\Delta l_l}{l_l}\right) + \sum_{-\lambda_{n_{\rm sat}}}^{\lambda_n} 2\delta\left(\frac{\Delta l_n}{l_n}\right) \right\}, \qquad \ldots\ldots(4)$$

where λ_l, $\lambda_{l\,\rm sat}$, λ_n, $\lambda_{n\,\rm sat}$ are the longitudinal and transverse magnetostrictions at (H, I) and at saturation respectively. This equation gives the total thermal energy change between saturation and any value H of the applied field, and is the equation used in calculating the curves.

It will be observed that no actual mechanism of energy transfer between the various forms of energy visualized has been assumed. Also, no means by which the energy $H^2/8\pi$ may affect the thermal energy has been suggested apart from the usual magnetic effects. The validity of the theory is to be tested by comparison of observed and calculated curves.

The application of the theory to the cases of annealed and strained nickel will now be described. The values of $H\,dB/4\pi$ were calculated from the measured (I, H) curves. The increments of $\Sigma\Delta Q_0$ were calculated from equation (2), the value of $(\partial I_0/\partial T)_H$ being obtained by interpolation between the values at 0° c. and 50° c. calculated by Stoner from Weiss' and Forrer's results. The temperature used was the mean temperature of the specimen during the measurement of each of the experimental thermal curves. (Variation of solenoid temperature may introduce an error of about 4% in the value of $\Sigma\Delta Q_0$.) The values of σ_i, the mean internal stress, were calculated by Kersten's reversible work method modified as described previously, the values being as shown in Table 7. Values derived from rough measurements of initial permeability, μ_i, omitting transverse magnetostriction, are given for comparison.

Table 7. Calculation of Mean Internal Stress

State	From reversible work		From μ_i
	kg/mm²	dynes/cm²	kg/mm²
Annealed	0·89	$87{\cdot}7\times10^6$	2·7
Strain 6	3·16	310×10^6	—
Strain 7	3·43	337×10^6	7·9

Transverse magnetostriction figures were those of Fricke (1933) whose values of longitudinal magnetostriction are very similar to those taken in the present work. Fricke's transverse values were taken in a hysteresis cycle only up to 30 oersteds, but are symmetrically disposed about and very close to his virgin magnetization values which extend to 400 oersteds. The virgin curve figures were therefore used in both virgin curves and closed cycles in the annealed state but for the strained state the same figures were used after scaling down in the ratio of the longitudinal magnetostriction figures after strain 7 and after re-annealing. This procedure appears to be the only way of obtaining figures, apart from actual measurements, since very little work on transverse magnetostriction has been done.

The observed and calculated curves are given in Figures 8 and 9. Figure 8 shows the virgin (Q, H) curves and Figure 9 the 400-oersted cycle curves in the annealed state and after strain 7. Very close agreement between calculated and observed curves cannot be expected because the values of longitudinal magnetostriction were not measured on the specimen in its initial condition, but only after re-annealing. Further, the estimates of transverse magnetostriction and the values of $(\partial I_0/\partial T_H)$ were not taken on the actual specimen used. Finally, the curve is the difference of four quantities of which three are large, so that small percentage errors in these latter may have a disproportionately large effect on the curve.

The calculated curves all show the general curve shape observed, in spite of the large difference between the shapes of the annealed and strained-state curves.

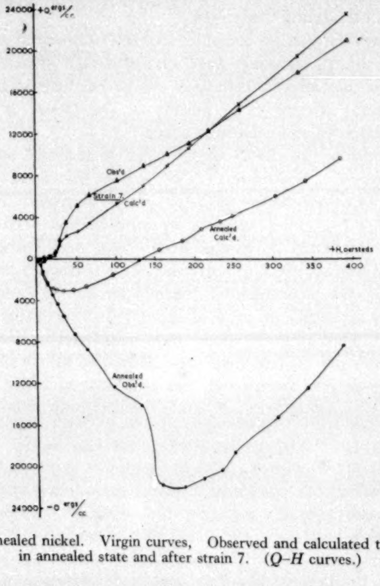

Figure 8. Annealed nickel. Virgin curves, Observed and calculated thermal curves in annealed state and after strain 7. (Q–H curves.)

The agreement in the strained state is remarkable, in view of the difficulties mentioned in the preceding paragraph. In the annealed state, the discrepancy between the curves shows the effect of the crystal anisotropy. The sign and (roughly) the magnitude of the difference are what might be expected. It is interesting that the sudden cooling at small positive values of H, in the 400-oersted cycles, which is found experimentally and has been previously reported (Bates and Harrison 1948), is predicted by the theory in the fully strained case.

Virgin curves after strains 3 and 5 are not shown, but were calculated using estimated values of transverse magnetostriction. The four curves showed the correct curve shapes with a gradual transition between the annealed and strained types. In particular, the increase of agreement as the crystal anisotropy gave place to strain anisotropy was striking. In the two curves shown, the initial irregular variation at small fields is again predicted.

§ 8. PHYSICAL INTERPRETATION OF THE CURVES

Consider the maximum negative field, $-H_{\max}$, applied to the specimen. As the field is reduced the specimen cools under the ordinary magneto-caloric effect. The cooling is increased, actually, because of the simultaneous abstraction of energy $H\,dB/4\pi$. As the field reduction reaches the point where hysteresis effects become noticeable, $H\,dH/4\pi$ becomes less but $H\,dI$ becomes larger as the rate of change of intensity of magnetization with field increases.

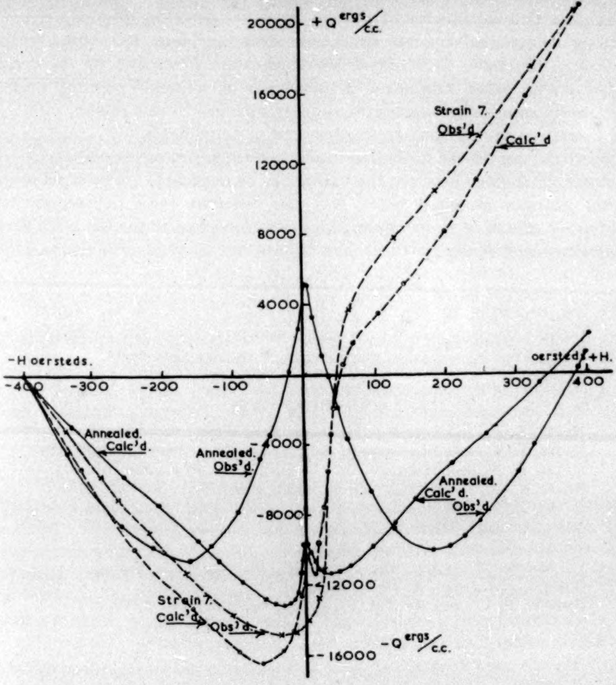

Figure 9. Nickel: 400-oersted cycle: Observed and calculated thermal curves in annealed state and after strain 7. (Q–H curves.)

When the intensity of magnetization is so reduced that magnetostriction changes begin to occur these will be in the form of reducing deformation, so that potential energy of magnetostrictive strain will be transferred to the thermal (kinetic) energy of the specimen. This transfer will supply thermal energy at a rate increasing with the decreasing strain until it exceeds the rate of abstraction of energy as $H\,dB/4\pi$ or by the ordinary magneto-caloric effect. There will then result a heating of the specimen. Thus the formation of the first trough of the curve is explained. After reversal of the field the same effects occur in the opposite order, and with transfer of energy in the opposite directions.

In annealed specimens the curve is strongly accentuated by the transfer of energy between the magneto-crystalline potential energy and the thermal energy. In strained specimens the hysteresis loop is wider, $H\,dI$ being larger, so that the first trough is deepened and broadened. At positive values of H, where the greatest increase in $H\,dI$ has occurred, the increase is sufficient to outweigh the cooling due to expenditure of energy in domain-vector rotations out of the directions determined by the strain anisotropy. Thus the second trough is wiped out. Further, in strained specimens the hysteresis of the magnetostriction curve gives minimum deformation at a small positive field with consequently rapid magnetostriction energy changes in this region. The result is the formation of the small kinks observed in small fields.

The virgin curves are explained in the same manner as the 400-oersted cycle, so that the similarities between the two are to be expected. The rapid magnetostriction changes at small fields and the different rates of increase of the contributory effects of the magnetization process account for the irregularity of the curve at small fields.

ACKNOWLEDGMENTS

We are indebted to Dr. L. B. Pfeil and Mr. H. W. G. Hignett of the Mond Nickel Company for the provision and analysis of the nickel rod, and to Mr. E. W. Lee for his valuable magnetostriction measurements.

REFERENCES

BATES, L. F., and DAVIS, J. H., 1948, *Proc. Phys. Soc.*, **60,** 307.
BATES, L. F., and EDMONDSON, A. S., 1947, *Proc. Phys. Soc.*, **59,** 329.
BATES, L. F., and HARRISON, E. G., 1948, *Proc. Phys. Soc.*, **60,** 213, 225.
BATES, L. F., and HEALEY, D. R., 1943, *Proc. Phys. Soc.*, **55,** 188.
BATES, L. F., and WESTON, J. C., 1941, *Proc. Phys. Soc.*, **53,** 5.
ESAU, A., 1931, *Phys. Z.*, **32,** 483.
FRICKE, W., 1933, *Z. Phys.*, **80,** 324.
GUILLAUME, C., 1920, *Proc. Phys. Soc.*, **38,** 374.
KERSTEN, M., 1932, *Z. Phys.*, **76,** 505.
STONER, E. C. and RHODES, P., 1949, *Phil. Mag.*, ser. 7, **40,** 481.

The Luminescence of Diamonds

By C. BULL and G. F. J. GARLICK
Physics Department, University of Birmingham

MS. received 18*th May* 1950

ABSTRACT. Studies of the luminescence characteristics of different types of industrial diamonds (80–100 mesh dust) have been made. Blue fluorescent diamonds (3,650 A. exciting radiation) exhibit thermoluminescence characteristics of two groups of metastable electronic states, with mean activation energies of 0·5 and 0·7 ev. respectively. Transitions of a forbidden nature from these states to the normal states of emission centres give rise to a temperature-independent, green-yellow phosphorescence, whose longest-lived component has a decay constant of 2×10^{-5} sec^{-1}. Most yellow luminescent and non-luminescent diamonds (3,650 A. exciting radiation) exhibit a blue luminescence when excited by energetic particles or by x-rays, but no thermoluminescence is observed after any type of excitation. The luminescence of diamonds appears to be characteristic of the matrix crystal, and a tentative model for the emission centres is given.

---

§ 1. INTRODUCTION

THE systematic study of the optical and electrical properties of diamonds began with the work of Robertson, Fox and Martin (1934). They showed that diamonds could be divided into two main types according to these properties. For example, diamonds classified as Type I are opaque to ultra-violet radiation of wavelength shorter than 3,000 A., while diamonds of Type II are transparent to radiations as short as 2,250 A. Many diamonds show characteristics of an intermediate nature. The two main types are also distinguished by their infra-red absorption spectra, their birefringence, luminescence and photoconductivity. A comparison of the properties of the two classes has recently been given by Blackwell and Sutherland (1949).

Extensive studies of the luminescence characteristics of many specimens of diamond have been made by Raman and his school (see *Symposia on Diamond* 1944, 1946). However, these do not include quantitative investigations of the thermoluminescence and phosphorescence, which form the main subject of this paper. It is useful here to summarize the experimental results of the Raman school, without acknowledging the validity of some of their theoretical postulates. According to these workers, diamonds of Type I show a blue fluorescence and a feeble yellow-green phosphorescence when excited by ultra-violet radiation at room temperature. The fluorescence and phosphorescence become more intense with increasing lack of crystal perfection of the specimens. Miss Bai (1944) has found that an increase in the optical transparency in the 2,250–3,000 A. region accompanies this increase in luminescence efficiency. Chandresekharan (1946) has shown qualitatively that, after excitation by ultra-violet radiation, these blue fluorescent diamonds exhibit an intense blue thermoluminescence when heated to about 540° K. He states that the thermoluminescence is more intense when the wavelength of the exciting radiation is shorter than 3,200 A. than when longer wavelength radiation is used, but that the shorter wavelength radiation is less efficient in exciting the yellow-green phosphorescence at room temperature. The intensity of the phosphorescence is said to be independent of the duration of excitation. Chandresekharan also found that a blue emission is produced when blue fluorescent diamonds, after excitation at room temperature, are irradiated with light of wavelength longer than 4,200 A.

According to the Raman group, diamonds of Type II are non-luminescent, but diamonds of intermediate type show a yellow fluorescence and a feeble yellow phosphorescence at room temperature. However, Blackwell and Sutherland (1949) have recently shown that some yellow fluorescent diamonds are of Type II.

Raman suggests that the results obtained by his workers show that luminescence in diamond is a characteristic of the pure substance and is not due to extraneous impurities. Since the luminescence intensity increases with the degree of crystal imperfection, it is probable that the luminescence emission is associated with regions of the crystal near lattice defects. Blackwell and Sutherland have reached a similar conclusion from their experimental studies.

The fluorescence spectra of blue and yellow fluorescent diamonds have been measured by Miss Mani (1944) and an attempt has been made by Ramachandran and Chandresekharan (1946) to relate the main features of these spectra to electronic transitions occurring in isolated carbon atoms. The fluorescence spectrum of blue fluorescent diamonds, at 90° K., consists of a strong close doublet at 4,152 A. and a banded continuum of comparable intensity lying to longer wavelengths. (We cannot accept Miss Mani's statement that ' lines ' can be selected from a microphotometer trace of this continuum.) Since it occurs in both emission and absorption spectra, it is assumed that the doublet is due to electronic transitions in carbon atoms, but, since no corresponding anomalous dispersion is observed in blue fluorescent diamonds, this transition must normally be forbidden. This doublet is ascribed to the transitions ${}^1S_0-{}^3P_1$ and ${}^1S_0-{}^3P_2$, since in the isolated atom these form a doublet with similar separation; the mean wave number of the doublet in diamond is 1·114 times that of the doublet in the isolated atom. Atomic interaction in the homopolar crystal and the destruction of symmetry in the neighbourhood of lattice defects could modify the energy levels to this extent. These transitions are forbidden in the isolated carbon atom and, from symmetry considerations, should also be forbidden in the perfect lattice. However, they may become allowed in regions where the symmetry is destroyed, that is, near lattice faults. Thus certain types of defects in the diamond lattice may be capable of functioning as luminescence centres.

No adequate explanation has been given for the line at 5,032 A. which Miss Mani claims to observe in the fluorescence spectrum of yellow fluorescent diamonds, nor for the banded continua, though the latter are probably associated with the vibration spectrum of the diamond crystal lattice.

The extensive studies of the luminescence properties of many different specimens of diamond, reported below, provide more complete information about the nature of luminescence processes in these crystals.

§ 2. EXPERIMENTAL STUDIES

(i) *Classification of Diamonds*

Because of their suitability for thermoluminescence experiments very small industrial diamonds were used in these studies. About 0·4 gramme of 80–100 mesh crushed diamonds (50,000 diamonds) were sorted according to the colour of their fluorescence when excited by 3,650 A. radiation. Of these specimens, about one-quarter showed a moderate or intense blue fluorescence, one-sixth were non-fluorescent, and about twenty specimens showed a strong yellow fluorescence. The remainder showed either a weak blue or a weak yellow-green fluorescence.

All specimens, including those classified above as non-fluorescent, showed a blue fluorescence when excited by x-rays or by ionic bombardment in a discharge tube.

(ii) *Experimental Apparatus*

In order to measure their thermoluminescence and phosphorescence characteristics, the diamonds were mounted either singly or in small numbers in recesses in a copper disc forming part of a vacuum Dewar system, described elsewhere (Garlick and Wilkins 1945). By the use of liquid oxygen and other refrigerants, and a small electric heater situated at the rear of the copper disc, the diamonds could be retained at different temperatures or warmed at a uniform rate over the temperature range from 90° to 600° K. A heating rate of 2·5° K. per second was used in all the thermoluminescence experiments.

The diamonds were excited by focused radiation from a high pressure, 125-watt, mercury-in-quartz lamp, and suitable filters. A Wood's glass filter was used for isolating 3,650 A. radiation and a Corning 986 filter for selecting radiation of wavelengths between 2,400 and 4,000 A. Suitable optical filters were used to select particular emission bands and to remove undesirable radiation.

The luminescence emission from the diamonds was focused on to the cathode of a photomultiplier of the RCA 931A type, whose output current was measured with a d'Arsonval galvanometer. The deflections of the latter were recorded with a manually-operated pen recorder. The apparatus was sufficiently sensitive to record the variation of thermoluminescence with temperature of a single diamond particle.

Measurements of short period phosphorescence and of the rate of increase of fluorescence intensity were made with a Becquerel type of phosphoroscope, photomultiplier and cathode-ray oscilloscope.

(iii) *The Fluorescence Spectra of Diamonds*

It was found that the blue fluorescence of diamonds could be excited by radiation of any wavelength shorter than 4,000 A. Although Miss Mani states that yellow fluorescent diamonds can be excited by radiation of wavelengths as long as 5,200 A., we have found that the excitation efficiency is very small when the wavelength is greater than 4,000 A.

The emission spectra of blue and yellow fluorescent diamonds, at room temperature, were recorded photographically, using a Hilger constant deviation spectrograph and Ilford S.R. Panchromatic plates. Microphotometer traces of two photographs obtained with 3,650 A. wavelength excitation are reproduced in Figure 1. A sharp line is observed at 4,152 A., in agreement with Miss Mani's observation, but the 5,032 A. line reported by her was not found in either spectrum. When radiation of shorter wavelengths (2,500–4,000 A.) was used to excite the diamonds, the long wavelength emission of blue fluorescent diamonds was enhanced. This is not in accord with Chandresekharan's results, but agrees with those deduced from the differences in the thermoluminescence characteristics obtained with these different excitation conditions.

Because of the very low emission intensity, attempts to record the phosphorescence spectrum of blue fluorescent diamonds by using a phosphoroscope in conjunction with the spectrograph were unsuccessful.

(iv) *The Phosphorescence of Blue Fluorescent Diamonds*

At temperatures below 350° K. excitation by radiation of 3,650 A. wavelength produces a yellow-green phosphorescence in blue fluorescent diamonds. When exciting radiations of shorter wavelength are used this phosphorescence is much more intense. At higher temperatures excitation produces a blue phosphorescence whose intensity and duration are strongly temperature-dependent. The rate of decay of the yellow-green phosphorescence is very little affected by temperature, indicating that the emission is due to a forbidden electronic transition in the luminescence centre. Measurements with a Becquerel phosphoroscope system using cathode-ray tube presentation show that, at room temperature, the blue fluorescence of these diamonds rises and decays in a time less than one millisecond after excitation commences or ceases.

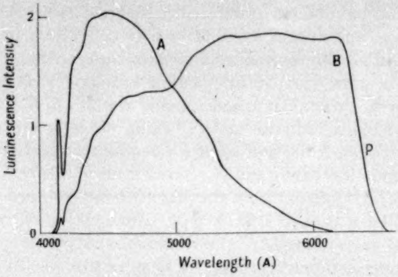

Figure 1. Luminescence emission spectra of diamond at room temperature with 3,650 A. excitation.
A. Blue fluorescent specimens.
B. Yellow fluorescent specimens.
P. Photographic plate cut-off.

(v) *The Thermoluminescence of Blue Fluorescent Diamonds*

After excitation, all blue fluorescent diamonds show a blue thermoluminescence when heated to temperatures above 350° K., with a maximum emission intensity near 520° K. Curves A and B of Figure 2 show the variation of thermoluminescence intensity with temperature after excitation at 90° K. with short wavelength radiation (Corning 986 filter) and with 3,650 A. radiation respectively. The general forms of these two curves are seen to be the same, but the high temperature peak is relatively less intense when 3,650 A. exciting radiation is used.

The thermoluminescence curves obtained with various single blue fluorescent specimens or with several specimens together are all similar, indicating that the thermally metastable electronic states responsible for the thermoluminescence are probably characteristic of the diamond crystal lattice, and are not due to impurities.

It was found that to fill completely the metastable states the excitation must be continued for several minutes. Curves A and B of Figure 2 were obtained after long excitations, while curve C was obtained after exciting the same specimens at room temperature with short wavelength radiation for one second. Small shifts in the positions of the maxima indicate that a distribution of the thermal activation energies of the metastable states responsible for each of the two peaks exists. However, the spread in activation energies of the states responsible for the 520° K. thermoluminescence peak is relatively small, as shown below.

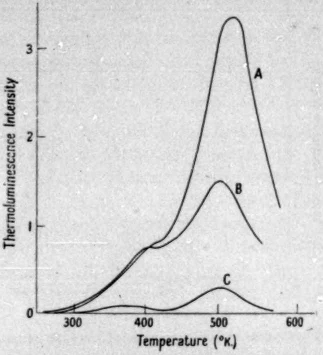

Figure 2. Thermoluminescence curves of blue fluorescent diamonds.
A. After excitation at 90° K. $\lambda_{exc} < 3{,}650$ A.
B. After excitation at 90° K. $\lambda_{exc} = 3{,}650$ A.
C. After excitation for 1 second at 289° K. $\lambda_{exc} < 3{,}650$ A.

(Area under curve A $\simeq 100 \times$ area under curve C.)

It was found that if the diamonds were retained in the dark at a low temperature for some time after excitation, and subsequently heated, the thermal light sum was smaller than that obtained when the same specimen, after identical excitation conditions, was heated immediately after being excited. Since the life-time of an electron in a metastable state whose activation energy corresponds to a thermoluminescence peak at 420° K. is about 10^{20} seconds at 90° K., this decrease in the thermal light sum must be due to direct transitions of electrons from the metastable states to the ground states of luminescence centres. These transitions are responsible for the temperature-independent yellow-green phosphorescence observed at low temperatures. In Figure 3 are shown thermoluminescence curves obtained after the diamonds have been retained for various times after excitation before being heated. These curves show that at 90° K. the probabilities of transitions from the metastable states responsible for the two thermoluminescence peaks are of the same order of magnitude, and that at 289° K. some of the electrons in metastable states giving thermoluminescence at about 400° K. are released by thermal activation. From the variation of the thermal light sum with the time of retention in the dark, the phosphorescence decay curve at low temperatures can be deduced. This is shown in Figure 4. The non-linear form of the curve shows that a range of transition probabilities exists. The lowest value, given by the rate of decay at long decay times, is about 2×10^{-5} sec^{-1}. A similar value is obtained from measurements at 90° K.

The thermal activation energy of the metastable states has been estimated in several ways from theory already established (Randall and Wilkins 1945). It can be shown that the initial rise of the thermoluminescence curve is given by

$$I = n_0 s \exp\left(-E/\boldsymbol{k}T\right),$$

where I is the emission intensity, n_0 is the number of electrons in metastable

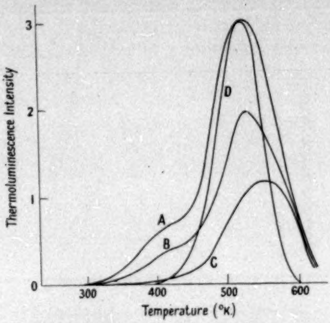

Figure 3. Thermoluminescence curves of blue fluorescent diamonds.

A. After excitation at 289° K. with short wavelength radiation. Phosphorescence decay for 20 seconds at 289° K.
B. After excitation at 90° K. with short wavelength radiation. Phosphorescence decay for 360 minutes at 90° K.
C. After excitation at 289° K. with short wavelength radiation. Phosphorescence decay for 660 minutes at 289° K.
D. Theoretical thermoluminescence curve ($s = 10^6$ sec^{-1}, $E = 0{\cdot}74$ ev.).

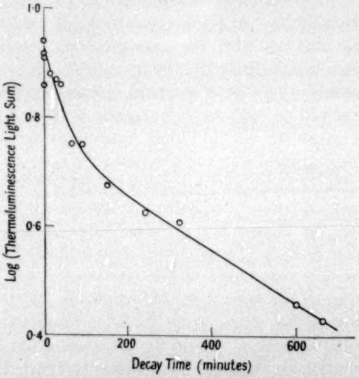

Figure 4. Variation of the thermoluminescence light sum with time of retention at 289° K. after excitation with short wavelength radiation at 289° K.

states, s is a normalizing constant, $\boldsymbol{k}$ is Boltzmann's constant, T is the absolute temperature and E is the activation energy of the states responsible for the thermoluminescence (in this case at about 380° K.). The mean value obtained was 0·43 ev. If the same value of s applies to the two groups of metastable states, a value of 0·65 ev. is obtained for the activation energy of those responsible for the thermoluminescence at 520° K.

The constant s was determined by the method due to Randall and Wilkins (1945). A value of $s = 10^{7 \pm 1}$ sec^{-1} was obtained. Using the relation between the temperature at which thermoluminescence occurs and the activation energy, the energy of the states giving thermoluminescence at 520° K. is found to be 0·8 ev. if $s = 10^7$ sec^{-1} and 0·68 ev. if $s = 10^6$ sec^{-1}.

A third method of estimating E is available in which the rate of decay of phosphorescence at elevated temperatures is related to the thermoluminescence curve by a selection of the correct values of E and s. The values obtained were: $E = 0{\cdot}7$ ev. if $s = 10^6$ sec^{-1}, or $E = 0{\cdot}8$ ev. if $s = 10^7$.

Thus the most probable value of E for thermoluminescence at 520° K. is about 0·7 ev., and that of s is of the order of 10^6 sec^{-1}.

A curve was plotted of the variation of the thermoluminescence intensity with temperature for electrons in metastable states with the single activation energy of 0·74 ev. and $s = 10^6$ sec^{-1} (curve D, Figure 3). This had a half-width of 75° K., compared with the experimentally determined half-width of the main thermoluminescence peak of 110° K., indicating that there is a spread in thermal activation energies in the states responsible for this peak, but that the spread is small.

When blue fluorescent diamonds are excited by X-rays or high-speed particles, they exhibit blue fluorescence and thermoluminescence, the characteristics of which are similar to those produced by ultra-violet excitation.

(vi) *Sensitivity of Blue Fluorescent Diamonds to Long Wavelength Radiation*

Chandresekharan (1946) found that irradiation of excited diamonds by radiation of wavelengths longer than 4,200 A. produced a blue emission (the stimulated emission) and that 5,500 A. radiation was most efficient in stimulating this emission.

By irradiating excited diamonds with radiation of the mercury line wavelengths, 4,358 A., 5,461 A. and 5,770 A., it was shown that the action of the stimulating radiation is to eject electrons from the metastable states.

The stimulation spectrum (that is, the variation of the efficiency of stimulation, as shown by the intensity of the stimulated emission, with the wavelength of the stimulating radiation) of blue fluorescent diamonds was determined using apparatus similar to that described by Garlick and Mason (1949). As the stimulated emission is very low, it was necessary to allow all the stimulated emission to reach the photomultiplier, so that stimulating radiations of wavelengths less than 6,000 A. could not be used without scattered radiation from the monochromator reaching the photomultiplier. The stimulation spectrum after excitation by short wavelength radiation or by 3,650 A. rises from zero at 1·0 μ and increases steadily in value into the visible region. The stimulated emission is greater after excitation of the diamonds by short wavelength radiation than after excitation by 3,650 A., but the shape of the stimulation spectrum was found to be independent of the excitation wavelength, of the temperature of stimulation below 290° K., and of whether one or both groups of metastable states are filled.

The decay of the stimulated emission at 290° K. under 7,000 A. radiation approximates to two superimposed exponential decays, which may correspond to the two mean activation energies of the metastable states.

§ 3. CONCLUSION

The thermoluminescence curves of all diamonds exhibiting thermoluminescence are similar in form, indicating that luminescence in diamond is a property of the matrix and is not due to impurities. This is supported by other experimental results given above, and also by those previously reported by Raman and his co-workers.

The sharp doublet at 4,152 A. in the emission spectrum of blue fluorescent diamonds can be related to electronic transitions between well-defined energy levels. The banded structure of the longer wavelength emission is probably due to interaction of the electronic states with vibrational states of the lattice.

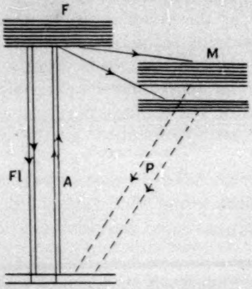

Figure 5. Energy level scheme for the luminescence centres of blue fluorescent diamonds. G. Ground states (doublet). F. Excited states. M. Metastable states. A. Absorption transitions. Fl. Fluorescence transitions. P. Phosphorescence transitions (temperature independent).

The electronic transitions producing the luminescence are highly forbidden, due to the high symmetry conditions of the perfect lattice, but the transition probability is increased where the symmetry is disturbed, as happens near lattice defects. No evidence is found for the sharp lines reported by Miss Mani in the long wavelength emission.

The structure of the spectrum suggests a lattice vibration spectrum of the form given by the Born–Kármán theory. The 5,032 A. line reported to occur in the emission spectrum of yellow fluorescent diamonds was not found in our investigations.

We suggest that the energy level scheme for the luminescence centre of blue fluorescent diamonds is probably that shown in Figure 5. Two groups of metastable states are assumed to exist, corresponding to the two groups found in the thermoluminescence experiments. Direct electronic transitions from these states to the ground states give rise to the temperature-independent, long wavelength phosphorescence observed at low temperatures, while thermal activation of electrons to the F states gives rise to thermoluminescence and the strongly temperature-dependent, short wavelength phosphorescence observed at higher temperatures. Electronic transitions from the upper levels to the ground states are allowed, and account for the rapid rise and decay of the blue luminescence, but the direct transitions from the metastable levels to the ground states are highly forbidden. Figure 4 indicates that a range of probabilities for these transitions exists, probably due to the different metastable levels. To explain the increase in thermal light sum obtained by using exciting radiation of shorter wavelength, it is assumed that states with higher energies than those of F states, shown in Figure 5, exist, and that some of the metastable levels can only be reached by transitions from these higher levels. The existence of these higher energy states may also account for the blue emission of most yellow- and non-fluorescent specimens when excited by high energy ions or electrons or by x-rays. In these cases no thermoluminescence or phosphorescence is observed. We may also conclude that the electron trapping states found in Type II diamonds (used as ' conductivity counters ' for energetic particles) are of a different nature from those found in the luminescence centres of blue fluorescent diamonds.

From measurements of the blue and yellow components of the luminescence spectrum it is found that the optical transition M–F should involve a minimum energy of about 0·5 ev. Absorption due to these transitions would therefore be expected in the 1–2 μ region. No well-defined bands are found in the stimulation spectrum, and no absorption measurements in this region have been reported. The absorption bands would be weak compared with those occurring at 8 μ, since the number of metastable states is not likely to exceed 1 per 10^4 lattice atoms.

These studies would be made more complete by repetition with large diamonds, for which careful optical absorption measurements could be made during excitation and emission.

REFERENCES

Bai, K. S., 1944, *Proc. Ind. Acad. Sci.* A, **19,** 253.

Blackwell, D. E., and Sutherland, G. B. B. M., 1949, *J. Chim. Phys.*, **46,** 9.

Chandresekharan, V., 1946, *Proc. Ind. Acad. Sci.* A, **24,** 187, 193.

Garlick, G. F. J., and Mason, D. E., 1949, *J. Electrochem. Soc.*, **96,** 90.

Garlick, G. F. J., and Wilkins, M. H. F., 1945, *Proc. Roy. Soc.* A, **184,** 408.

Mani, A., 1944, *Proc. Ind. Acad. Sci.* A, **19,** 231.

Ramachandran, G. N., and Chandresekharan, V., 1946, *Proc. Ind. Acad. Sci.* A, **24,** 176.

Randall, J. T., and Wilkins, M. H. F., 1945, *Proc. Roy. Soc.* A, **184,** 347.

Robertson, R., Fox, J. J., and Martin, A. E., 1934, *Phil. Trans. Roy. Soc.* A, **232,** 463.

Symposia on Diamond, 1944, *Proc. Ind. Acad. Sci.* A, **19,** and 1946, *Ibid.* A, **24.**

LETTERS TO THE EDITOR

The Ultra-Violet Spectrum of Ethylene

In 1934, Snow and Allsopp investigated the ultra-violet spectrum of ethylene. They found that a very weak diffuse absorption begins near 2,100 A. which appears to rise to a flat continuous maximum at 1,630 A. They suggested that this broad and diffuse system corresponds to two distinct electronic transitions: the weak long-wave system near 2,000 A. was attributed to the $^1A_g \rightarrow {}^3B_{1u}$ singlet–triplet transition, and the intense region near 1,630 A. to the allowed transition $^1A_g \rightarrow {}^1B_{1u}$. Recently, Craig (1950) has criticized the former assignment and has suggested that the weak band near 2,000 A. is due to a forbidden transition $^1A \rightarrow {}^1A_g$. His conclusions were based, very largely, on theoretical considerations in which the method of antisymmetrized molecular orbitals (a.s.m.o.) was used.

A critical test of a.s.m.o. procedure, which has just been completed (Moffitt and Scanlan, to be published), indicates that this method is most unreliable. In particular, it has been shown that the predicted and observed degrees of excitation of the $^3\Sigma_u^-$, $^3\Sigma_u^+$, $^1\Sigma_g^+$ and $^1\Delta_g$ states of the oxygen molecule, with respect to its $^3\Sigma_g^-$ ground state, do not correspond at all closely. The causes for this failure have been analysed and it has been demonstrated, similarly, that the $^1B_{1u} - {}^3B_{1u}$ separation for ethylene, which is predicted in this way, is systematically exaggerated.

Accordingly the author has developed a modified a.s.m.o. theory which is free from these objections, and which gives a very satisfactory account of the observed oxygen spectrum. These improvements have been attained by ensuring the correct asymptotic behaviour of the approximate energy matrix, as the internuclear distance increases indefinitely. For it is in this respect that the conventional a.s.m.o. theory is most seriously in error. Applying this new method to the ethylene molecule, it is estimated that the $^1B_{1u} - {}^3B_{1u}$ interval, for a C–C distance of 1·34 A., is $1{\cdot}1 \pm 0{\cdot}3$ ev., and, further, that Craig's excited ^1A_g state lies, at the very least, some 7 ev. above the $^1B_{1u}$ state. Since the assignment of the 1,630 A. system to the allowed transition $^1A_g \rightarrow {}^1B_{1u}$ has been substantiated both empirically and theoretically, it is seen that Snow and Allsopp's assignment also for the weak 2,000 A. band is in excellent agreement with these predictions.

It is concluded that the weak region of diffuse absorption which occurs near 2,000 A. in the ultra-violet spectrum of ethylene is due to the forbidden electronic transition $^1A_g \rightarrow {}^3B_{1u}$, as was originally suggested by Snow and Allsopp in 1934. A full account of these calculations is being prepared for publication.

British Rubber Producers' Research Association,
Welwyn Garden City, Hertfordshire.
W. E. Moffitt.

17th August 1950.

Craig, D. P., 1950, *Proc. Roy. Soc.* A, **200**, 272.
Snow, C. P. and Allsopp, C. B., 1934, *Trans. Faraday Soc.*, **30**, 93.

The Spectra of Flames Supported by Fluorine

The reaction of fluorine with most organic and many inorganic substances is accompanied by the emission of light in the form of a flame which is not dependent on the presence of oxygen. The spectroscopic study of these flames of 'combustion' of hydrocarbons and other substances in fluorine may yield valuable information concerning combustion processes, besides possibly providing a source for new band-systems.

These flames are now being studied at Imperial College in collaboration with Dr. A. G. Gaydon as part of the research project now in progress to determine the mechanism of the formation of the C_2 and CH radicals in flames and the excitation processes involved (Gaydon and Wolfhard 1949, 1950).

The fluorine was obtained from a 10 amp. fluorine cell, kindly lent by Imperial Chemical Industries Ltd., capable of delivering up to 4 litres of fluorine per hour. Both copper and nickel burners have been used, these consisting of three concentric tubes, the inner tube ($\frac{1}{8}$ in. o.d.) carrying the fluorine, the second tube ($\frac{5}{16}$ in. o.d.) carrying the fuel, and the outer tube ($\frac{1}{2}$ in. o.d.) carrying a steady flow of nitrogen to isolate the flame from the atmosphere. A steady flame is obtained on the tip of the inner tube. The flames have been small, and contributions by surface effects due to the burner walls may be large.

The hydrocarbons *methane*, *ethane*, *ethylene*, *acetylene*, *benzene* and *toluene* all burn with a bright blue-green flame which becomes luminous as soon as either the burner tip becomes heated or the fuel flow is increased, giving copious carbon formation. The spectrum in every case contains strong C_2 Swan bands and strong CH bands with high excitation at 3143 A. Weak CN violet bands and a trace of the 3360 A. NH band also appear.

Methyl alcohol burns with a weak blue-green flame giving C_2 Swan and CH bands with strong OH. There is also a trace of the CN violet bands.

Ethyl nitrate gives a blue-violet flame with no evidence of carbon formation. The spectrum contains strong CN violet, NOγ and OH band-systems with weaker C_2 Swan and CH bands.

Carbon disulphide gives a bright pale-blue flame, the spectrum consisting of a weak continuum superimposed with S_2 bands between 2500 A. and 4900 A.

Carbon tetrachloride burns with a weak greenish-yellow flame, the spectrum consisting of a yellow-green continuum extending down to 2800 A. superimposed with CN violet bands. The introduction of a trace of hydrogen causes the flame to brighten and eventually become luminous, giving heavy carbon formation. The spectrum now contains C_2 and CH bands with the CCl 2790 A. and strong CN violet bands.

Chloroform gives a fairly bright greenish-yellow flame. The spectrum is mainly continuous, but several unidentified closely-spaced bands appear between 5600 A. and 6400 A. The addition of a trace of hydrogen brightens the flame, and it eventually becomes luminous, with heavy carbon formation. Strong C_2 and CN violet bands now appear; the CH bands appears to be missing.

Methyl bromide burns with a very bright luminous flame with heavy carbon formation. It is difficult to obtain a spectrum unmasked by the continuous emission from the hot carbon. However, small flows of methyl bromide, diluted with nitrogen, give a weak yellow-green flame which yields a continuum superimposed with weak bands between 5100 A. and 6400 A. A trace of hydrogen increases the brightness and adds a blue-green tint, ultimately leading to carbon formation. The spectrum now contains strong CN violet and C_2 Swan with weak CH bands, the bands between 5100 A. and 6400 A. being increased in intensity.

These bands occur much more strongly in the flame of *bromine*, containing a trace of hydrogen, burning in fluorine. An analysis of these bands shows that they belong to, and form an extension of, the system already known in absorption for the BrF molecule (Brodersen and Schumacher 1947). This system has not previously been reported in emission.

Methyl iodide gives a greenish-yellow flame emitting an unknown system of red-degraded bands between 5200 A. and 6500 A. The addition of hydrogen brightens the flame and, besides increasing the intensity of the new bands, gives strong C_2 Swan and weak CH bands.

These bands also occur in the *iodine*-fluorine flame and have therefore been provisionally attributed to IF. They form a fairly strong red degraded system with marked progressions —probably the $v'=0$ and the $v''=0$ progressions. The approximate wavelengths of the strongest heads together with a provisional assignment of vibrational quantum numbers are: 6249 (0,5), 6032 (0,4), 5826 (0,3), 5632 (0,2), and 4869 (4,0), 4781 (5,0), 4697 (6,0).

Hydrogen gives a weak greenish-blue flame with a weak violet mantle. Instead of the expected continuous emission, strong S_2 and the SH 3240 A. bands appear (cf. sulphur impurities in the hydrogen-oxygen flame (Gaydon 1948)).

Carbon monoxide burns with a steady blue flame which emits a continuum extending from 4900 to 2900 A.

Ammonia gives a yellow-green flame. The spectrum contains strong NH 3360 A. and the ammonia α (NH_2) bands, with OH and NOγ bands due to the presence of oxygen impurities.

All these flames are very sensitive to traces of impurities: S_2 bands appear in the hydrogen, CS bands in the hydrocarbon, and CuCl in the carbon monoxide flames.

These results are sufficient to show that a detailed study of these flames may yield much valuable information and surprising and interesting results, such as the formation of C_2 and CH and the influence of hydrogen on the organic halides, causing the appearance of strong C_2 bands followed by heavy carbon formation.

A more detailed study of this type of flame is now in progress and the results will be published later. The systems attributed to IF and BrF are receiving further attention, and the analyses will be published shortly.

The author is indebted to the Australian Department of Supply for a scholarship.

Imperial College,
London, S.W.7.
17th August 1950.

R. A. Durie.

Brodersen, P. H., and Schumacher, H. J., 1947, *Z. Naturforsch.*, **2a**, 358.
Gaydon, A. G., 1948, *Spectroscopy and Combustion Theory*, 2nd Edn., p. 91.
Gaydon, A. G., and Wolfhard, H. G., 1949, *Proc. Roy. Soc.* A, **199**, 89; 1950, *Ibid.*, **201**, 561, 570.

Scintillation Efficiency of Anthracene Crystals

An extensive investigation is being made of the scintillations excited in organic crystals by ionizing radiations. In this note some preliminary results obtained with a pure anthracene crystal are reported. The crystal, 1 cm. square by 1 mm. thick, was mounted on a 5,311 photo-multiplier tube, with a Po α-particle source directly above it. The air spacing d between the source and the crystal, and hence the mean energy E of the incident radiation, were varied by a micrometer screw attached to the source. The photo-tube output was fed through a cathode follower to a linear amplifier, discriminator and scaler, and the integral pulse size distributions were observed for different values of d. The mean pulse size V, derived from the integral distribution, is plotted against d in Figure 1. It is found that V increases linearly with the residual air range $r=r_0-d$ (where $r_0=38$ mm.) of the incident α-particles, from $r=8$ to 38 mm., corresponding to $E=1{\cdot}6$ to $5{\cdot}3$ Mev. Hence at these energies the number of fluorescent photons emitted is directly proportional to the range of the α-particle within the crystal, and it is independent of the specific energy loss $-dE/dx$, which changes by more than 2 : 1 in this energy interval.

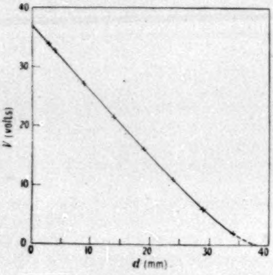

Figure 1.

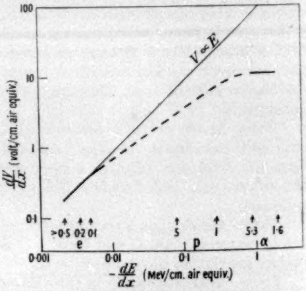

Figure 2.
Values relating to e, p and α are in Mev.

Observations have also been made of the scintillations excited in the crystal by the 162 kev. and 186 kev. internal conversion electrons from ^{114}In. In these measurements a single channel pulse analyser was substituted for the discriminator. Two separate peaks were resolved, which were of equal intensity, and of mean pulse sizes $V = 11{\cdot}1$ and $13{\cdot}2$ volts, measured on the same scale as the α-particle pulses. Hopkins (1950) has found that the scintillations excited in anthracene by electrons increase linearly with electron energy from 125 kev. to more than 1 MeV., but non-linearly at lower energies. The ^{114}In electron peaks have been used as calibration points to convert Hopkins' experimental curve to the same scale of V.

The response of the crystal to different ionizing radiations has been compared by considering the variation of the specific fluorescence dV/dx (expressed in the arbitrary units of v/cm. air equivalent) with the specific energy loss $-dE/dx$, measured in MeV/cm. air equivalent. These quantities have been computed from the experimental curves, using the range–energy data of Bethe (1950) for α-particles, and of Curie (1935) for electrons; they are plotted in Figure 2. At low values of $-dE/dx$ (electrons > 125 kev.) the specific fluorescence increases linearly, corresponding to V proportional to E, but at high values of $-dE/dx$ (α-particles of 1·6 to 5·3 MeV.) it saturates, attaining a constant value independent of $-dE/dx$. The data for α-particles of $r < 8$ mm. indicates a decrease in dV/dx beyond saturation, but as no corrections for straggling, source thickness, etc., were applied in these preliminary measurements, this has been omitted from Figure 2. The response to particles of intermediate energy loss can be estimated by interpolation, and comparison with the linear ($V \propto E$) curve. Thus the scintillations produced by 5 MeV. protons ($-dE/dx = 0{\cdot}08$) are expected to be about 50% of those excited by electrons of the same energy. Measurements of the proton response of the crystal are being made to obtain experimental data in this region.

The relative response to α-particles and electrons is found to be the same for naphthalene and anthracene, so that the behaviour of anthracene is probably typical of the organic crystals. It differs from inorganic crystals, like NaI(Tl), in which the response is proportional to E, and is independent of the nature of the incident particles. It is estimated, from the widths of the observed pulse size distributions, that for fast electrons in anthracene about 100 ev. of incident energy are expended per emitted photon, so that a pulse size V of 1 volt on the scale adopted is equivalent to the emission of about 120 photons. The specific fluorescence, expressed in photons/cm. air equivalent, increases from about 22 for fast electrons to about 1,300 at saturation. The calculated α-particle stopping power of anthracene relative to air is 1,200, so that the path length per emitted photon decreases from about 4000 A. for fast electrons to about 60 A. at saturation.

Most of the energy of the α-particle is dissipated within the crystal in non-fluorescent processes, such as chemical dissociation. In preliminary observations on an anthracene crystal irradiated by an intense source of α-radiation for a period of an hour, the crystal surface turned brown and lost its property of fluorescence. This effect, which is attributable to the removal of the loosely bound hydrogen atoms from the molecules, is being further investigated.

Department of Natural Philosophy,
The University, Glasgow.
11th August 1950.

J. B. BIRKS.

BETHE, H. A., 1950, *Rev. Mod. Phys.*, **22,** 213.
CURIE, Mme P., 1935, *Radioactivité* (Paris : Hermann et Cie).
HOPKINS, J. I., 1950, *Phys. Rev.*, **77,** 406.

Dissociation Cross Sections for Fast Hydrogen Molecule Ions

Dr. J. H. Fremlin has informed the present author that measurements will soon be carried out of the cross section for the dissociation of a hydrogen molecule ion (H_2^+), accelerated to energies of 1 to 20 MeV., during a collision with stationary gas molecules or atoms. It therefore seemed of interest to attempt to calculate these cross sections theoretically. Because of the complex structure of both the hydrogen molecule ion and the gas atoms with which it collides, it seemed impracticable to attempt an exact calculation. An estimate of the order of magnitude of these cross sections has been obtained, however, using a method outlined below.

Teller (1930) has calculated binding energies of H_2^+, for the ground state as well as for excited electronic states, as a function of internuclear distance. Teller's calculations show that a hydrogen molecule ion in its ground state can be dissociated in either of the following two ways. (i) By exciting nuclear vibrations: if we assume the ion to be in its lowest vibrational state initially this requires an energy transfer (in the reference frame in which the ion is at rest) equal to or bigger than E_{N}, the dissociation energy of H_2^+, which is about 2·8 ev. (ii) By exciting higher electronic states of H_2^+: we assume the Franck–Condon principle to apply, i.e. that the internuclear distance of the H_2^+ ion is not altered appreciably during the collision and excitation from its equilibrium value for the ground state (1sσ). The lowest state which can be excited is the 2pσ-state, which requires an energy transfer E_{e} of 12·5 ev. for the internuclear distance we are considering. This state is unstable, dissociating into a free proton and a hydrogen atom in its ground state with total kinetic energy 9·7 ev. Excitation of any of the other discrete electronic states of H_2^+ requires an energy transfer of between 19 and 30 ev. for this internuclear distance; these states then also lead to dissociation, resulting in a free proton, a hydrogen atom in an excited discrete state and some kinetic energy. Excitation of a continuum state, resulting in two free protons and a free electron, requires an energy transfer E_{e}' of 30 ev. (or more).

We note that E_{N}, E_{e} and E_{e}' are all very small compared with the kinetic energies of either the two protons or the electron making up the H_2^+ ion, measured in the laboratory system in which the hit gas atoms are at rest. We cannot calculate exactly cross sections for the energy transfer to a H_2^+ ion in a collision with a gas atom, but we can calculate the total cross section for a free proton (or electron) with the velocity of the impinging H_2^+ ion to undergo a momentum change K in a small angle collision with a gas atom (both with and without excitation of the gas atom). It seems plausible that the cross section for this process is of the same order of magnitude as one half (since there are two protons in H_2^+), the cross section for an energy of $K^2/2M$ being transferred to nuclear vibrations of the impinging hydrogen molecule ion in a collision with the same gas atom, provided that $K^2/2M$ is about equal to or larger than E_{N}. Similarly the total cross section for a free electron of the same velocity to undergo a momentum change K should be of the same order of magnitude as that for an energy transfer of $K^2/2m$ to the electronic excitation of a hydrogen molecule ion in such a collision, provided that $K^2/2m$ is larger than E_{e}'. M and m are the proton and electron mass respectively. The total cross section for exciting the discrete states of H_2^+ requiring energies between E_{e} and E_{e}' is presumably of the same order of magnitude as, but smaller than, the total cross section for a free electron to suffer a momentum change between $(2mE_{\mathrm{e}})^{1/2}$ and $(2mE_{\mathrm{e}}')^{1/2}$. We therefore use as two estimates of the total dissociation cross section for a H_2^+ ion of a certain velocity the sum of (i) twice the total cross section for a free proton of the same velocity to undergo a momentum change of $(2mE_{\mathrm{N}})^{1/2}$ or more, and (ii) the total cross section for one free electron of the same velocity to undergo a momentum change of more than $(2mE_{\mathrm{e}})^{1/2}$ for the one estimate, $(2mE_{\mathrm{e}}')^{1/2}$ for the other. It is hoped that the true answer lies between these two estimates.

In calculating cross sections the following further approximations were made. Any molecular structure of the stationary gas was disregarded and cross sections were calculated for single atoms of hydrogen, nitrogen, oxygen and argon. Born approximation was used throughout. For kinetic energies of the hydrogen molecule ion of about 2 Mev. or more this should be quite reliable if the stationary gas is hydrogen, nitrogen or oxygen and at least a reasonable approximation for argon. For the scattering cross sections for the protons, screening of the nuclear field and binding of the electrons in the gas atom can be neglected. The estimate for the total dissociation cross section due to excitation of nuclear vibrations is then $[4\pi(Z+Z^2)e^4/EE_{\mathrm{N}}]$ or $[(Z+Z^2)/E]\times 9{\cdot}3\times 10^{-20}$ cm^2, where Z is the atomic charge of the stationary gas atom and E is the kinetic energy of the hydrogen molecule ion in Mev. In evaluating scattering cross sections for the electron, however, both screening and binding have to be considered for the gas atoms since $(2mE_{\mathrm{e}})^{1/2}$ is of the same order of magnitude as the Bohr momenta in these atoms. The estimates for the dissociation cross section due to electronic excitation are then $[3{,}670\pi(g_1Z+g_2Z^2)e^4/EE_{\mathrm{e}}]$ and the same expression with E_{e} replaced by E_{e}'. There g_1 and g_2 are factors of the order of magnitude of, but smaller than, unity which take account of screening and binding. These factors g_1 and g_2 were calculated separately for each of the gas atoms considered, both for E_{e} and E_{e}', by numerical integration using tables given by Mott and Massey (1949) which are based partly on Hartree and partly on Thomas–Fermi wave functions for nitrogen, oxygen and argon (and exact wave functions for hydrogen).

In the first column of the Table we give the limits between which the product of

	$\sigma_{tot} \times E$ $(10^{-18}$ cm^2 Mev.)	M.F.P./E (cm/Mev.) for 10^{-3} mm. Hg	P_{nuc}(%)	P_{ion}(%)	P_{exc}(%)
Hydrogen	12·5 to 22·5	1200 to 2200	1	60	65
Nitrogen	210 to 340	85 to 140	2	65	25
Oxygen	255 to 370	75 to 110	2	70	20
Argon	900 to 1300	22 to 31	3	70	10

σ_{tot} in 10^{-18} cm^2, and of E in Mev., is estimated to lie; σ_{tot} is the total cross section for a H_2^+ ion with kinetic energy E to be dissociated in a collision with a single H, N, O or A atom. In the second column we give estimates for the mean free path for dissociation of a H_2^+ ion in H_2, N_2, O_2 or A gas at a pressure of 10^{-3} mm. Hg expressed in cm. (M.F.P.) divided by the energy E expressed in Mev. In the remaining columns we give estimates for P_{nuc} the percentage of the dissociations due to excitation of nuclear vibrations of the H_2^+ ion, P_{ion} the percentage of dissociations in which the H-atom resulting from the dissociation is further ionized, and P_{exc} the percentage of dissociations in which the hit atom is excited into higher electronic states. According to these estimates the dissociations take place mainly through electronic excitation of the hydrogen molecule ion; the cross section is inversely proportional to the kinetic energy E and increases with the atomic number Z of the hit atom, faster than Z but more slowly than Z^2. A comparison of these theoretical estimates of the dissociation cross sections for H_2^+ with experimental measurements will show just how reliable or unreliable methods of the type used here are for estimating cross sections for complicated collision processes.

The author wishes to express his gratitude to the Department for Scientific and Industrial Research for a Senior Research Award, during the tenure of which part of this work was carried out.

Laboratory of Nuclear Studies,
Cornell University,
Ithaca, New York.
10th August 1950.

E. E. Salpeter.

Mott, N. F., and Massey, H. S. W., 1949, *The Theory of Atomic Collisions* (Oxford: Clarendon Press).
Teller, E., 1930, *Z. Phys.*, **61**, 458.

The Reaction ^{7}Li γp ^{6}He

Becker, Hansen and Diven (1947) reported finding a β-emitting body of half-life 1 second following irradiation of lithium with γ-rays from the Illinois 20 Mev. betatron. Assuming this to be ^{6}He resulting from the ^{7}Li γp reaction, they determined the threshold of the reaction to be 9·5±0·3 Mev.

In the course of experiments to investigate the reaction ^{7}LiγT^{4}He (Titterton 1950) lithium loaded nuclear emulsions were exposed to the radiation from the reaction ^{7}Lipγ^{8}Be, ^{8}Be*. Definite evidence has been obtained for the reaction

$$^7\mathrm{Li} + h\nu = {}^1\mathrm{H} + {}^6\mathrm{He} - 10{\cdot}1 \text{ Mev.},$$

the ^{6}He being formed in the ground state.

Nine events, one of which is shown in the Figure, have been found; seven correspond to the 17·6 Mev. γ-ray and two to the 14·8 Mev. γ-ray. The events can be identified by the difference in ionization of the ^{6}He recoil and the proton and are confirmed by energy and momentum balances. The range–energy relation for the ^{6}He was derived from the known relation for α-particles. The scattering of the tracks indicates that the two particles are moving in opposite directions.

A cross section for the reaction can be estimated in terms of the $^{12}C\gamma3\alpha$ reaction following the procedure given in the earlier note (Titterton 1950), and the value obtained is

$$\sigma^7\mathrm{Li}\,(\gamma p)(17{\cdot}6+14{\cdot}8)=(2{\cdot}0\pm0{\cdot}9)\times10^{-28}\ \mathrm{cm}^2.$$

Attention is being given to the possibility that ^{6}He may be formed in an excited state which de-excites by γ-ray emission before the fragment has moved an appreciable distance in the emulsion, and one event has been observed which might be attributed to this. Further work now in progress should establish or refute this possibility.

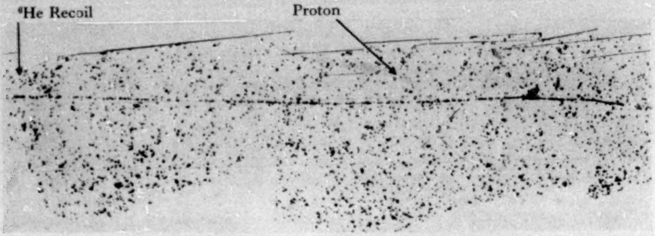

The reaction $^7\mathrm{Li}\,\gamma p\,^6\mathrm{He}$. Proton range 238 μ. ^{6}He recoil 4μ.

Thanks are due to Miss P. Port for microscope work on this problem.

Ministry of Supply,
Atomic Energy Research Establishment,
Harwell, Didcot, Berkshire.
E. W. Titterton.

1st August 1950.

Becker, R. A., Hansen, A. O , and Diven, B. C., 1947, *Phys. Rev.*, **71**, 466 (Abstract).
Titterton, E. W., 1950, *Proc. Phys. Soc.* A, **63**, 915.

Forbidden β-Decay in ^{24}Na

The decay scheme of ^{24}Na is very well established (Siegbahn 1946, Elliott *et al.* 1943) and is shown in the Figure (roman type). The order of emission of the two γ-rays is not obtainable from coincidence experiments, but it is definitely established that they are in cascade and follow the β-ray emission. Experiments on the inelastic scattering of protons (Rhoderick 1949), and of neutrons (Beghian *et al.* 1950), and measurements of the intensity of the 4·14 Mev. ' cross-over ' γ-ray transition (Bishop *et al.* 1950), suggest that the order of emission is that shown in the Figure. Experiments on the angular correlation of the γ-rays (Brady and Deutsch 1948) suggest the spin assignments 0, 2, 4 for the ground state and first and second excited states of ^{24}Mg.

In view of the larger energy-release in the β-ray transitions $^{24}\mathrm{Na}\rightarrow{}^{24}\mathrm{Mg}^*$ (1·38 Mev.) or $^{24}\mathrm{Na}\rightarrow{}^{24}\mathrm{Mg}$ (ground state) a search has been made for electrons belonging to either of these two spectra. The only result has been to place an upper limit on the probability of occurrence of these processes.

The investigation has been carried out by means of a short magnetic lens β-ray spectrometer. The normal background counting rate due to Compton electrons ejected by the γ-radiation from the walls and baffles of the counter, and to γ-rays scattered into the counter, was greatly reduced by using as detector a pair of counters in coincidence with an aluminium absorber about 1/16 inch thick between them; for example, with no current in the lens-coil the coincidence counting rate was only 6·6 counts/minute when the counting rate in the first counter was 7,000/minute.

A source of about 3 millicuries of ^{24}Na in the form of carbonate was used and the procedure was as follows : the counting rate beyond the limit of the known spectrum was measured by means of the double counter; the experiment was then repeated with the same value of the lens-coil current but with an absorber in front of the source to remove any β-particles. Neglecting the very slight absorption of the γ-radiation in the absorber, this second measurement shows what proportion of the first counting rate should be attributed to the γ-ray background and hence, by difference, the counting rate due to β-rays from the source. In order to eliminate the effect of drifting of the counter characteristics the measurements were taken alternately for ten-minute periods. After allowing time for the known spectrum to decay to a measurable intensity it was examined using a single counter. After correction for the lower efficiency of the double counter the intensity of the 'non-existent' spectra could be compared with that of the known spectrum.

For an element of small Z like ^{24}Na the shape of the β-spectrum is given approximately by the expression $P(\eta)\,d\eta = C\eta^2(W_0 - W)^2\,d\eta$ and hence $N_x = C_x f(\eta_{0x})$, where the suffix x refers to the particular spectrum under consideration, N_x is the number of particles in the spectrum, η_{0x} is the maximum momentum of the β-particles in the spectrum in m_0c units. The partial half-life is inversely proportional to the number of particles emitted, N_x, and hence the relative ft values are given by $(ft)_2/(ft)_1 = C_1/C_2$. If the known spectrum is designated (1) and the spectrum leading to the 1·38 Mev. level is designated (2), in a typical experiment $C_1 = 5 \times 10^3$, and if the reasonable assumption is made that almost all the residual counting rate at 3·5 Mev. is due to (2), then $C_2 = (1{\cdot}7 \pm 1{\cdot}6) \times 10^{-3}$, and hence

$$(ft)_2/(ft)_1 \nless 1{\cdot}5 \times 10^6, \qquad N_2/N_1 \ngtr 1/12{,}500.$$

From the ratio of the ft values it is seen that the second spectrum must be at least three degrees more forbidden than the known spectrum (1). If the known spectrum is 'allowed but unfavoured', then it follows that the spin of ^{24}Na must be 5 units in order that spectrum (2) should be 'third forbidden', and it is further necessary that the two levels in ^{24}Mg should differ in parity. The two possible schemes are shown in the Figure (italics). If the known spectrum is 'first forbidden' then it is impossible for the β-ray theory in its present form to explain the low intensity of the second spectrum.

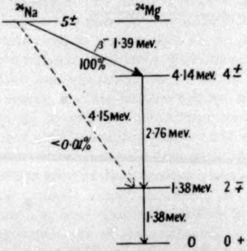

The explanation given of the low intensity of the higher-energy β-ray transitions is not very convincing since the 4·15 Mev. transition is almost 'fourth forbidden' by its ft value and may be much less intense than the upper limit given above. If the spin of ^{24}Na is measured to be less than 5 units, or if the predicted parity assignments are shown to be incorrect, then the presence will have been established of other factors besides spin and parity selection rules capable of reducing the transition probability by about one thousand times.

I wish to thank Professor S. Devons for suggesting this problem.

Cavendish Laboratory,
Cambridge.
18th August 1950.

P. J. Grant.

Beghian, L. E., Grace, M. A., Preston, G., and Halban, H., 1950, *Phys. Rev.*, **77**, 286.
Bishop, G. R., Wilson, R., and Halban, H., 1950, *Phys. Rev.*, **77**, 416.
Brady, E. L., and Deutsch, M., 1948, *Phys. Rev.*, **74**, 1541.
Elliott, L. G., Deutsch, M., and Roberts, A., 1943, *Phys. Rev.*, **63**, 386.
Rhoderick, E. H., 1949, *Nature, Lond.*, **163**, 898.
Siegbahn, K., 1946, *Phys. Rev.*, **70**, 127.

REVIEWS OF BOOKS

Heat Transfer, Volume I, by MAX JAKOB. Pp. xxix + 758. 1st Edition. (New York: John Wiley and Sons, Inc.; London: Chapman and Hall, Ltd.) 96*s*.

This is a book of wide scope. Scarcely any of the properties of matter, physical laws and underlying theories of interest in the study of heat transfer do not receive at least some attention. A student of physics cannot fail to be impressed by the way in which the different branches of his subject are intertwined in the discussion of topics which are generally grouped together under the heading of heat transfer. The reader will find, for example, in the appropriate context in the book, an account of Planck's law of radiation, the hydrodynamics of viscous flow, Drude's theory of conduction in metals, the theory of similarity, the Laplace transformation method applied to the heat conduction equation and the relaxation method for the numerical solution of differential equations. The author has, however, imposed upon himself the restriction of keeping the mathematical treatment on an elementary level, in order to make the work accessible to a wider class of readers. He sets out to show the worker in heat transfer how to set up his boundary value problems in mathematical form and to solve them in the simpler cases, but refers him elsewhere for the more difficult matters of technique. For instance, although the Laplace transformation method is explained in principle, the inversion theorem is only briefly mentioned.

The book, of thirty chapters, is divided into five parts excluding the appendices and bibliography. In the first part, which is of an introductory nature, the basic equations of conduction, convection and radiation are developed. The second contains an account of the properties of matter that are of importance in heat transfer. The third, fourth and fifth parts of the book deal respectively with heat conduction in bodies of simple shape, convection without change of phase or constitution and convection including changes of phase. Problems to be solved by the reader are not given at the ends of the chapters, but are collected together in an appendix. There is an extensive bibliography. The author states that he intends, in the second volume of this work, to deal with heat radiation in spaces of simple configuration and with selected fields of application.

There is, in the present volume, a great deal of information on the physical properties of materials, a discussion of the physical theory leading to an understanding of these properties, an account of experimental methods and numerous references to published literature. Work carried out in Germany up to the nineteen-thirties is particularly well covered in the text, both because of the author's participation in it and because of his fear that the unhappy history of that country will diminish the incentive to learn German among English-speaking science students. The section on heat conduction contains chapters on the solution of the heat conduction equation with simple boundary conditions. These are followed by an account of finite difference approximation methods which are useful when an analytical solution is not practicable—the relaxation method for steady state problems and a numerical method, similar in principle to the Schmidt graphical method, for the calculation of transient flow. Graphical and experimental analogy methods are also described. The methods used for dealing with the more difficult problems involving free and forced convection are discussed at some length and the reader is given a good idea of the present state of knowledge in this field. There is a discussion of similarity considerations which are of fundamental importance in the complicated heat transfer problems that arise in industrial practice.

The book is likely to be useful both to the student and to anyone who has to deal with heat transfer problems in the course of his work. The price of the book, however, even after making allowances for present trends, is much too high. M. R. HOPKINS.

CONTENTS FOR SECTION B

PAGE

Dr. H. R. **Thirsk**. A Note on the Orientated Overgrowths of Metal Films on Single Crystal Inorganic Substrates 833
Dr. D. J. **Phillips** and Dr. N. **Thompson**. Surface Effects in Creep of Cadmium Crystals 839
Dr. M. **Davis** and Dr. N. **Thompson**. Creep in a Precipitation-Hardened Alloy . 847
Dr. H. K. **Henisch** and Mr. J. **Ewels**. A Study of Electrical Forming Phenomena at Selenium Contacts 861
Dr. D. **Greene**. Secondary Electron Emission from Molybdenum produced by Helium, Neon, Argon and Hydrogen 876
Mr. A. C. **Lynch**. The Variation with Temperature of the Piezoelectric Coefficients of Quartz 890
Mr. I. G. **Ross** and Dr. R. A. **Sack**. Solvent Effects in Dipole Moment Measurements 893
Mr. B. H. **Briggs** and Mr. G. J. **Phillips**. A Study of the Horizontal Irregularities of the Ionosphere 907
Dr. S. R. **Khastgir** and Mr. P. M. **Das**. Periodic Fading of Short-Wave Radio Signals 924
Dr. J. McG. **Bruckshaw** and Dr. B. S. **Rao**. Magnetic Hysteresis of Igneous Rocks 931
Mr. W. **Culshaw**. The Michelson Interferometer at Millimetre Wavelengths . 939
Mr. P. A. **Sturrock**. Note on the Focusing of Electron Beams in certain Magnetic Fields 954
Dr. J. F. W. **Bell**. Satellite Resonances in Ultrasonic Interferometry . . 958
Letters to the Editor :
  Dr. J. R. **Bristow**: Dr. R. C. **Parker** and Mr. D. **Hatch**. Frictional Relaxation Oscillations 964
Contents for Section A 965
Abstracts for Section A 966

ABSTRACTS FOR SECTION B

A Note on the Orientated Overgrowths of Metal Films on Single Crystal Inorganic Substrates, by H. R. Thirsk.

ABSTRACT. Some new examples of metal crystal orientations on inorganic substrates are described. They include silver and iron on mica, platinum on the cube face of potassium chloride, iron and silver on the (111) face of potassium chloride, silver and nickel on the cube face of magnesium oxide. Some of the problems involved in the study of the types of crystal growth are discussed briefly for the cases examined.

Surface Effects in Creep of Cadmium Crystals, by D. J. Phillips and N. Thompson.

ABSTRACT. A recording rate-of-strain meter has been used to investigate the changes in creep rate when the chemical environment of a stressed cadmium crystal is altered. Experiments were made with aqueous solutions of a number of inorganic salts of cadmium. The observations are explicable in terms of variations in the thickness of a surface film of cadmium hydroxide, the presence of such a film having the effect of reducing the creep rate by an amount depending on its thickness. Measurements were also made on the effect of very thin films, formed by immersion in distilled water; these were estimated to be about 10^{-8} to 10^{-7} cm. thick. When the films were removed with dilute sulphuric acid a sudden small strain increment was observed, the magnitude of which depended on the film thickness. Possible explanations are discussed.

Creep in a Precipitation-Hardened Alloy, by M. Davis and N. Thompson.

ABSTRACT. Measurements have been made of the creep shown by polycrystalline wires of a hardened alloy (Cu+3% Ag) both at room temperature and 90° K. The results are interpreted in terms of the Mott–Nabarro theory of transient creep. The agreement between theory and experiment is qualitatively good, and the quantitative discrepancies suggest directions in which the existing theory might be refined.

A Study of Electrical Forming Phenomena at Selenium Contacts, by H. K. Henisch and J. Ewels.

ABSTRACT. An account is given of current-creep experiments at various temperatures on Se specimens of different impurity content. The dependence of these phenomena on the electrical and thermal history of the specimens and on the nature of the counter-electrode is investigated. It is shown that two opposing creep mechanisms are, in general, active simultaneously. One is due to power dissipation within the barrier layer, the other due to structural changes which take place under the influence of the applied field. It was found, contrary to theoretical expectations, that creep processes cannot be 'frozen out' at low temperatures (e.g. −183° c.). Measurements of the self-capacitance of the barrier were carried out at suitable stages of the experiment. These show that the thickness of the barrier increases slightly during forming. A theory of current creep is proposed on the basis of the present observations.

Secondary Electron Emission from Molybdenum produced by Helium, Neon, Argon and Hydrogen, by D. Greene.

ABSTRACT. Experiments have been carried out on the secondary electron emission produced at very low pressure from a degassed metal surface by neutral particles resulting from the neutralization of positive ions of about 1,000 electron volts energy in a metal canal. The gases used were helium, neon, argon and hydrogen. For the first three the energy distribution of the secondary electrons is compatible with the view that a large part of the emission is due to communication of the energy of excitation of a metastable atom to a metallic electron. With hydrogen there is evidence that a similar process occurs with normally excited states of the atom or molecule. In all cases there is evidence that some emission occurs through local heating or disruption of the metal lattice by the mechanical impact of swift atoms, the extent of this increasing from helium and neon to argon and hydrogen. Some reflection of the swift atoms occurs from the metal target.

The Variation with Temperature of the Piezoelectric Coefficients of Quartz, by A. C. Lynch.

ABSTRACT. The equivalent electrical circuits of three bars in longitudinal vibration were measured at approximately 25, 52·5 and 80° c. In this range of temperature the temperature coefficients of d_{11} and d_{14} are respectively -2_{30} and $+13_{60}$ parts/million/° c., and there is no evidence to support Cady's suggestion that d_{11} passes through a maximum near room temperature.

The measurements suggested a rather high value for d_{14}: $(-2{\cdot}21 \pm 0{\cdot}1) \times 10^{-8}$ cm/E.S.U. of potential at 25° c.

Solvent Effects in Dipole Moment Measurements, by I. G. Ross and R. A. Sack.

ABSTRACT. Previous theories advanced to account for the differences between the moments of polar molecules, as measured in dilute solution (in non-polar solvents) and from gas measurements, are discussed on the basis of an internal field function ξ, determining the field inside an ellipsoidal obstacle in a polarized uniform medium. Contours of ξ as a function of the axial ratios of the ellipsoid have been calculated. Onsager's theory of the

static dielectric constant is extended to account for the solvent effect in ellipsoidal solute molecules of uniform polarizability, in which the dipole is parallel to one of the axes of the ellipsoid; the new equation thus obtained gives results in better agreement with experimental data than previous theoretical treatments.

The rule that the sign of the solvent effect of a substance should be opposite to that of its Kerr constant is shown not to be of general applicability.

A Study of the Horizontal Irregularities of the Ionosphere, by B. H. BRIGGS and G. J. PHILLIPS.

ABSTRACT. The theory of diffraction by a random screen developed by Booker, Ratcliffe and Shinn is presented in a convenient form for practical application in ionospheric experiments. It is shown that measurements of the correlation of the fading of the reflected wave observed at spaced receiving points can be used to find the extent of the angular spreading of the downcoming wave.

Histograms are given to show the frequency of occurrence of different degrees of angular spreading observed during a series of experiments using pulse transmissions at vertical incidence.

For a frequency of 2·4 Mc/s. it is most common to find that the downcoming wave has an angular spread such that the amplitude falls to half value at an angle of 5° for regions E and F. For region F observed on 4·8 Mc/s., the corresponding value is 2·5°. There is no evidence for any pronounced seasonal or diurnal variations.

Periodic Fading of Short-Wave Radio Signals, by S. R. KHASTGIR and P. M. DAS.

ABSTRACT. Periodic fading patterns were recorded photographically with Calcutta signals of frequency 4,840 kc/s. received at Dacca (distance 240 km.) during the evening and early night hours of December 1948 and January 1949. The main features in the experimental conditions were: (i) the operating frequency was much less than the maximum usable frequency (M.U.F.) for the F layer transmission, (ii) the frequency was slightly greater than the M.U.F. for the ordinary wave transmission through the E layer and (iii) it was slightly less than the M.U.F. for the extraordinary wave transmission through the E-layer between the transmitting and receiving stations. The following patterns of periodic or rhythmic fading were observed:

(i) Sinuous fading of comparatively quick period: this is considered to be of magneto-ionic origin, due to the interference between the upper and lower trajectory extraordinary waves in the E layer, the ordinary waves having passed through the E layer.

(ii) Periodic or rhythmic fading of comparatively slow period: the slow periodic fading is considered to be due to the beat-effect between the singly and doubly reflected waves from the F2 region or between the singly reflected waves from the E and F2 regions, the two interfering waves in different directions having suffered different amounts of Doppler change of frequency due to the vertical movement of the ionospheric layer or layers. The vertical velocity of the ionosphere as computed from this view agrees with the observed value.

(iii) Slow periodic fading with superposed ripples: this was observed when the ionospheric conditions were favourable for the simultaneous occurrence of the magneto-ionic type of sinuous fading and the Doppler beat type of slow periodic fading. In a few patterns of periodic fading there was evidence of extremely high frequencies (4–12 cycles/second) the origin of which is unknown.

Magnetic Hysteresis of Igneous Rocks, by J. McG. BRUCKSHAW and B. S. RAO.

ABSTRACT. A rapid method has been developed for the investigation of the magnetic properties of igneous rocks. The specimens examined show the normal properties to be expected from a mixture of magnetically different constituents. In particular, high coercivities have been found. The significance of the results in relation to natural permanent magnetism in rocks is discussed.

The Michelson Interferometer at Millimetre Wavelengths, by W. Culshaw.

ABSTRACT. The design and operation of an interferometer of the Michelson type at a wavelength of 12·5 mm. is discussed.

The required frequency stabilization of the 12·5 mm. source is achieved by using a high Q cavity as an R.F. discriminator.

Wavelength measurements have been made with various spacings of the interferometer, the measured wavelength increasing as the spacing is reduced. Results indicate that the interferometer gives more accurate measurements of the wavelength when operated well in the Fraunhofer region of diffraction.

The operating frequency has been measured using a calibrated frequency meter, and hence the velocity of electromagnetic waves deduced. The value obtained for this velocity agrees, within the accuracy attempted with the present instrument, viz. one part in 10^4, with the generally accepted value for this velocity. The possibilities of increasing the accuracy of its determination with the interferometer are discussed.

Measurements of the dielectric constants of low-loss materials by means of the interferometer have been made. Results obtained using ordinary commercial sheets of materials agree within a few per cent with values obtained otherwise.

The use of the interferometer as a substandard of length is also discussed.

Note on the Focusing of Electron Beams in certain Magnetic Fields, by P. A. Sturrock.

ABSTRACT. Equations are set out which determine the focusing properties of electron beams in magnetic fields whose scalar potential has a plane of antisymmetry. From these is derived the condition that a proposed ray-axis and associated focusing requirements should be physically realizable. It is also shown that the fringe-effect of fields with sharply defined boundaries may be characterized by a pair of focal lengths for which formulae are given.

Satellite Resonances in Ultrasonic Interferometry, by J. F. W. Bell.

ABSTRACT. An experimental investigation into the origin of satellite resonances has been carried out by the author. They are identified as mode resonances of the gas in the interferometer tube and are of the type described by Lord Rayleigh.

The presence of unresolved satellites in the principal interferometer resonance introduces a considerable error into absorption measurements. Results obtained by Van Itterbeek and his co-workers are shown to be in agreement with the Krasnooshkin interferometer theory, which takes into account the effect of the multiple nature of the principal resonance.

A criterion for the choice of crystals for ultrasonic absorption measurements is given.